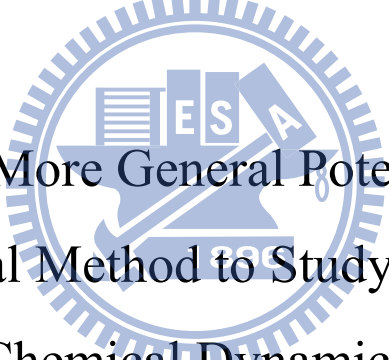


國立交通大學

應用化學系分子科學碩士班

碩士論文

一個更普遍用於半經典理論研究化學反應動態
學的絕熱勢能曲線



Constructing a More General Potential Curves for
Semi-Classical Method to Study State to State
Chemical Dynamics

研究生：孔令鈞 (Ling-Ging Kaung)

指導教授：朱超原 博士 (Dr. Chao-Yaun Zhu)

中華民國一百年十二月

一個更普遍用於半經典理論研究化學反應動態 學的絕熱勢能曲線

研究生：孔令鈞

指導教授：朱超原

國立交通大學應用化學系分子科學碩士班

摘要

此研究利用了現今發展完善的反應途徑(Reaction coordinate)以及正交於反應座標系的 $3N-7$ 震動模(Normal modes)所建構的 $J=0$ 絕熱曲線(adiabatic curves)來進行 $\text{OH} + \text{H}_2 \rightarrow \text{H}_2\text{O} + \text{H}$ 化學反應動態學的研究。發現由此絕熱曲線在只考慮穿隧效應下得到的 $J=0$ 累積反應機率(Cumulative reaction probability)比 Miller 的 $J=0$ 累積反應機率(Cumulative reaction probability)小很多。可能原因是反應端跟生成端轉動相關的震動模的數目不相符。吾人也利用了絕熱模型(adiabatic model)，改裝過的絕熱模型(modified adiabatic model)和透熱模型(diabatic model)來計算累積反應機率，並得到三個可能與 Miller 結果差異的原因。第一是能量曲線並不是拋物線的模型，第二是非絕熱耦合(non-adiabatic coupling)的貢獻和最後一個是延反應途徑的頻率分析的準確度。為了確定哪個是最主要的原因，吾人利用上述的三個模型到比較大的體系， $\text{Cl} + \text{CH}_4 \rightarrow \text{CH}_3 + \text{HCl}$ 。可是對於大於五個原子以上的

體系，並沒有一個精確的解。所以只有降維度的資料可以比較，也就是說，吾人只能用降維度的絕熱模型來做比較。在與 Nyman 三個降維度；RLA, RLU 和 RBU, 的結果比較，吾人發現絕熱模型的結果與 Nynam 的結果的趨勢很近，並且發現考慮的維度越小，共振的現象越大。從比較的結果，吾人發現以上三個原因中，以第三個原因為決定累積反應機率準確度的最主要原因。



Constructing a More General Potential Curves for Semi-Classical Method to Study State to State Chemical Dynamics

Student: Ling-Ging Kaung

Advisor: Dr. Chao-Yaun Zhu

M.S. Program, Institute of Molecular Science, Department of
Applied Chemistry, National Chiao Tung University



We constructed more general adiabatic energy curves of $J=0$ for $\text{OH} + \text{H}_2 \rightarrow \text{H}_2\text{O} + \text{H}$ by using the reaction coordinate and $3N-7$ normal modes which is orthogonal to the reaction coordinate, but found the cumulative reaction probability of these adiabatic energy curves (without the effect of non-adiabatic coupling, only the effect of tunneling) is lower than the result of Miller. The possible reason would be the linkage between reactants and products. Since three rotational related vibration modes in reactant side, but two in product side. And we also applied the adiabatic model, modified adiabatic model and diabatic model to the cumulative reaction probability and then got three main possible reasons for the deviation from Miller's

result. First is that the energy curves are not parabolic model, the second one is that the contribution of non-adiabatic coupling and the last one is the accuracies of the frequencies along the reaction path. In order to make sure which one is the main reason, we applied these three models to a larger but prototypical system, $\text{Cl} + \text{CH}_4 \rightarrow \text{HCl} + \text{CH}_3$. But for more than 5-atoms system, there's no exact solution no matter hyper-spherical (projected one is the same) or Jacobi coordinate. So only reduced dimensions information is available, that is, only the adiabatic model with reduced dimension could be applied to do comparisons. After comparing with the three models; RLA, RLU, RBU, by Nyman, we found that the trends of our adiabatic models goes well Nyman's results and the effect of resonance becomes larger as the degree of freedom becomes smaller. From the result, we conclude that the last reason; the accuracies of the frequencies along the reaction coordinate dominate the accuracy of the result for the cumulative reaction probability.

謝誌

在交大已經待了快六年半了，時間真是一轉眼就過了！這幾年經歷的各種快樂、痛苦和挫折。這一路上很謝謝有你們。

首先我要感謝的是我的指導教授朱超原老師，感謝您在這一年半忍耐著我異想天開的想法，並且給予我機會思考我做的每件事情，也很謝謝老師您對我耐心的教導，讓我了解到理論的重要性。謝謝偉哥在我一開始進入實驗室，耐心的回答我每一個很蠢的問題。謝謝俊吉學弟這個開心果，不論怎樣鬧你，你都嘻嘻哈哈的。最後要感謝的是那些在我最痛苦的時候陪伴在我身邊的大學同學以及家人，謝謝金毛、信良(後半年真的是謝謝你，要不是你陪我睡那燈超亮來以及蚊子多到爆的實驗室，我大概會瘋掉)、誠帥仔以及蝌蚪在這段時間總是靜靜聽我吐苦水(雖然事後總是機車我，尤其是金毛)更要謝謝我母親總是在我挫折的時候鼓勵我，並且完全的相信我。謝謝你們給我這些美好的回憶。

Table of Contents

Chapter 1 Introduction	1
1-1 Quasi-classical trajectory, quantum and semi-classical methods	2
1-1.1 Quasi-classical trajectory method	2
1-1.2 Quantum method	4
1-1.3 Semi-classical method	5
1-2 Motivation	5
References	9
Chapter 2 Theory	11
2-1 Born-Oppenheimer approximation	14
2-1.1 Hartree–Fock method (HF)	18
2-1.2 Post- HF methods	23
2-2 Adiabatic approximation for the motion of nuclei on single PES	27
2-2.1 Min energy path	28
2-2.2 Semi-classical theory	31
2-2.2.1 Zhu and Nakamura theory	31
2-3 Application to adiabatic curves on MEP	33
References:	44
Chapter 3 Results and Discussions	45
3-1 Theoretical results for $\text{OH}+\text{H}_2 \rightarrow \text{H}+\text{H}_2\text{O}$ reaction	45
3-1.1 Theoretical calculation for MEP	45
3-1.2 Geometry of transition state	46
3-1.3 Normal modes along reaction path	46
3-2. Construct the adiabatic curves of $J = 0$ on MEP	50
3-3. Cumulative reaction probability	51
3-3.1 Cumulative reaction probability for $\text{OH}+\text{H}_2 \rightarrow \text{HCl}+\text{H}_2\text{O}$	51
3-3.2 Cumulative reaction probability for $\text{Cl} + \text{CH}_4 \rightarrow \text{HCl} + \text{CH}_3$	59

3-3.2.1 Theoretical results for the MEP of $\text{Cl} + \text{CH}_4 \rightarrow \text{HCl} + \text{CH}_3$	59
3-3.2.2 Geometries of transition state, products and reactants	60
3-3.2.3 Normal modes along reaction path	60
3-3.2.4 Cumulative reaction probability for $\text{Cl} + \text{CH}_4 \rightarrow \text{HCl} + \text{CH}_3$	61
Chapter4 Conclusions.....	99
Reference.....	101



Chapter 1 Introduction

One of the basic purposes of chemical reaction dynamics including state-to-state reaction is to understanding reaction mechanism by analyzing the evolution relationships between quantum states of products and reactants. These relationships show the information of how bonds break and form gradually from reactant to product through the transition state. Within Born-Oppenheimer approximation, the motion of atoms in the molecule relies on the force created by the potential energy surface which is formed by averaging motion of all electrons in the molecule.

A tri-atomic reaction, $AB+C \rightarrow A+BC$, is the most basic reaction for state-to-state reaction dynamical studies. In this fundamental reaction involving only three normal-mode vibrations plus rotation and translation, both experiments and theoretical research have very much advanced in order to obtain the complete information for diatom-atom reactions. These indicate that vibrational or translational excitation may produce dramatic effects on chemical reactions. One of the most obvious effects is the influence of chemical reactivity. ¹ Polanyi has shown that the vibrational excitation is more efficient than the translation excitation for increasing endoergic chemical reactivity for atom-diatom-reaction, namely late barrier. The concept of early barrier/late barrier becomes not so apparent for reactions containing polyatomic reagents since many degree of freedoms involves in polyatomic molecules in which

there are a large number of vibrational modes. The quantum⁵⁻⁷ and quasiclassical trajectory⁸ methods for atom-diatom reaction have been extended for studying polyatomic reactions. At the same time, several exciting experimental results for state-to-state reaction dynamics of polyatomic reactions have been found. Both these experiments and theoretical research have pointed out that there are essential differences between atom-diatom reactions and polyatomic reactions. Studying these differences open new horizons for scientists.

1-1 Quasi-classical trajectory, quantum and semi-classical methods

Quasi-classical trajectory (QCT), quantum scattering and semi-classical methods are three general methods to study chemical reaction dynamics theoretically. I would like to introduce a brief review of QCT first, the second is quantum method, and the third is semi-classical method. Finally, I will mention problems for each of three methods.

1-1.1 Quasi-classical trajectory method

As mentioned above from Born-Oppenheimer approximation, the motion of atoms in molecule is just experiencing force induced by PES formed. If potential energy surface can be constructed as an analytical function of the internal coordinates

of the constituent atoms, it is possible to solve the motion of atoms on the surface for collision trajectory in classical way. The initial conditions can be determined by using coordinates and momentums of reactant molecule semi-classically, and then numerical integration of the Hamilton equation of motion for coordinate Q_j and it's conjugate momentum $P_j = m \frac{dQ_j}{dt}$ are evaluated. Because of classical mechanical approach, there are several quantum effects that have to be added separately:

1. Particles penetrating into the region are classical forbidden.
2. The zero point energy (ZPE) is absence. Several approaches⁹⁻¹⁵ have been done to fix the problem of ZPE, but none of them are that reliable.
3. Classical mechanics does not recognize that reactants/products have quantum states, the given integration results may produce the vibrational energy of products different from quantum mechanics. But what we're interested in is the quantum mechanic features as the vibrational or rotational product distribution, in order to obtain the correspondence, a binning process is needed. How to bin the region for different vibration and rotation quantum number will influence the accuracy of state to state dynamics, but this defect may cancel out for overall distribution.
4. Some of the initial-condition parameters of reactants would not be specified during experiments, but the specification of these parameters is required in doing calculation, such as impact parameter, the orientation of the reactants, the phase of

the reactant vibration with respect to the time of collision, and so on. So, averaging over these uncontrolled parameters of collision in the classical mechanic calculation is required.

The defects of QCT can be easily seen from the mentioned above, the omission of the quantum effects make it experienced difficulties at threshold; when the total energy is slightly above the minimum required to cross the potential barrier, the ZPE energy tends to be converted into translation energy, which is not allowed in quantum mechanics. Besides this general problem for QCT, dealing with large system by QCT is still a challenging problem. The reason for this is that determination of vibrational actions; binning process, for large system is not a standard process. Even if there is standard process for binning, obtaining the PES for large system is still difficult.

1-1.2 Quantum method

Apart from using the Newton mechanics to describe the motion of atoms; their motion is governed by a wave equation in quantum mechanics. The general strategy is to solve the time dependent or time independent Schrodinger equation in the superposition wave function of channels interested and then obtain the quantities needed, e.g. state to state cross section, by giving suitable boundary condition.

For exact quantum calculation, it may consume large amount of computational

time. Since all accessible states; rotational and vibrational states, should be considered in the calculation. Of course, one could calculate all the information, but are these considerable quantities that demanding? Doing that requires huge effort, so a modified method; reduced dimension quantum method is developed for this need. For four, five, or six atoms system, this method is accessible. But for larger system, it's a big problem. So there's reduced dimension quantum method (modified quantum method). However for too large system, the modified quantum method is still not ok.

1-1.3 Semi-classical method

This method would be explained clearly in chapter 2. Same as the two methods mentioned above. There is no general strategy for large system.

1-2 Motivation

As mentioned above, no matter quasi-classical trajectory, modified quantum method or semi-classical method, there still exist difficulties for studying dynamics of large system. So, this motivates us to produce a more general way; which is practical to large system for dealing with state-to-state reaction dynamics. For system more than 5 atoms, it's not that easy to obtain exact quantum results for reactions. In order to make sure the feasibility of our method, we would like to apply this approach to

$\text{OH} + \text{H}_2 \rightarrow \text{H}_2\text{O} + \text{H}$; which has been studied thoroughly from both theory and experiments. Firstly, I would like to give a brief review of the calculations and experiments which have been done for $\text{OH} + \text{H}_2 \rightarrow \text{H}_2\text{O} + \text{H}$.

$\text{OH} + \text{H}_2 \rightarrow \text{H}_2\text{O} + \text{H}$

The thermal rate constant for $\text{OH} + \text{H}_2$; which is important in combustion chemistry, has been measured over a wide range of temperature ($T = 250 \sim 2000 \text{K}$) for both thermal distribution of reactants¹⁶⁻¹⁸ and there is obvious evidence¹⁸ that $k(T)$ shows non-Arrhenius behavior with a suggested best fit expression $k(T) = 1.66 \times 10^{-16} \cdot T^{1.6} \cdot \exp(-1660 \text{K}/T)$ cm³/molecule*s. G.P. Glass¹⁹, Spencer et al²⁰ and R. Zellner^{18,21} investigate the influence of vibrational excitation on reaction rate. They^{18,19-20} found that not small amount of enhancement ($\text{H}_2(v=1)/\text{H}_2(v=0) > 100$) for $\text{H}_2(v=1)$, but smaller effect (50% less than the excitation of H_2) for $\text{OH}(v=1)$; which is reasonable since OH can be seen as a spectator in the reaction. Later, R. Zellner²¹ thought the large enhancement may be due to the possibilities of the contribution of a translational rate acceleration of $\text{OH} + \text{H}_2$ in the flow system. After correction, the enhancement is rather small (5~66) compared to before (>100). Many fast-atom experiments²²⁻²⁹ have been done for $\text{H} + \text{H}_2\text{O}$ (and its isotopomers) in the final vibrational and rotational distribution of H_2 and OH were determined.

Isaacson's³⁰ group reported a reaction path potential, based on Walch and

Dunning's calculation, and use it in transition state theory calculation for rate constant with complex tunneling effect. Cohen et al³¹ used Isaacson's reaction path potential in transition state theory calculation of rate constant with new treatments of anharmonicity of the transition state force field. A potential curve along a tunneling path is also calculated by Truong and Evans³²; which is used in calculating the rate constant.

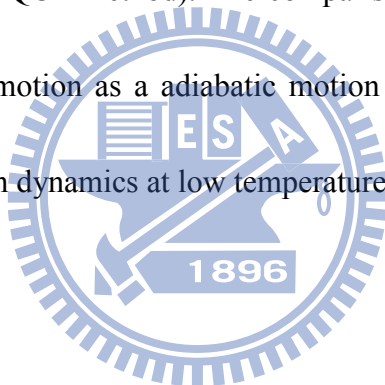
Schatz and Elgersma³³ based on the method for saddle point properties developed by Walch and Dunning³⁴ to construct a global potential energy surface. Extensive quasiclassical trajectory calculations^{33,35,36} based on this PES have been done, they point out interesting mode specificity in the H+H₂O reaction in highly vibrational excited states. There are several other QCT studies being reported later³⁷⁻⁴⁰

Quantum dynamics studies for the OH+H₂ reaction have been reported by Wang & Bownan⁴¹, Clary and coworkers⁴², Miller and coworkers⁴³, Zhang⁴⁴, and Neuhauser⁴⁵. Those of Miller and coworkers, Zhang, and Neuhauser are full dimension. Wang & Bownan RD-AB theory. Clary and coworkers use RBA-AB theory.

The cumulative reaction probability for J=0 has been calculated with full dimension; by Miller, RD-AB; by Wang, and RBA-AB, by Clary. The results show that there is a quite good agreement for RD-AB and RBA-AB with full dimension at low E, but a little deviation at higher E.

Miller also calculated the thermal rate constant for OH+H₂ by J-shift

approximation. The result for thermal rate constant along RD-AB (J-shift approximation), RBA-AB (centrifugal-sudden approximation), and QCT are also calculated. The RD-AB result is in good agreement with full dimension (RD-AB results are reasonable, since $J=0$ CPR are almost the same and they both use J shift method), but RBA-AB somewhat higher (The difference comes from using centrifugal-sudden approximation). Finally, QCT's result show good agreement with full dimension at higher temperatures, but underestimate at lower temperatures (The lack of tunneling effect for QCT method). The comparisons between full dimensions show that taking bending motion as a adiabatic motion still give reliable result and QCT method can't deal with dynamics at low temperature.



References

1. J. C. Polanyi, *Acc. Chem. Res.* **5**, 161 (1972).
2. F. F. Crim, *J. Phys. Chem.* **100**, 12725 (1996).
3. R. N. Zare, *Science* **279**, 1875 (1998)
4. F. F. Crim, *Acc. Chem. Res.* **32**, 877 (1999)
5. Bowman JM, ed. *Advances in Molecular Vibrations and Collision Dynamics: Quantum Reactive Scattering*, 187 (1994)
6. Clary DC, Echave I. See reference 5 ,2: 203(1994)
7. Clary DC. *J. Phys. Chem.* **98**, 10678 (1994)
8. Schatz Ge. *J. Phys. Chem.* **99**, 516(1995)
9. Schatz GC. *J. Chem. Phys.* **79**, 5386 (1983)
10. LuD-H, Hase WL. *J. Chem. Phys.* **89**, 6723 (1988)
11. Miller WH, Hase WL, Darling L. *J. Chem. Phys.* **91**, 2863 (1989)
- 12 Bowman JM, Gazdy B, Sun Q. *J. Chem. Phys.* **91**, 2859 (1989)
13. Sewell TD, Thompson DL, Gezelter JD, Miller WHO. *Chem. Phys. Lett.* **193**, 512 (1992)
14. Peslherbe GL, Hase WL. *J. Chem. Phys.* **100**, 1179 (1994)
15. Ben-Nun M , Levine RD. *J. Chem. Phys.* **101**, 8768 (1994)
16. Tully FP, Ravishankara AR. *J. Phys. Chem.* **84**, 3226 (1980)
17. Ravishankara AR, Nocovich JM, Thompson RL, Tully FP. *J. Phys. Chem.* **85**, 2498 (1981)
18. R. Zellner, *J. Phys. Chem.* **83**, 18. (1979)
19. Glass OP, Chaturvedi BK. *J. Chem. Phys.* **75**, 2749 (1981)
20. J.E. Spencer, H. Endo and G.P. Glass, 16th Symposium (International) on Combustion (The Combustion Institute, Pittsburgh) 829 (1976)
21. Zellner R, Steinert W. *Chem. Phys. Lett.* **81**, 568 (1981)
22. Kleinermanns K, Wolfrum J. *Appl. Phys. B* **34**, 5 (1984)
23. Honda K, Takayanagi M, Nishiya T, Ohoyama H, Hanazaki I. *Chem. Phys. Lett.* **180**, 321 (1991)
24. Kessler K, Kleinermanns K. *Chem. Phys. Lett.* **190**, 145 (1992)
25. Jacobs A, Volpp H-R, Wolfrum J. *Chem. Phys. Lett.* **196**, 249 (1992)
27. Jacobs A, Volpp H-R, Wolfrum J.J. *Chem. Phys.* **100**, 1936 (1994)
28. Kippe S, Laurent T, Naik PD, Volpp H-R, Wolfrum J. *Can. J. Chem.* **74**, 615 (1994)
29. Adelman DE, Filseth SV, Zare RN. *J. Chem. Phys.* **98**, 4636 (1993)
30. Isaacson AD. *J. Phys. Chem.* **96**, 531(1992)
31. Cohen MJ, Willetts A, Handy NC. *J. Chem. Phys.* **99**, 5885 (1993)

32. Truong TN, Evans TJ. J. Phys. Chem. **98**, 9558 (1994)
33. Schatz GC, Elgersma H. Chem. Phys. Lett. **73**, 21(1980)
34. Walch SP, Dunning TH Jr. J. Chem. Phys. **72**, 1303 (1980)
35. Schatz Ge. J. Chem. Phys. **79**, 5386 (1983)
37. Schatz OC, Colton MC, Grant JL. J. Phys. Chem. **88**, 2971 (1984)
38. Rashed O, Brown NJ. J. Chem. Phys. **82**, 5506 (1985)
39. Harrison JA, Mayne HR. J. Chem. Phys. **87**, 3698(1987)
40. Harrison JA, Mayne HR. J. Chem. Phys. **88**, 7424(1988)
41. Wang D, Bowman JM. J. Chem. Phys. **96**, 8906 (1992)
42. Echave J, Clary DC. J. Chem. Phys. **100**, 402 (1994)
43. Manthe U, Seideman T, Miller Who. J. Chem. Phys. **99**, 10078 (1993)
44. Zhang DH, Zhang JZH. J. Chem. Phys. **99**, 5615 (1993)
45. Neuhauser DJ. J. Chem. Phys. **100**, 9272 (1994)



Chapter 2 Theory

As mentioned in chapter 1, state-to-state dynamics provide mechanism understanding of reactions by indirect probing of transition state. What is probed are the connections made between products and reactants, that is, these connections reveal how bond break and form in the transition state. So the question is how to obtain the information of state-to-state dynamics theoretically. In order to achieve this goal, knowing how atoms move in the electron clouds of the molecule system is necessary. In general, this kind of information would be gained by Born-Oppenheimer approximation (or adiabatic approximation). Within Born-Oppenheimer approximation, the motion of atoms in the molecule relies on the force created by the potential energy surface which is formed by averaging motion of all electrons in the molecule, that is, the motion of atoms and electrons could be considered separately as bellow

$$\Psi_T = \Psi_{Elec} \Psi_{Nuc} \quad (2.1)$$

, where Ψ_T is the total wave function, Ψ_{Elec} is the wave function of electrons and Ψ_{Nuc} the wave function of nucleuses. Since the state-to-state dynamics here are talking about the states in the same electronic state, that is to say, only the rovibrational states of the ground electronic state are necessary and non-adiabatic coupling would occur between the rovibrational states. There are three general methods; quasi-classical trajectory (QCT), quantum and semi-classical methods.

However, no matter which method, there is still a big problem for dealing with large system. It motivates us to generate a general way for polyatomic reaction. Our method is based on the semi-classical theory developed by Zhu and Nakamura¹, but chooses a different reaction scattering axis for adiabatic curves, which is more general for normal system (small or large system). Bellow I would like to talk about the general concept for adiabatic approximation. Then, there will be explanation of the reason for the chosen of this coordinate and the difference of semi-classical theory for dealing with non-adiabatic coupling and its application.

General concept of adiabatic approximation

In a study of systems with many degrees of freedom, such as those consisting several interacting particles, one general seeks to use the same way, a successive reduction of multidimensional problem to several lower dimensional problems that are simpler to deal with. There are two general way to do this, symmetry and adiabatic separation. Adiabatic separation is main thought in Born-Oppenheimer approximation, which is settled on the assumption that the motion associated with some part of the variables (Fast) can be treated with other part (Slow) seen as frozen; taking the energy of these fast variables at different slow variables produce effective PES for the motion of slow variables. A general operator of this thought:

$$H(Q_f, Q_s) = K(Q_s) + H_{ad}(Q_f, Q_s) \quad (2.2)$$

, in which Q_f and Q_s represents the fast and slow variables, $K(Q_s)$ is the kinetic energy for the motion in Q_s which does not depends on Q_f , and the adiabatic Hamiltonian $H_{ad}(Q_f, Q_s)$ is the operator of Q_f which depends on Q_s parametrically. The schrodinger equation would be:

$$\{K(Q_s) + H_{ad}(Q_f, Q_s) - E\}\Psi(Q_s) = 0 \quad (2.3)$$

with total wave function to be:

$$\Psi(Q_s) = \sum F_n(Q_s)\varphi_n(Q_f, Q_s) \quad (2.4)$$

, in which $\varphi_n(Q_f, Q_s)$ is from equation (2.5)

$$H_{ad}(Q_f, Q_s)\varphi_n(Q_f, Q_s) = E_n(Q_s)\varphi_n(Q_f, Q_s) \quad (2.5)$$

where E_n is the adiabatic energy and φ_n is the adiabatic state. Take equation (2.4) into equation (2.3) and integrate the coordinate of fast variables with φ_m , you could obtain the non-adiabatic coupling terms as equation (2.6) and equation (2.7):

$$\langle \phi_m(Q_f, Q_s) | \nabla_{Q_s} | \phi_n(Q_f, Q_s) \rangle \quad (2.6)$$

And

$$\langle \phi_m(Q_f, Q_s) | \nabla_{Q_s}^2 | \phi_n(Q_f, Q_s) \rangle \quad (2.7)$$

If the adiabaticity is pretty good, then the contribution of these two terms would be pretty small, that is, we could omit these effects and obtain

$$\{K(Q_s) + E_n(Q_s) - E\}F_n(Q_s) = 0 \quad (2.8)$$

And the approximated total wave function as

$$\Psi_n(Q_s) = F_n(Q_s)\varphi_n(Q_f, Q_s) \quad (2.9)$$

From equation (2.2) to (2.7), there is no approximation inside until the function $\varphi_n(Q_f, Q_s)$ is specified. Since it's impossible to consider infinite basis in equation (2.5), we must do truncation. If the adiabaticity is good, then the non-adiabatic coupling between adiabatic states; equation (2.6) and (2.7), would be small, that is, the total wave function; equation (2.5), would be much more similar to the adiabatic one, which means lesser basis are needed and this is where the approximation originated. In order to obtain good approximation, the way of how to choose the fast and slow variables is important, since the adiabaticity will be depended on how you choose them. Born-Oppenheimer approximation is a good approximation of adiabatic approximation. Bellow I would like to introduce this approximation.

2-1 Born-Oppenheimer approximation

Born-Oppenheimer approximation; named after Max Born and J. Robert Oppenheimer, is a kind of adiabatic approximation which is used to describe the motion of nuclei and electrons in the molecular system. As mentioned above, the adiabaticity controls the accuracy of the approximation. Why adiabatic approximation is a good approximation for the motion of nucleus and electrons in the molecular system? From the view of physical meanings, since the motion of nuclei is much

slower than the motion of electrons, that is, we could see the movements of nuclei as frozen when electrons are moving at every instant, which is pretty reasonable, since the weight of nucleus is much larger than the weight of electron (even the lightest one; hydrogen, are larger than electron in a factor of 1836). So it's obvious to take the motion of nuclei as slow variables and the motion of electrons as fast variables. From the view of derivation, the nonrealistic Hamiltonian of the molecular system could be written as

$$\hat{H} = -\sum_A \frac{\hbar^2}{2m_A} \nabla_A^2 - \sum_i \frac{\hbar^2}{2m_e} \nabla_i^2 - \sum_A \sum_i \frac{Z_A e^2}{4\pi\epsilon_0 r_{Ai}} + \sum_i \sum_{j>i} \frac{e^2}{4\pi\epsilon_0 r_{ij}} + \sum_A \sum_{B>A} \frac{Z_A Z_B e^2}{4\pi\epsilon_0 r_{AB}} \quad (2.10)$$

, where A, B refer to nuclei and i, j refer to electrons. The Hamiltonian may be written explicitly as

$$\hat{H} = \hat{T}_N(R) + \hat{T}_e(r) + V_{Ne}(R, r) + V_{ee}(r) + V_{NN}(R) \quad (2.11)$$

, where R is the set of nuclear coordinates, r is the set of electronic coordinates. In equation (2.11), it is V_{Ne} this term that makes the separation of electrons and nuclei becoming impossible. But as mentioned above, since the motion of nuclei is much slower than the motion of electrons, it is reasonable to rewrite the Hamiltonian as

$$\hat{H} = \hat{T}_N(R) + \hat{H}_e(R, r) \quad (2.12)$$

Where $\hat{H}_e(R, r)$ is as bellow

$$\hat{H}_e(R, r) = \sum_i \frac{\hbar^2}{2m_e} \nabla_i^2 - \sum_A \sum_i \frac{Z_A e^2}{4\pi\epsilon_0 r_{Ai}} + \sum_i \sum_{j>i} \frac{e^2}{4\pi\epsilon_0 r_{ij}} + \sum_A \sum_{B>A} \frac{Z_A Z_B e^2}{4\pi\epsilon_0 r_{AB}} \quad (2.13)$$

Or

$$\hat{H}_e(R, r) = \hat{T}_e(r) + V_{Ne}(R, r) + V_{ee}(r) + V_{NN}(R) \quad (2.14)$$

And the total schrodinger equation of the molecular system would be

$$(\hat{H} - E)\Psi_t = (\hat{T}_N(R) + \hat{H}_e(R, r) - E)\Psi_t = 0 \quad (2.15)$$

, where H_e is the Hamiltonian of electrons at fixed nuclei configuration, R is the set of nuclear coordinates; the slow variables, and r is the set of electronic coordinates: the fast variables. The total wave function would be

$$\Psi_t(R) = \sum_n F_n^{Nuc}(R) \varphi_n^e(R, r) \quad (2.16)$$

, where $\varphi_n^e(R, r)$ is from

$$H_e(R, r) \varphi_n^e(R, r) = E_n(R) \varphi_n^e(R, r) \quad (2.17)$$

, in which E_n is the adiabatic electronic energy and $\varphi_n^e(R, r)$ is the adiabatic electronic state. Take equation (2.16) back to equation (2.15) and integrate the coordinates of electrons with $\varphi_m^e(R, r)$, then we get

$$\sum_n \langle \varphi_m^e | \hat{T}_N | F_n^{Nuc} \varphi_n^e \rangle_r + E_m F_m^{Nuc} - E F_m^{Nuc} = 0 \quad (2.18)$$

And the term $\sum_n \langle \varphi_m^e | \hat{T}_N | F_n^{Nuc} \varphi_n^e \rangle_r$ could be further derived by

$$T_N = -\sum_A \frac{\hbar^2}{2m_A} \nabla_A^2 \quad (2.19)$$

Then we obtain

$$\left[\sum_A \frac{-\hbar^2}{2m_A} \nabla_A^2 + E_m - E \right] F_m^{Nuc} - \sum_n \sum_A \frac{\hbar^2}{2m_A} \left[\langle \varphi_m^e | \nabla_A^2 \varphi_n^e \rangle_r F_n^{Nuc} + 2 \langle \varphi_m^e | \nabla_A \varphi_n^e \rangle_r \nabla_A F_n^{Nuc} \right] = 0 \quad (2.20)$$

A more compact notation is needed for equation (2.20), so we introduced the following quantities used by Tully²

$$d_{mn}^{(A)}(R) = \left\langle \varphi_m^e \left| \nabla_A \varphi_n^e \right. \right\rangle_r \quad (2.21)$$

$$D_{mn}^{(A)}(R) = \left\langle \varphi_m^e \left| \nabla_A^2 \varphi_n^e \right. \right\rangle_r \quad (2.22)$$

These two terms are the non-adiabatic terms shown in equation (2.6) and (2.7). The neglect of these two terms is the Born-Oppenheimer approximation, which is reasonable since the weight of nucleus is much larger than the weight of electron, that is, $\nabla_A \varphi_n^e$ is much smaller than $\nabla_A F_n^{Nuc}$. So we could obtain

$$\left[\sum_A \frac{-\hbar^2}{2m_A} \nabla_A^2 + E_m - E \right] F_m = 0 \quad (2.23)$$

And total wave function would be

$$\Psi_t(R) = F_n^{Nuc}(R) \varphi_n^e(R, r) \quad (2.24)$$

Equation (2.17) and (2.23) are the two basic equations of Born-Oppenheimer approximation, where E_m is obtained by equation (2.17); the adiabatic electronic energy, which is seen as the average field of the motion of nuclei. This average field is calculated before dealing with the motion of nuclei, that is, solve the Shcrondinger equation at every fixed nuclei configuration. Now the question comes to how to obtain the adiabatic electronic energy state and energy, that is how to solve equation (2.17). In general, there are two general methods for quantum calculation; Hartree–Fock or self-consistent field (SCF) method and Post–Hartree–Fock, where

the Post-Hartree-Fock are the set of methods developed to improve on the Hartree-Fock (HF), which considered the electron correlation energy that HF method didn't consider. Bellow we would to introduce the HF method and then some Post-HF methods.

2-1.1 Hartree-Fock method (HF)

Hartree-Fock theory is one of the simplest approximate theories for solving the many-body Hamiltonian, which reduce the many-body problem into several one-body problems. It is based on the independent particle models, that is, the total wave function of the electrons are the product of wave function of each single electrons, as bellow

$$\Psi_t^e = \varphi_{a_1}^e(R, r_1) \varphi_{a_2}^e(R, r_2) \cdots \varphi_{a_{N_e}}^e(R, r_{N_e}) \quad (2.25)$$

Where R is the set of nuclear coordinates, r_i is the i th electronic coordinate and a_i is the i th spin orbital function. In order to contain the property of anti-symmetry for the total wave function of electrons, single Slater determinant is used to represent the total wave function, as the form bellow

$$\Psi_{SD}^e = \frac{1}{\sqrt{N_e!}} \begin{vmatrix} \varphi_{a_1}^e(r_1) & \varphi_{a_1}^e(r_2) & \cdots & \varphi_{a_1}^e(r_{N_e}) \\ \varphi_{a_2}^e(r_1) & \varphi_{a_2}^e(r_2) & \cdots & \varphi_{a_2}^e(r_{N_e}) \\ \vdots & \vdots & \cdots & \vdots \\ \varphi_{a_{N_e}}^e(r_1) & \varphi_{a_{N_e}}^e(r_2) & \cdots & \varphi_{a_{N_e}}^e(r_{N_e}) \end{vmatrix} \quad (2.26)$$

With

$$\int \varphi_{a_A}^e * (r_j) \varphi_{a_B}^e (r_j) dr_j = \delta_{a_A a_B} \quad (2.27)$$

That is

$$\int \Psi_{SD}^e * \Psi_{SD}^e dr_1 dr_2 \cdots dr_{N_e} = 1 \quad (2.28)$$

. So the energy would be

$$E = \langle \Psi_{SD}^e | \hat{H}_e | \Psi_{SD}^e \rangle \quad (2.29)$$

Where \hat{H}_e is the form as equation (2.13) or (2.14) which could be rewritten as

$$\hat{H}_e(R, r) = \sum_i^{N_e} H_i^0 + \sum_i^{N_e} \sum_{j>i}^{N_e} \frac{1}{r_{ij}} + \sum_A^M \sum_{B>A}^M \frac{Z_A Z_B}{r_{AB}} \quad (2.30)$$

Where H_i^0 is the operator of single electron at the same nuclei configuration as

bellow

$$H_i^0 = \frac{\hbar^2}{2m_e} \nabla_i^2 - \sum_A \frac{Z_A e^2}{4\pi\epsilon_0 r_{Ai}} \quad (2.31)$$

If N_e equals to $2N$, and the form of Slater determinant changed to

$$\Psi_{SD}^e = \frac{1}{\sqrt{N_e!}} \begin{vmatrix} \varphi_{B_1}^e \alpha(r_1) & \varphi_{B_1}^e \alpha(r_2) & \cdots & \varphi_{B_1}^e \alpha(r_{2N}) \\ \varphi_{B_1}^e \beta(r_1) & \varphi_{B_1}^e \beta(r_2) & \cdots & \varphi_{B_1}^e \beta(r_{2N}) \\ \vdots & \vdots & \cdots & \vdots \\ \varphi_{B_N}^e \beta(r_1) & \varphi_{B_N}^e \beta(r_2) & \cdots & \varphi_{B_N}^e \beta(r_{2N}) \end{vmatrix} \quad (2.32)$$

Then equation (2.29) can be further written as

$$E = 2 \sum_j^N I_{B_j} + \sum_i^N \sum_j^N (2J_{B_i B_j} - K_{B_i B_j}) \quad (2.33)$$

Where the third term of equation (2.30) is not considered, since it is just an effect of a

constant and shifts to the eigenvalues and

$$I_{B_j} = \langle \varphi_{B_j}^e (r_i) | H_i^0 | \varphi_{B_j}^e (r_i) \rangle_{r_i} \quad (2.34)$$

$$J_{B_i B_j} = \left\langle \varphi_{B_i}^e(r_l) \varphi_{B_j}^e(r_m) \left| \frac{1}{r_{lm}} \right| \varphi_{B_i}^e(r_l) \varphi_{B_j}^e(r_m) \right\rangle_{r_l r_m} \quad (2.35)$$

$$K_{B_i B_j} = \left\langle \varphi_{B_i}^e(r_l) \varphi_{B_j}^e(r_m) \left| \frac{1}{r_{lm}} \right| \varphi_{B_j}^e(r_m) \varphi_{B_i}^e(r_l) \right\rangle_{r_l r_m} \quad (2.36)$$

$J_{B_i B_j}$ is called coulomb integral and the $K_{B_i B_j}$ is called the exchange integral if i is not equals to j . By applying the vibration method to equation (2.34), we could find that the form of spatial orbital will satisfy the following equation (2.37) in order to minimize the energy; which is the famous Fock equation

$$\hat{F}(r_j) \varphi_{B_i}^e(r_j) = \varepsilon_{B_i} \varphi_{B_i}^e(r_j) \quad i = 1, 2, \dots, N \quad (2.37)$$

Where $\hat{F}(r_j)$ is the Fock operator, which is given by

$$\hat{F}(r_j) = \hat{f}(r_j) + \sum_k^N [2\hat{J}_{B_k}(r_j) - \hat{K}_{B_k}(r_j)] \quad (2.38)$$

Where

$$\hat{f}(r_j) = -\frac{1}{2} \nabla_j^2 - \sum_A \frac{Z_A}{r_{jA}} \quad (2.39)$$

$\hat{J}_{B_k}(r_j)$ is the coulomb operator given by

$$\hat{J}_{B_k}(r_j) \varphi_{B_i}^e(r_j) = \varphi_{B_i}^e(r_j) \left\langle \varphi_{B_k}^e(r_m) \left| \frac{1}{r_{mj}} \right| \varphi_{B_k}^e(r_m) \right\rangle_{r_m} \quad (2.40)$$

And $\hat{K}_{B_k}(r_j)$ is the exchange operator given by

$$\hat{K}_{B_k}(r_j) \varphi_{B_i}^e(r_j) = \varphi_{B_k}^e(r_j) \left\langle \varphi_{B_k}^e(r_m) \left| \frac{1}{r_{mj}} \right| \varphi_{B_i}^e(r_m) \right\rangle_{r_m} \quad (2.41)$$

So the expression for the i th molecular orbital would be

$$\varepsilon_{B_i} = \left\langle \varphi_{B_i}^e(r_j) \left| \hat{F}(r_j) \right| \varphi_{B_i}^e(r_j) \right\rangle_{r_j} \quad (2.42)$$

Or

$$\varepsilon_{B_i} = I_{B_i} + \sum_j^N (2J_{B_i B_j} - K_{B_i B_j}) \quad (2.43)$$

Comparing with equation (2.33), we could get the total energy in the form of

$$E = \sum_i^N I_{B_j} + \varepsilon_{B_i} \quad (2.44)$$

,which is not just the summation of the orbital energy, since the interaction between electrons will give contribution to the total energy. As it comes to solve the equation (2.37), we found that equation (2.40) and (2.41) cannot be evaluated until all the orbital are known. So self-consistent procedure is needed, in which you guess a set of N coupled basis. Using the Fock equation, we could get a set of new orbital. Then this new set of orbital are used to calculate the new Fock equation. Repeating this process until the new set of orbital is almost same as the previous set, in other words, until they are self-consistent. Now the problem comes to how to guess the orbital. This problem is pretty important, since it controls the convergence time for the self-consistent and the accuracy of the convergent result. The most general procedure is developed by Clemens Roothaan. He expressed the molecular orbital φ_{MO}^e as the linear combinations of basis functions ϕ_v , which in general is atomic orbital

$$\varphi_{MO}^e = \sum_v^k c_v \phi_v \quad (2.45)$$

Take equation (2.45) back into equation (2.37) and integrate the electron coordinate r_j

with $\phi_\mu^*(r_j)$. Then we can get

$$\sum_v^k F_{\mu v} c_v = \varepsilon \sum_v^k S_{\mu v} c_v \quad \mu = 1, 2, \dots, k \quad (2.46)$$

Where $F_{\mu v}$ is given by

$$F_{\mu\nu} = \langle \phi_{\mu}(r_j) | \hat{F}(r_j) | \phi_{\nu}(r_j) \rangle_{r_j} \quad (2.47)$$

and $S_{\mu\nu}$ is given by

$$S_{\mu\nu} = \langle \phi_{\mu}(r_j) | \phi_{\nu}(r_j) \rangle_{r_j} \quad (2.48)$$

If ϕ is chosen a set of real functions; which is general the case. Then both $F_{\mu\nu}$ and $S_{\mu\nu}$ are $k \times k$ Hermitian matrices. The equation (2.46) could be rewritten in matrix notation as bellow

$$Fc = \epsilon Sc \quad (2.49)$$

Which is the most general form used in the computational calculation for HF method, because of the convenience of matrix notation. Up to now, we have shown the derivation of HF method. From this, we could see that there is a principle for making sure the accuracy of the HF ground state result; the lower the ground state energy the more accurate the ground state result, since it is derived from variation method. Besides that advantage, from equation (2.37) we found that the best form after vibration method is one electron schrodinger equation with the effect of taking other electrons as average field, that is, this not only reduce the multi-electrons problem into several one-electron problems but also improve the molecular orbital; the Fock orbital, which has the information of considered electron interacting with other electrons and it is much better than normal single electron orbital. Although there are several advantages above, but there exist one big defect, that is, the independent

particle model approximation for the total wave function, which is absolutely not the form of exact wave function. Because of the second term in the right side of equation (2.30), they are no longer independent. So it is impossible for the total wave function in the form of the product by each single electrons wave function. In other words, the result of HF for ground state will never same as the exact one and it will always higher than the exact one (Since it is derived from variation method.), even if we used infinite basis equation (2.45); which we call this HF limit. The difference between HF limit and the exact one is in the order that will influence the accuracy of chemical reaction. Since HF omit the effect of the instant interaction of electrons (because of the form for total wave function); which is called electron correlation energy, and this is very important for chemical reactions. In order to consider the effect of correlation energy, there is the development of the post-HF method, which would be introduced bellow.

2-1.2 Post- HF methods

As mentioned above, Post- HF method is the method improved to consider the correlation energy that HF didn't consider, which could be defined in the form of bellow equation

$$E_{corr} = E_{exact} - E_{HF\ limit} \quad (2.50)$$

There are several Post- HF methods. Here we would only mention the MP2 for Moller-Plesset Perturbation theory and the CCSD, CCSD(T) for couple cluster method.

Moller-Plesset Perturbation Theory

The basis of Moller-Plesset is to take the Slater determinants constructed by Fock orbitals as the zero order function and further improve the energy and wave function by perturbation theory. So the zero order schrodinger equation would be as bellow

$$\hat{H}^{(0)}\Phi_i^{(0)} = E_i^{(0)}\Phi_i^{(0)} \quad (2.51)$$

Where

$$\hat{H}^{(0)} = \sum_i^{N_e} F(r_i) \quad (2.52)$$

In which $F(r_i)$ is the Fock operator

$$E_i^{(0)} = \sum_i \varepsilon_{a_i} \quad (2.53)$$

and $\Phi_i^{(0)}$ is constructed by Fock orbital(The excited state is simply obtained by exciting the electrons to virtual Fock orbital and then construct its correspond Slater determinants.) Since \hat{H} is in the form of equation (2.30) and $\hat{H}^{(0)}$ is in the form of equation (2.52), then we could expected the first order Hamiltonian would be

$$\hat{H}^{(1)} = \hat{H} - \hat{H}^{(0)} \quad (2.54)$$

Or

$$\hat{H}^{(1)} = \frac{1}{2} \sum_i^{N_e} \sum_j^{N_e} g_{ij} - \sum_i^{N_e} \sum_{a_j} \hat{J}_{a_j}(i) - \hat{K}_{a_j}(i) \quad (2.55)$$

Where

$$g_{ij} = \frac{1}{r_{ij}} \quad (2.56)$$

From the basic of perturbation we would find that the energy considered to first order

(MP1) is the result of HF, which is pretty reasonable since

$$E_i = E_i^{(0)} + E_i^{(1)} = \langle \Phi_i^{(0)} | \hat{H} | \Phi_i^{(0)} \rangle = \langle \Phi_i^{HF} | \hat{H} | \Phi_i^{HF} \rangle = E_i^{HF} = E_i^{MP1} \quad (2.57)$$

So considering to second order energy (MP2), the energy would be

$$E_i = E_i^{(0)} + E_i^{(1)} + E_i^{(2)} = E_i^{HF} - \sum_{A \neq 0} \frac{\langle \Phi_i^{(0)} | \frac{1}{2} \sum_i^{N_e} \sum_j^{N_e} g_{ij} | \Phi_A^{(0)} \rangle \langle \Phi_A^{(0)} | \frac{1}{2} \sum_i^{N_e} \sum_j^{N_e} g_{ij} | \Phi_i^{(0)} \rangle}{E_A^{(0)} - E_i^{(0)}} \quad (2.58)$$

From equation (2.58), it is easy to see that the second order energy correction must be negative. So if we are talking about the ground state, and the basis already make HF limit, then it's obvious that the second order energy correction would be the electron correlation energy.

Coupled-Cluster Theory

The concept of coupled-cluster is little bit same as configuration interaction, but sort the groups in the order of number of electrons excited (same as MP2), where CI sort them in the order of spin (converge too slow.). So total wave function would in the following form

$$\Psi_{CI} = \Phi_0 + \sum_{i,a} a_i^a \Phi_i^a + \sum_{ij,ab} a_{ij}^{ab} \Phi_{ij}^{ab} + \sum_{ijk,abc} a_{ijk}^{abc} \Phi_{ijk}^{abc} + \dots \quad (2.59)$$

Where Φ_0 is the HF ground wave function, i; j; k is the occupied orbitals and a; b; c is the virtual orbitals. The coefficients in equation (2.59) are obtained by variation method, but not the case for coupled-cluster method, which are obtained by second excitation as bellow, where the coefficients are not obtained by variation method

$$\hat{T}_1 \Phi_0 = \sum_i^{occ} \sum_a^{vir} t_i^a \Phi_i^a \quad (2.60)$$

$$\hat{T}_2 \Phi_0 = \sum_{i<j}^{occ} \sum_{a<b}^{vir} t_{ij}^{ab} \Phi_{ij}^{ab} \quad (2.61)$$

$$\hat{T}_3 \Phi_0 = \sum_{i<j<k}^{occ} \sum_{a<b<c}^{vir} t_{ijk}^{abc} \Phi_{ijk}^{abc} \quad (2.62)$$

So equation (2.59) would be

$$\Psi_{CC} = (1 + \hat{T}_1 + \hat{T}_2 + \hat{T}_3 + \dots) \Phi_0 \quad (2.63)$$

By non linear transformation we could get

$$\Psi_{CC} = e^{(\hat{T}_1 + \hat{T}_2 + \hat{T}_3 + \dots)} \Phi_0 = e^{\hat{T}} \Phi_0 \quad (2.64)$$

, which is the exact solution to the equation (2.17). By multiplying $e^{-\hat{T}}$ and integrate with Φ_α , which is at least single excitation, then we can get the information of coefficient in it as bellow

$$\langle \Phi_\alpha | e^{-\hat{T}} \hat{H}_e e^{\hat{T}} | \Phi_0 \rangle = \langle \Phi_\alpha | \Phi_0 \rangle = 0 \quad (2.65)$$

By multiplying $e^{-\hat{T}}$ and integrate with Φ_0 , then we can get the total energy as bellow

$$\langle \Phi_0 | e^{-\hat{T}} \hat{H}_e e^{\hat{T}} | \Phi_0 \rangle = E = E_{HF} + \langle \Phi_0 | \hat{H}_e (\hat{T}_2 + \frac{1}{2} \hat{T}_1^2) | \Phi_0 \rangle \quad (2.66)$$

And CCSD and CCSD(T) is the truncated coupled-cluster method, where CCSD take

$e^{(\hat{T})}$ as bellow

$$e^{(\hat{T})} \approx 1 + \hat{T}_1 + \hat{T}_2 \quad (2.67)$$

And CCSD(T) is same as CCSD but consider some effect of triple excitation, but not entirely as CCSDT.

2-2 Adiabatic approximation for the motion of nuclei on single PES

Now the question is how to deal with the nuclei motion on the single adiabatic electronic PES. Adiabatic approximation is the general strategy for this kind of problem. But electronic transition, vibrational transition seems cannot be a good candidate for good adiabaticity. But in fact, reactive transitions occur in the rovibronal states in physical different regions, reactants and products and occur efficiently only in the region that two parts come closer. So using adiabatic separation for state to state dynamics problem seems reasonable. Still, the adiabaticity is not that good as electronic transition, that is, non-adiabatic transition still play an important rule inside the state to state dynamics. But the adiabaticity is good enough that the region of strong non-adiabatic coupling would be separated from each other, each of them can be seen freely from others. Because of the properties of localized region, the semi-classical method developed by Zhu and Nakamura^{3,4} could be used to deal with this case. The information needed is the E_n in equation (2.5) without solving the

non-adiabatic coupling by equation (2.6) and (2.7). Now The question is how to make sure the quality of adiabaticity, that is, how to choose a coordinate that improve the adiabaticity. Previously, Jacobi⁵ (non-adiabatic coupling did not die out in asymptotic region), hyper-spherical⁶ and hyper-spherical elliptic coordinates⁷ are being used. But there is no analytical form for more than 5 atoms, the work become tedious even for obtaining the adiabatic curves only. A general coordinate is needed for this semi-classical method, since the main issue is to obtain the adiabatic curves, and the following steps will be just like a service pattern. So how to choose this coordinate, in fact, it's min energy path (MEP), which has been developed thoroughly. How can min energy path be an appropriate slow variable will be explained in 2-2.1. Then, I would like to introduce how the semi-classical theory developed by Zhu and Nakamura^{3,4} can be applied to this coordinate in section 2-2.2.

2-2.1 Min energy path

In order to explain why MEP could be proper slow variable for adiabatic approximation, knowing the basics of MEP is necessary. Let's recall the fundamental concept for min energy path, there would be $3N-7$ mode with gradient equal to zero, orthogonal to the min energy path which may contains non zero gradient. So for the general point one could has

$$v(x) = v(a) + \frac{\partial v(a)}{\partial a} \cdot \zeta + \frac{1}{2} \zeta \cdot k \cdot \zeta \quad (2.68)$$

where x is arbitrary point; $x = \{x_{ir}\}$, a is a point on the reaction path; $a = \{a_{ir}\}$, $k =$

$\{k_{ir,i'r'}\}$ with

$$k_{ir,i'r'} = \frac{\partial^2 v}{\partial x_{ir} \partial x_{i'r'}} \quad (2.69)$$

, and ζ is the displacement vector. Here $i = 1, 2, 3, \dots, N$, $r = x, y, z$. For

displacement ζ that is orthogonal in the $3N$ dimensional vector space component of

the gradient part in the equation (2.68). In order to get the normal modes for vibration

that are orthogonal to the reaction path, it is also necessary for ζ to orthogonal to

the $3N$ space vector component of the rotation and translation for the complete

N -atom system. Since it's not the case of minimum or saddle point, it is necessary to

project out the infinitesimal rotation, translation and the unit vector along the reaction

path, otherwise there will contamination of rotation and translation during normal

analysis. So at each point, one define projected force constant matrix k^P for normal

analysis as

$$k^P = (1 - P) \cdot k \cdot (1 - P) \quad (2.70)$$

After doing normal analysis at harmonic approximation, one could expect there will

be $3N-7$ nonzero eigenvalues; which give frequencies orthogonal to the reaction path,

seven zero with six correspond to rotation and translation, one for reaction coordinate.

So this provides the following approximated potential surface,

$$v(s, Q_1, Q_2, Q_3, \dots, Q_{3N-7}) = v_0(s) + \sum_{k=1}^{k=3N-7} \frac{1}{2} w_k(s)^2 Q_k^2 \quad (2.71)$$

where s is reaction path, Q_k is the normal coordinate orthogonal to s and v_0 is the potential energy on the reaction path. The classical one-dimension motion Hamiltonian along reaction path for $3N-7 > 2$ has been reported as

$$H_n(p_s, s) = \frac{1}{2} p_s^2 A(s) + v_0(s) + \sum_{k=1}^{k=3N-7} \frac{1}{2} w_k(s) \left(n_k + \frac{1}{2} \right) \quad (2.72)$$

by Miller⁸, where $A(s)$ is the correction factor and p_s is the momentum along reaction coordinate. From equation (2.72), we can easily find that the first term is equal to the kinetic energy of slow variable in equation (2.2), the second and third term then correspond to adiabatic potential, which is the E_n in (2.5). This term (E_n) is only information needed for semi-classical theory. Up to now, I have not explained why reaction path could be the right coordinate to choose. Since the reaction coordinate separate reactant and product into two regions, there's no problem of non-adiabatic coupling between reactants and products in asymptotic region as Jacobi coordinate does. And the reactive transitions mostly occur around the saddle point (transition state). Besides that, the way of obtaining the adiabatic curves (E_n) is much more general than Jacobi, hyper-spherical and hyper-spherical elliptic coordinate, since the theory for normal mode analysis on reaction coordinate⁸ has been developed completely. E_n here is correspond to $J = 0$ adiabatic curves, since equation (2.72) only contains vibrational part, where J is the total angular momentum, which is conserved

during the reaction, so the information of chemical dynamics preserved in constant J , that is the dynamics won't be mixed between each J . But in order to obtain the total dynamics, the message of $J > 0$ is needed. The J -shift approximation^{11,12,13}, which relates the state to state reaction probability for arbitrary J and its body-fixed projection k to the one actually calculated for $J = 0$:

$$P_{i \rightarrow f}^{J,K}(E) \approx P_{i \rightarrow f}^{J=0}(E - E_{J,K}^*) \quad (2.73)$$

, will be used to gain case for $J > 0$, where $E_{J,K}^*$ is the rotational energy of transition state.

2-2.2 Semi-classical theory

As mentioned above, MEP divides the reactant and product into two different regions; no problem of non-adiabatic coupling in the asymptotic region, and reactive transitions mainly occur around saddle point (transition), so it make it possible to treat the chemical reaction in ordinary scattering problem. That is to say, we can apply the semi-classical theory of non-adiabatic transition developed by Zhu and Nakamura^{9,10}.

2-2.2.1 Zhu and Nakamura theory

The theoretical studies of non-adiabatic of transitions between potential energy curves should be date back to 1932, when Landau¹⁴, Zener¹⁵, and Stueckelberg¹⁶

published the pioneering paper independently. They have shown the non-adiabatic transition probability at curve crossing point between two curves :

$$P_{LZ} = \exp\left(-\frac{2\pi\Delta E^2}{\hbar v|F|}\right) \quad (2.74)$$

, so called famous Landau-Zener formula, where ΔE is the diabatic coupling:

$$\Delta E = \frac{W_2 - W_1}{2} \quad (2.75)$$

and F is the difference of the slopes of the two diabatic potential (V_1 and V_2) at R_x ,

which is the crossing point between V_1 and V_2 as shown in figure 2.1. But there are

five general defects for this formula, which are summarized¹⁷ as follows: (1) Not

work at energies near and lower than the crossing point. (2) No good formula exists

for transmission when the two diabatic curves cross with different signs of slopes. (3)

The available accurate formulas, which are valid only at energies higher than the

crossing point, contain inconvenient complex contour integrals and are not very useful

for experimentalists. (4) The Landau-Zener formula requires the knowledge of

diabatic potential, which can't be uniquely obtained from adiabatic potentials. (5) The

accurate phases to define the scattering matrixs are not available for all cases. In this

report, we would take advantages of point (2), (3) and (4), that is, we only consider

the transition point lower than total energy and no phase consideration. The main

purpose of this report is to check whether taking MEP as the slow variable is valid or

not.

2-3 Application to adiabatic curves on MEP

Since the properties of MEP, the adiabaticity holds in localized region. Then the most important non-adiabatic transition occur between two adjacent adiabatic curves.

(Non-adiabatic transition between non-adjacent may contribute a little, but not that important, which may be considered after obtaining the diabatic curves from adiabatic curves as ref 1 does. This won't be shown in this report.) So let us look at the easiest

case; two adiabatic curves, as Figure 2.2. The scattering wave function for asymptotic region can be written in WKB form:

$$\Psi_R(s) = \frac{A_n}{\sqrt{k_n(s)} \exp(i \int_{T_n^R}^s k_n(s) ds)} + \frac{B_n}{\sqrt{k_n(s)} \exp(-i \int_{T_n^R}^s k_n(s) ds)} \quad (s \rightarrow \infty) \quad (2.76)$$

$$\Psi_L(s) = \frac{C_n}{\sqrt{k_n(s)} \exp(i \int_{T_n^L}^s k_n(s) ds)} + \frac{D_n}{\sqrt{k_n(s)} \exp(-i \int_{T_n^L}^s k_n(s) ds)} \quad (s \rightarrow -\infty) \quad (2.77)$$

,where T_n^L and T_n^R are the same for transition point lower than the total energy considered, but left-side turning point and right-side turning point for tunneling case,

and

$$k_n(s) = \sqrt{2\mu(E - En(s))}. \quad (2.78)$$

The scattering matrix is defined by

$$\begin{pmatrix} A_1 \\ A_2 \\ D_1 \\ D_2 \end{pmatrix} = S \begin{pmatrix} B_1 \\ B_2 \\ C_1 \\ C_2 \end{pmatrix} = \begin{pmatrix} S_{11} & S_{21} & S_{31} & S_{41} \\ S_{12} & S_{22} & S_{32} & S_{42} \\ S_{13} & S_{23} & S_{33} & S_{43} \\ S_{14} & S_{24} & S_{34} & S_{44} \end{pmatrix} \begin{pmatrix} B_1 \\ B_2 \\ C_1 \\ C_2 \end{pmatrix} = \begin{pmatrix} S_{11} & S_{12} & S_{13} & S_{14} \\ S_{21} & S_{22} & S_{23} & S_{24} \\ S_{31} & S_{32} & S_{33} & S_{34} \\ S_{41} & S_{42} & S_{43} & S_{44} \end{pmatrix} \begin{pmatrix} B_1 \\ B_2 \\ C_1 \\ C_2 \end{pmatrix} \quad (2.79)$$

, where the outgoing coefficients (purple one in the figure 2.2) are represented by the incoming coefficients (black one in the figure 2.2), and $S_{ij}=S_{ji}$. It's not unexpected to obtain S matrix in the form of equation (2.79). Since the outgoing part is contributed by the outgoing part, that is to say, S_{ij} itself is related to the probability that outgoing coefficient formed from the incoming coefficient. In fact, it is in the form of square root of probability with phase; because it is the square of coefficient that gives the meaning of probability not coefficient itself. Take A_1 for example:

$$A_1 = S_{11}B_1 + S_{21}B_2 + S_{31}C_1 + S_{41}C_2 \quad (2.80)$$

, where S_{11} is related to the probability of the reflection of the incoming wave B_1 , S_{12} is the probability of the reflection of the incoming wave of B_2 which transmit to lower curve, S_{31} is the probability that C_1 stay at lower curve and S_{41} is the probability that C_2 stay at upper curve. In this model, there two kinds of S matrix:

1. Non-adiabatic transition between two curves, so called I matrix ; like point I_1 and point I_2 in figure 2.3:

$$\begin{pmatrix} A_1 \\ A_2 \\ D_1 \\ D_2 \end{pmatrix} = \begin{pmatrix} 0 & 0 & \sqrt{1-p_1}e^{ix_1} & \sqrt{p_1} \\ 0 & 0 & \sqrt{p_1} & -\sqrt{1-p_1}e^{-ix_1} \\ \sqrt{1-p_1}e^{ix_1} & \sqrt{p_1} & 0 & 0 \\ \sqrt{p_1} & -\sqrt{1-p_1}e^{-ix_1} & 0 & 0 \end{pmatrix} \begin{pmatrix} B_1 \\ B_2 \\ C_1 \\ C_2 \end{pmatrix}$$

$$\text{Or } \begin{pmatrix} A_1 \\ A_2 \\ D_1 \\ D_2 \end{pmatrix} = I_1 \begin{pmatrix} B_1 \\ B_2 \\ C_1 \\ C_2 \end{pmatrix} = \begin{pmatrix} 0 & T_1 \\ T_1 & 0 \end{pmatrix} \begin{pmatrix} B_1 \\ B_2 \\ C_1 \\ C_2 \end{pmatrix} \text{ with } T_1 = \begin{pmatrix} \sqrt{1-p_1}e^{ix_1} & \sqrt{p_1} \\ \sqrt{p_1} & -\sqrt{1-p_1}e^{-ix_1} \end{pmatrix}$$

for I_1 (2.81)

$$\begin{pmatrix} A'_1 \\ A'_2 \\ D'_1 \\ D'_2 \end{pmatrix} = \begin{pmatrix} 0 & 0 & \sqrt{1-p_2}e^{ix_2} & \sqrt{p_2} \\ 0 & 0 & \sqrt{p_2} & -\sqrt{1-p_2}e^{-ix_2} \\ \sqrt{1-p_2}e^{ix_2} & \sqrt{p_2} & 0 & 0 \\ \sqrt{p_2} & -\sqrt{1-p_2}e^{-ix_2} & 0 & 0 \end{pmatrix} \begin{pmatrix} B'_1 \\ B'_2 \\ C'_1 \\ C'_2 \end{pmatrix}$$

$$\text{Or } \begin{pmatrix} A'_1 \\ A'_2 \\ D'_1 \\ D'_2 \end{pmatrix} = I_2 \begin{pmatrix} B'_1 \\ B'_2 \\ C'_1 \\ C'_2 \end{pmatrix} = \begin{pmatrix} 0 & T_2 \\ T_2 & 0 \end{pmatrix} \begin{pmatrix} B'_1 \\ B'_2 \\ C'_1 \\ C'_2 \end{pmatrix} \text{ with } T_2 = \begin{pmatrix} \sqrt{1-p_2}e^{ix_2} & \sqrt{p_2} \\ \sqrt{p_2} & -\sqrt{1-p_2}e^{-ix_2} \end{pmatrix}$$

for I_2 (2.82)

, where p_1 and p_2 are the probability of the transition between lower curve and upper curve at position of I_1 and I_2

2. Tunneling; like the E_1 case in figure 2.3:

$$\begin{pmatrix} C_1 \\ C_2 \\ B'_1 \\ B'_2 \end{pmatrix} = \begin{pmatrix} e^{i\phi_{t1}}\sqrt{p_{t1}} & 0 & e^{i\phi_{t1}}e^{ix_{t1}}\sqrt{1-p_{t1}} & 0 \\ 0 & e^{i\phi_{t2}}\sqrt{p_{t2}} & 0 & e^{i\phi_{t2}}e^{ix_{t2}}\sqrt{1-p_{t2}} \\ -e^{i\phi_{t1}}e^{-ix_{t1}}\sqrt{1-p_{t1}} & 0 & e^{i\phi_{t1}}\sqrt{p_{t1}} & 0 \\ 0 & -e^{i\phi_{t2}}e^{-ix_{t2}}\sqrt{1-p_{t2}} & 0 & e^{i\phi_{t2}}\sqrt{p_{t2}} \end{pmatrix} \begin{pmatrix} A'_1 \\ A'_2 \\ D_1 \\ D_2 \end{pmatrix}$$

(2.83)

, where p_{t1} and p_{t2} represents the probability of transmittance at lower and upper curve for energy equals to E_1 . These two kinds shown above are only single S matrix. In order to obtain the final s matrix; which connects incoming and outgoing of the very beginning and end, one should know how to link the multiple s matrix. From figure 2.3, we could find that there are two types of linkage; one is that energy contains

all two curves (E_2 in fig. 2.3), another one is tunneling exist between two transition matrix (E_1 in fig. 2.3). It seems these two types are totally different, but in fact E_2 is just a special case of E_1 with the transmittance probability equal to 1. So the discussion of E_1 's case is enough. In order to do this, the transformation of the S matrix is necessary. Since we can't just multiple each single S matrix to obtain the last one, the transformed one could, which links . After obtaining the total matrix, we need convert it back to S matrix. The transformed one for transition and tunneling matrix would be:

1. Transition matrix:

$$\begin{pmatrix} C_1 \\ C_2 \\ D_1 \\ D_2 \end{pmatrix} = \begin{pmatrix} 0 & T_1^* \\ T_1 & 0 \end{pmatrix} \begin{pmatrix} B_1 \\ B_2 \\ A_1 \\ A_2 \end{pmatrix} = I_1' \begin{pmatrix} B_1 \\ B_2 \\ A_1 \\ A_2 \end{pmatrix} \quad (2.84)$$


, where I_1' is the modified matrix of I_1

$$\begin{pmatrix} C_1' \\ C_2' \\ D_1' \\ D_2' \end{pmatrix} = \begin{pmatrix} 0 & T_2^* \\ T_2 & 0 \end{pmatrix} \begin{pmatrix} B_1' \\ B_2' \\ A_1' \\ A_2' \end{pmatrix} = I_2' \begin{pmatrix} B_1' \\ B_2' \\ A_1' \\ A_2' \end{pmatrix} \quad (2.85)$$

, where I_2' is the modified matrix of I_2

2. Tunneling matrix

$$\begin{pmatrix} B_1' \\ B_2' \\ A_1' \\ A_2' \end{pmatrix} = \begin{pmatrix} -\sqrt{\frac{1-p_{t1}}{p_{t1}}}e^{ix_{r1}} & 0 & \frac{1}{\sqrt{p_{t1}}}e^{i\phi_{t1}} & 0 \\ 0 & -\sqrt{\frac{1-p_{t2}}{p_{t2}}}e^{ix_{r2}} & 0 & \frac{1}{\sqrt{p_{t2}}}e^{i\phi_{t2}} \\ \frac{1}{\sqrt{p_{t1}}}e^{-i\phi_{t1}} & 0 & -\sqrt{\frac{1-p_{t1}}{p_{t1}}}e^{-ix_{r1}} & 0 \\ 0 & \frac{1}{\sqrt{p_{t2}}}e^{-i\phi_{t2}} & 0 & -\sqrt{\frac{1-p_{t2}}{p_{t2}}}e^{-ix_{r2}} \end{pmatrix} \begin{pmatrix} C_1 \\ C_2 \\ D_1 \\ D_2 \end{pmatrix}$$

$$\text{or } \begin{pmatrix} B_1' \\ B_2' \\ A_1' \\ A_2' \end{pmatrix} = \begin{pmatrix} r & t \\ t^* & r^* \end{pmatrix} \begin{pmatrix} C_1 \\ C_2 \\ D_1 \\ D_2 \end{pmatrix} = P \begin{pmatrix} C_1 \\ C_2 \\ D_1 \\ D_2 \end{pmatrix} \quad \text{with}$$

$$r = \begin{pmatrix} -\sqrt{\frac{1-p_{t1}}{p_{t1}}}e^{-ix_{t1}} & 0 \\ 0 & -\sqrt{\frac{1-p_{t2}}{p_{t2}}}e^{-ix_{t2}} \end{pmatrix} \quad \text{and } t = \begin{pmatrix} \frac{1}{\sqrt{p_{t1}}}e^{i\phi_{t1}} & 0 \\ 0 & \frac{1}{\sqrt{p_{t2}}}e^{i\phi_{t2}} \end{pmatrix} \quad (2.86)$$

So the total matrix would be manipulated as bellow for E₁ case:

$$\begin{pmatrix} C_1' \\ C_2' \\ D_1' \\ D_2' \end{pmatrix} = \begin{pmatrix} 0 & T_2^* \\ T_2 & 0 \end{pmatrix} \begin{pmatrix} B_1' \\ B_2' \\ A_1' \\ A_2' \end{pmatrix} = \begin{pmatrix} 0 & T_2^* \\ T_2 & 0 \end{pmatrix} \begin{pmatrix} r & t \\ t^* & r^* \end{pmatrix} \begin{pmatrix} C_1 \\ C_2 \\ D_1 \\ D_2 \end{pmatrix} = \begin{pmatrix} 0 & T_2^* \\ T_2 & 0 \end{pmatrix} \begin{pmatrix} r & t \\ t^* & r^* \end{pmatrix} \begin{pmatrix} 0 & T_1^* \\ T_1 & 0 \end{pmatrix} \begin{pmatrix} B_1 \\ B_2 \\ A_1 \\ A_2 \end{pmatrix}$$

$$= \begin{pmatrix} T_2^* t^* T_1 & T_2^* p^* T_1^* \\ T_2 p T_1 & T_2 t T_1^* \end{pmatrix} \begin{pmatrix} B_1 \\ B_2 \\ A_1 \\ A_2 \end{pmatrix} = I_1 P I_2 \begin{pmatrix} B_1 \\ B_2 \\ A_1 \\ A_2 \end{pmatrix} = \begin{pmatrix} M_1^T & M_2^T \\ M_3^T & M_4^T \end{pmatrix} \begin{pmatrix} B_1 \\ B_2 \\ A_1 \\ A_2 \end{pmatrix} \quad (2.87)$$

The P matrix in equation (2.26) should always exist between two I matrix, since p is not unit matrix even for the case of total transmittance. The result of equation (2.87) could be applied to multiple s matrices, and you can obtain following form for modified total matrix F:

$$F = I'_n(s_{2n-1})P_{n-1}(s_{2n-2})I'_{n-1}(s_{2n-3})P_{n-1}(s_{2n-4})\cdots p_1(s_2)I'_1(s_1) = \begin{pmatrix} M_1^T & M_2^T \\ M_3^T & M_4^T \end{pmatrix}$$

with $s_1 < s_2 < s_3 < s_4 \cdots < s_{2n-1}$. (2.88)

, where s_i is the position on the reaction path. In fact Equation (2.88) is also the general result for multiple curves, but with (2.87) in the form of

$$\begin{pmatrix} C'_1 \\ \vdots \\ C'_i \\ D'_1 \\ \vdots \\ D'_i \end{pmatrix} = F \begin{pmatrix} B_1 \\ \vdots \\ B_i \\ A_1 \\ \vdots \\ A_i \end{pmatrix} = \begin{pmatrix} M_1^T & M_2^T \\ M_3^T & M_4^T \end{pmatrix} \begin{pmatrix} B_1 \\ \vdots \\ B_i \\ A_1 \\ \vdots \\ A_i \end{pmatrix} \quad (2.89)$$

, where i is the number of adiabatic curves. For multiple curves, the $T_j(s_j)$ in $I_j(s_j)$ matrix will be denoted as

$$\begin{pmatrix} \sqrt{1-p_1(s_j)}e^{ix_1(s_j)} & \sqrt{p_1(s_j)} & & 0 \\ \sqrt{p_1(s_j)} & -\sqrt{1-p_1(s_j)}e^{-ix_1(s_j)} & & \\ & \vdots & & \\ & & \ddots & \\ & & & \sqrt{1-p_n(s_j)}e^{ix_n(s_j)} & \sqrt{p_n(s_j)} \\ 0 & & & \sqrt{p_n(s_j)} & -\sqrt{1-p_n(s_j)}e^{-ix_n(s_j)} \end{pmatrix} \quad (2.90)$$

, where $p_n(s_j)$ is the transition probability between curve n and $n+1$ at position s_j (p_n would be equal to zero for those curves not involve in the transition point) and $n+1 < i$'s curves. Here, n is the number of n th curves, not the notation of right side or left side for the adiabatic curves. And the $r_j(s_j)$ and $t_j(s_j)$ in $P_j(s_j)$ would be

$$r_j(s_j) = \begin{pmatrix} -\sqrt{\frac{1-p_{11}(s_j)}{p_{11}(s_j)}} e^{-ix_1(s_j)} & & 0 \\ & \ddots & \\ 0 & & -\sqrt{\frac{1-p_{ii}(s_j)}{p_{ii}(s_j)}} e^{-ix_n(s_j)} \end{pmatrix} \quad (2.91)$$

$$p_j(s_j) = \begin{pmatrix} \frac{1}{\sqrt{p_{11}(s_j)}} e^{i\phi_1(s_j)} & & 0 \\ & \ddots & \\ 0 & & \frac{1}{\sqrt{p_{ii}(s_j)}} e^{i\phi_i(s_j)} \end{pmatrix} \quad (2.92)$$

, where $p_{in}(s_j)$ is the probability of transmittance in n th adiabatic, and $n \leq i$; the total number of adiabatic curves. Now we know the general form for modified total matrix in equation (2.89). Then we need to convert the transformed total matrix into S matrix.

A general step is shown below:

First,

$$\begin{pmatrix} C'_1 \\ \vdots \\ C'_n \end{pmatrix} = M_1^T \begin{pmatrix} B_1 \\ \vdots \\ B_n \end{pmatrix} + M_2^T \begin{pmatrix} A_1 \\ \vdots \\ A_n \end{pmatrix} \quad (2.93)$$

$$\begin{pmatrix} D'_1 \\ \vdots \\ D'_n \end{pmatrix} = M_3^T \begin{pmatrix} B_1 \\ \vdots \\ B_n \end{pmatrix} + M_4^T \begin{pmatrix} A_1 \\ \vdots \\ A_n \end{pmatrix} \quad (2.94)$$

Then, from equation (2.93) we can obtain

$$\begin{pmatrix} A_1 \\ \vdots \\ A_n \end{pmatrix} = (M_2^T)^{-1} \begin{pmatrix} C'_1 \\ \vdots \\ C'_n \end{pmatrix} - (M_2^T)^{-1} M_1^T \begin{pmatrix} B_1 \\ \vdots \\ B_n \end{pmatrix} \quad (2.95)$$

Finally take (2.94) into (2.93), we get

$$\begin{pmatrix} D'_1 \\ \vdots \\ D'_n \end{pmatrix} = \left[M_3^T - M_4^T (M_2^T)^{-1} M_1^T \right] \begin{pmatrix} B_1 \\ \vdots \\ B_n \end{pmatrix} + M_4^T (M_2^T)^{-1} \begin{pmatrix} C'_1 \\ \vdots \\ C'_n \end{pmatrix} \quad (2.96)$$

Thus we gain the representation for total S matrix:

$$\begin{pmatrix} A_n \\ \vdots \\ A_n \\ D'_1 \\ \vdots \\ D'_n \end{pmatrix} = \begin{pmatrix} -(M_2^T)^{-1} M_1^T & (M_2^T)^{-1} \\ M_3^T - M_4^T (M_2^T)^{-1} M_1^T & M_4^T (M_2^T)^{-1} \end{pmatrix} \begin{pmatrix} B_1 \\ \vdots \\ B_n \\ C'_1 \\ \vdots \\ C'_n \end{pmatrix} = S \begin{pmatrix} B_1 \\ \vdots \\ B_n \\ C'_1 \\ \vdots \\ C'_n \end{pmatrix} \quad (2.97)$$

No matter how many tunneling(barriers) exist in the dynamics, the process from equation (2.93) to (2.97) is general, which could be easily solved numerically. There four parts in S matrix, each has its correspond physical meanings:

1. **Upper left part:** relate to the probability for the waves from right side curves to go back.
2. **Upper right part:** relate to the probability for the waves from right side curves to go to left side curves.
3. **Lower left part:** relate to the probability for the waves from left side curves to go to right side curves
4. **Lower right part:** relate to the probability for the waves from left side curves to go to left side curves

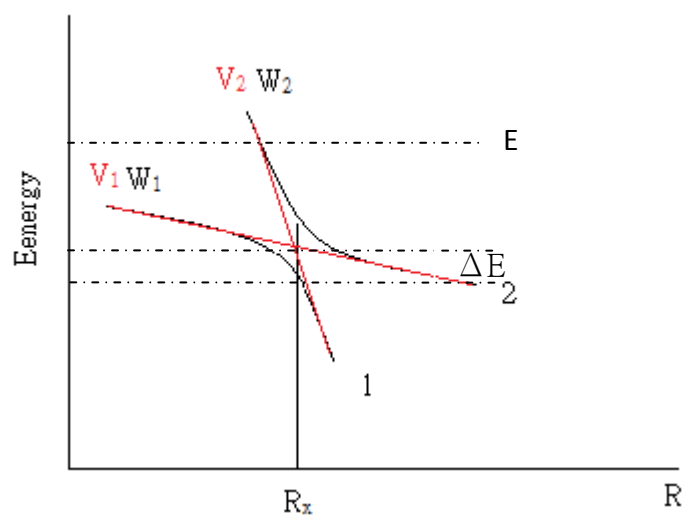
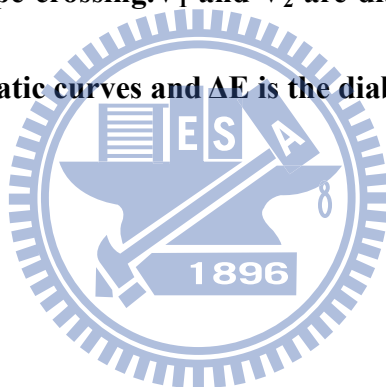


Figure 2.1 Schematic potential energy curves in the Landau-Zener type crossing. V_1 and V_2 are diabatic curves, W_1 and W_2 are adiabatic curves and ΔE is the diabatic coupling.



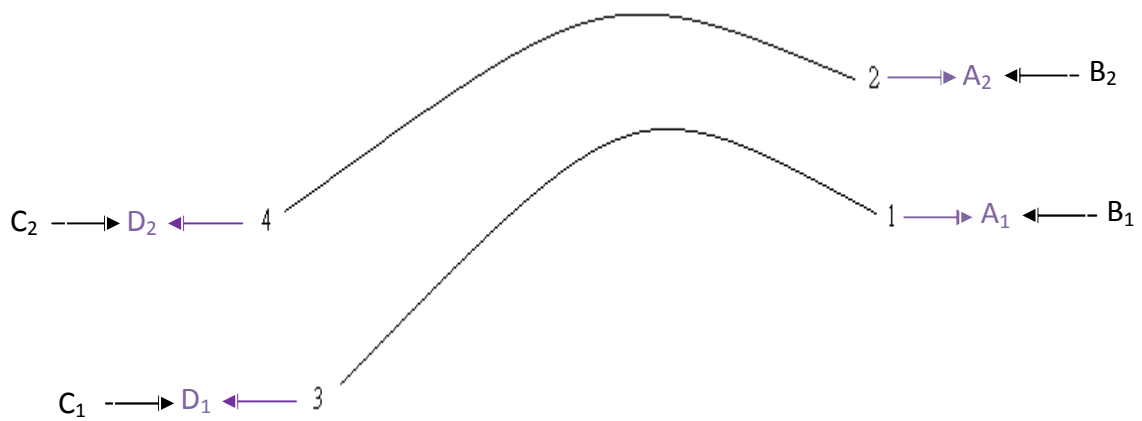


Figure 2.2 Schema of general case for two adiabatic curves on MEP coordinate. A_n and B_n are the coefficients of scattering wave function for asymptotic region ($s \rightarrow +\text{infinity}$) in WKB form as equation (2.76). C_n and D_n are the coefficients of scattering wave function for asymptotic region ($s \rightarrow -\text{infinity}$) in WKB form as equation (2.77).

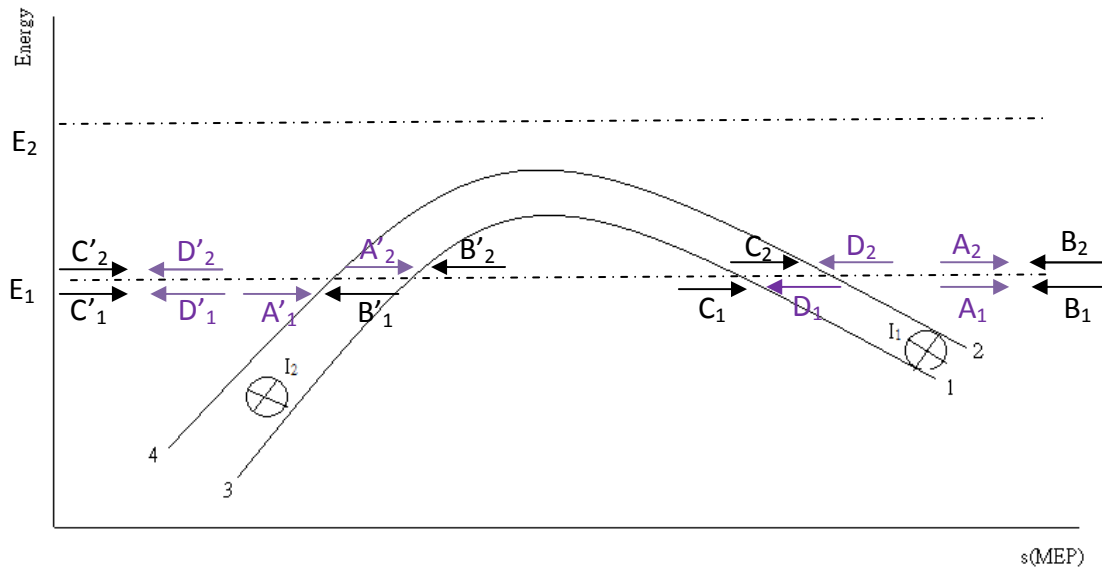
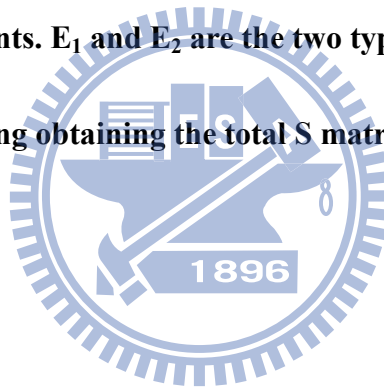


Figure 2.3 Schema of two adiabatic curves on MEP. I_1 and I_2 are the transition points. E_1 and E_2 are the two types of energy will be encountered during obtaining the total S matrix.



References:

1. C. Zhu, H. Nakamura and K. Nobusada, PCCP , **2**, 557 (2000)
2. J. C. Tully, Nonadiabatic processes in molecular collisions, in Dynamics of Molecular Collisions, edited by W. H. Miller, pages 217{267. Plenum, New York, 1976.2. H, Nakamura, Annu, Rev. phys. Chem. **48**, 293 (1997)
3. H, Nakamura, Annu, Rev. phys. Chem. **48**, 293 (1997)
4. H, Nakamura and C. Zhu, Comments At. Mol. Phys. **32**, 249 (1996)
5. C. Kubach, Chem. Phys. Lett. **164**, 475 (1997)
6. A. Kupperman and P. G. Hipes, J. Chem. Phys. **84**, 5962 (1986)
7. Oleg I. Tolstikhin and H. Nakamura, J. Chem. Phys. **108**, 21 (1998)
8. William H. Miller, Nicholas C. Handy and John E. Adams J. Chem. Phys. **72**, 1 (1980)
9. (a) C. Zhu and H. Nakamura, J. Chem. Phys. **102**, 7448 (1995); (b)C. Zhu and H. Nakamura, J. Chem. Phys. **106**, 2599 (1997) (c) C. Zhu and H. Nakamura, Chem. Phys. Lett. **258**, 342 (1996); (d)C. Zhu and H. Nakamura, J. Chem. Phys. **109**, 4689 (1998)
10. (a) C. Zhu and H. Nakamura, J. Chem. Phys. **101**, 10630 (1994); (b) C. Zhu and H. Nakamura. **107**, 7839 (1997); (c) C. Zhu and H. Nakamura, Chem. Phys. Lett. **274**, 205 (1997); (d) C. Zhu and H. Nakamura, J. Chem. Phys. **108**, 7501 (1998)
11. Bowman JM. J. Phys. Chem. **95**, 4960 (1991)
12. See ref. 5 in chapter 1
13. Sun Q, Bowman JM, Schatz GC, Sharp JR, Connor JNL. J. Chem. Phys. **92**, 1677 (1990)
14. L. D. Landau. Phys. Zts. Sov. **2**, 46 (1932)
15. C. Zener. Proc. Roy. Soc. **A137**, 696 (1932)
16. E. C. G. Stueckelberg. Hel. Phys. Acta. **5**, 369 (1932)
17. H. Nakamura. Nonadiabatic transition; concepts, basic theories and applications

Chapter 3 Results and Discussions

3-1 Theoretical results for $\text{OH}+\text{H}_2 \rightarrow \text{H}+\text{H}_2\text{O}$ reaction

3-1.1 Theoretical calculation for MEP

There are several theoretical groups devoted on the research of $\text{OH}+\text{H}_2 \rightarrow \text{H}+\text{H}_2\text{O}$ reaction; Smith and Zenner¹ use two different semi-empirical potential energy surface; LEPS and BEBO and they neglect tunneling with barrier same as experiment activation energy, Schatz used large scale POL-CI³ wave function with basis 3s3p1d/3s1p and 4s3p2d/3s2p and Truong⁴ used the PMP4/6-311++G(2d f,2pd)//QCISD/6-311+G(d,p) method. And in this report, Gaussian 09 is used to calculate the reaction path with CCSD/aug-cc-pvdz, CCSD(T)/ aug-cc-pvdz//CCSD/ aug-cc-pvdz and CCSD(T)/aug-cc-pvtz//CCSD/aug-cc-pvdz. All the results are shown in table 3.1. From table 3.1, we could see that the energy correction by CCSD(T) is necessary, which match pretty well with Schatz's larger basis and Truong, no matter aug-cc-pvdz or aug-cc-pvtz, but seems shown difference with Zener and the activation energy (E_a) at 300K, which Zener took the activation energy as barrier height in the semi-empirical potential energy surface. It could be contributed to the tunneling effect and temperature effect. Schatz⁴ and Truong⁵ have calculated the rate constant with the effect of tunneling, then they get pretty good results with experiments, that is to say, the results of CCSD(T) energy correction is ok. And the comparison for MEP of my work between before and after energy correction by CCSD(T) shown in figure 3.1 indicates that the saddle point does not change to much compared to the one without energy correction and almost no difference between the two different basis in energy correction, CCSD(T)/aug-cc-pvdz//CCSD/aug-cc-pvdz and CCSD(T)/aug-cc-pvtz//

CCSD /aug-cc-pvdz. So we use the MEP calculated by CCSD(T)/ aug-cc-pvdz // CCSD aug-cc-pvdz.

3-1.2 Geometry of transition state

Figure 3.2 displays the geometries of transition state with CCSD/aug-cc-pvdz method, which predicted that the O-H length of HOH'H'' is 0.976 Å, which almost same as the length of OH radical. This result match the concept that several studies bring out, which OH can be seen as a spectator group during the reaction. The geometry is almost same as Schatz² and Truong⁴'s result, but different from Zenner¹, which is no longer planar.

3-1.3 Normal modes along reaction path

Table 3.2 presents the frequencies along reaction path calculated by G09 with CCSD/aug-cc-pvdz. In general, there should be 7 zero or very small frequencies and $3N-7$ non-zero frequencies, here is 5. From table 3.2, you could see that it's not the case. For points near transition state ($s = 0$) are still ok, but points away from $s = 0$ show strong defects. Since there are two general problems exist in the G09 calculation for points on reaction coordinate:

1. Linear transformation of Cartesian coordinate to internal coordinate:

For non local maximum or minimum point, the transformation will be no longer linear, since the first order gradient will also contribute to it like Truhlar metioned⁶.

Bellow is the energy based on Cartesian (equation (3.1)) and internal coordinates (equation (3.2))

$$V = V_0 + \sum_i^{3N} G_i \Delta R_i + \frac{1}{2} \sum_{i,j}^{3N} F_{ij} \Delta R_i \Delta R_j + \dots \quad (3.1)$$

And

$$V = V_0 + \sum_i^{3N} g_i \Delta q_i + \frac{1}{2} \sum_{i,j}^{3N} f_{ij} \Delta q_i \Delta q_j + \dots \quad (3.2)$$

,in which ΔR_i and Δq_i are, respectively, the Cartesian and internal coordinate.

The internal coordinate can be expressed in terms of power series of the Cartesian coordinate as bellow:

$$\Delta q_i = \sum_j^{3N} B_{ij} \Delta R_j + \frac{1}{2} \sum_{j,k}^{3N} C_{jk}^i \Delta R_j \Delta R_k + \dots \quad (3.3)$$

From equation (3.1) to (3.3) yields the expressions for Cartesian gradient and force const matrix in terms of their internal coordinate counterpart as

$$G = B^T g \quad (3.4)$$

and

$$F = B^T fB + \sum_i^F g_i C^{[i]} \quad (3.5)$$

In above equation, it could be seen easily that it's not linear transformation, which is the only first term of equation (3.5)

2. The process of projecting out the unit component along reaction path, rotation and translation is not conducted.

Because of problem 1, we choose to use Molpro to calculate the frequencies by the same method and basis, CCSD/aug-cc-pvdz, with the geometries from G09. Since Molpro directly diagonalize the transformation matrix in Cartesian coordinate without changing to internal coordinate. The results of Molpro are indicated in table 3.3. It seems better but there is still some defects in it, because of problem 2 mentioned above. This program for this is not that easy to construct. In order to find the $3N-7$ nonzero frequencies, we've done the following steps:

1. Transform the first order gradient in Cartesian coordinate from Molpro to normal

mode coordinate with the transformation matrix from Molpro

2. Do mode-scanning for each coordinate with the transformation matrix obtained in Molpro for each mode at each point on reaction path.

From the gradient, reduced mass and the mode scan in normal mode, we could distinguish which is frequency of reaction path (gradient max one), rotation and translation. Then we obtained the organized frequencies in table 3.4 and. Figure 3.3. Those frequencies belong to the modes of reactants (OH, H₂) and products (H₂O); W₃~W₄ in table 3.4, are reasonable. But W₁ and W₂ have unphysical imaginary frequencies during the reaction path. It's due to the problem 2 mentioned above. The contamination of reaction coordinate, rotation and translation is stronger for smaller frequencies (those contribute to the rotation of reactants and products, that is, W₁ and W₂). But the program for dealing problem 2 is no easy to write. Even if we have done this, there will be still a big problem, which is shown by Truhlar⁶. You still may get unphysical imaginary frequencies not until you use curvilinear internal coordinate. This is even harder than dealing with problem 2, since it's a non linear process. So we modified the W₁ and W₂ by following the trends of frequencies around $s = 0$ and goes to frequencies of rotation in the asymptotic region (Originally, it should be zero, but we know it's contributed by the rotation in the asymptotic region, which won't be defined as frequency). Then, we fit the curves in the reaction region ($s > 0$) and product region ($s < 0$). This process is shown in figure 3.4. (Only show W₁ and W₂, since W₃~W₄ don't need to modification.) The fitting process will also be done for W₃, W₄, W₅ and MEP. The fitting result for W₁, W₂ and W₃ of OH+H₂ part (all change to rotation at asymptotic region) is shown as bellow:

W₁:

OH+H₂ part (The rotation of OH, $s > 0$) :

$$\tilde{E}(cm^{-1}) = 18.601 + 204.63869 \cdot 3 \cdot \exp(-s / 0.56019) \quad (3.6)$$

, where $18.601cm^{-1}$ is the rotation constant B of OH in asymptotic region.

H+H₂O part (The total rotational J of H₂O, here we approximate it as prolate with $I'_c=I'_b=1/2(I_c+I_b)$ and $I'_a=I_a$, where I' is the modified one and I is the real one):

$$\tilde{E}(cm^{-1}) = 11.92 + 674.23928 \cdot \exp(-0.5 \cdot [(s + 0.24983) / 0.48136]^2) \quad (3.7)$$

, where $11.92cm^{-1}$ is the rotation constant B' of H₂O in asymptotic region.

W₂:

OH+H₂ part (H₂ rotate around OH, $s > 0$):

$$\tilde{E}(cm^{-1}) = 200.5297 \cdot 3 \cdot \exp(-s / 0.51682) \quad (3.8)$$

, where $0cm^{-1}$ is the rotation constant B' of OH/H₂ in asymptotic region.

H+H₂O part (The k component of H₂O):

$$\tilde{E}(cm^{-1}) = 14.875 + 637.32359 \cdot \exp(-0.5 \cdot [(s + 0.08221) / 0.54214]^2) \quad (3.9)$$

, where $14.875cm^{-1}$ is the rotation constant A' of H₂O in asymptotic region.

W₃:

OH+H₂ part (The rotation of H₂, $s > 0$):

$$\tilde{E}(cm^{-1}) = 57.66 + 908.2709 \cdot \exp(-s / 1.22003) + 93.92793 \cdot \exp(-s / 0.1746) \quad (3.10)$$

, where $57.66cm^{-1}$ is the rotation constant B of H₂ in asymptotic region.

We fit these frequencies directly to certain rotation, which in fact is not the case. Since the motion of those rotations in asymptotic region are mixed together in the complex HOHH. In reality, it's not a big problem for two reasons: (1) The couplings between these rotations could be considered during the process of non-adiabatic transition. (2) We could take the rotation as an average field, that is, we only need to know this rotation belong to which vibration without knowing what kind of rotation it is, which is more general for large system. So from the result we can gain the fitted frequencies

along the reaction path as table 3.5 and figure 3.5

3-2. Construct the adiabatic curves of $J = 0$ on MEP

By the fitted frequencies along the MEP, we could construct the adiabatic curves of $J = 0$ on it with second and third term in the right side of the equation (2.9). But there are some modifications, which is necessary. Those frequencies that become rotation in the asymptotic region don't always preserved the form of $E_{ni} = w_i(n_i+1/2)$. It evolves into the form of rotation in regions that are away from transition state. Besides that, for W_2 of OH+H₂, the rotational quantum number itself is restricted to the rotational quantum numbers of OH and H₂ rotation, and for W_1 of H+H₂O, it's restricted by rotational total J of H₂O. The restriction seems unreasonable, but in fact ok as the two points I mentioned above. So the modification will be done as bellow:

$$E_J = a(s) \cdot J \cdot w + (1 - a(s)) \cdot (J^2 + J) \cdot w = n \cdot w - a(s) \cdot J^2 \cdot w \quad (3.11)$$

Or

$$E_K = a(s) \cdot K \cdot w + (1 - a(s)) \cdot (K^2) \cdot w \quad (3.12)$$

, in which J is the rotational total quantum number and K is the quantum number of z component of J in molecular axis. $a(s)$ is percentage for the portion of vibration and $(1-a(s))$ then is the portion of rotation. ZPE is directly considered with MEP, so no $1/2$ for vibration in equation (3.11) and (3.12). The way of how to obtain $a(s)$ is pretty easy, just follow the trends of how frequencies drop in equation (3.6)~(3.10). Take W_1 for example, you could get $a(s)$ for :

W_1 of OH+H₂:

$$a(s) = \exp(-s/0.56019) \quad (3.13)$$

W_1 of H+H₂O:

$$a(s) = \exp(-0.5 \cdot [(s + 0.24983) / 0.48136]^2) \quad (3.14)$$

So E_n for adiabatic curves would be:

OH+H₂ side :

$$E = [J_1 - a_1(s) \cdot J_1^2] \cdot W_1 + [J_2 - a_2(s) \cdot J_2^2] \cdot W_2 + [J_3 - a_3(s) \cdot J_3^2] \cdot W_3 + n_4 \cdot W_4 + n_5 \cdot W_5 \quad (3.15)$$

, in which $J_2 = J_1+J_3, J_1+J_3-1, J_1+J_3-2, \dots, |J_1-J_3|$, in order to make the total angular momentum equals to zero.

H+H₂O side :

$$E = [K_1 + (1 - a_1(s)) \cdot K_1^2] \cdot W_1 + [J_2 - a_2(s) \cdot J_2^2] \cdot W_2 + n_3 \cdot W_3 + n_4 \cdot W_4 + n_5 \cdot W_5 \quad (3.16)$$

, in which $J_2 = 0, 1, 2, \dots, J_1$, since it's the z component of J_2 (we didn't consider $J_2 < 0$). Thus from (3.15) and (3.16) we can gain the adiabatic curves as figure 3.6

3-3. Cumulative reaction probability

3-3.1 Cumulative reaction probability for OH+H₂→HCl+H₂O

Before talking about the state to state dynamics, we would like to show the cumulative reaction probability first. Cumulative reaction probability is the property that indicates how much reactants become products at certain total energy, which could be shown as below:

$$N(E)(J) = \sum_i \sum_f p_{i \rightarrow f}(E)(J) \quad (3.17)$$

$$N(E) = \sum_J N(E)(J) \quad (3.18)$$

, in which $N(E)(J)$ is cumulative reaction probability at total energy E , $p_{i \rightarrow f}(J)$ stands

for the reaction probability from certain state i of reactants to certain state f of products and both of them are the results of total angular momentum equals to J . From equation (3.18), it is easy to understand that $N(E)$ is macroscopic properties, which means that the result of $N(E)$ decides whether the potential energy curves we use is right or not, since it's a total effect, that is, it's easier to achieve than $p_{i \rightarrow f}(J)$, which is a microscopic property. Here, we only show the result of $N(E)(J=0)$, since other $N(E)(J)$ could be obtain by J shift approximation, that is, we only need to make sure $N(E)(J=0)$ is correct. Below we would like to display several results of $N(E)(J=0)$ from different types of model :

Type I :

We only consider the energy levels at the two sides of adiabatic curves, $s=-2.5\text{bohr}$ and $s=2.0\text{bohr}$ with the cumulative reaction probability as bellow

$$N(E)(J = 0) = \frac{N_r \cdot N_f}{N_r + N_f} \quad (3.19)$$

, where N_r , N_f are, respectively, the number of states available at E for $s=2.5\text{bohr}$ and $s=2.0\text{bohr}$. This $N(E)(J=0)$ is the result of barrierless and every states are equal partition if the states are available at that E . We do the same thing for reactants and products, where N_r , N_f would then, respectively, be the number of states available at E for reactants and products. Then we obtain the result as figure 3.7. The outcome is larger than Miller's result⁷, which is reasonable, since no barrier in this case. Th $S=-2.5\text{bohr}/s=2.0\text{bohr}$, these two positions are pretty close to the asymptotic region, and from figure 3.7, we could find that it goes well with the trend of reactant and product. That is, the linkage between the two sides of the energy curves and asymptotic region is pretty good.

Type II :

We consider the entire curves as shown in figure 3.6, but we didn't evaluate the total S matrix as equations (2.26) to (2.35) in reality. We only consider the effect of tunneling of each curve. Because of the macroscopic properties of cumulative reaction probability, it is easy to assume that the $N(E)$ is contributed mainly by the tunneling property of each adiabatic curve not by the non-adiabatic transition between them, which is a microscopic property that would easily vanish in the macroscopic properties. The strategy we applied is pretty easy, if there is only one barrier in each adiabatic curve, we just evaluate the tunneling probability of each curves and then do summation. But if any curve inside the adiabatic curves has more than one barrier, evaluating the S matrix becomes necessary. Since OH+H₂ side, reactant side, is higher than H₂O+H side in each adiabatic curve, that is, the possibilities of tunneling would be decided only by the energy levels of OH+H₂ in the asymptotic region. From figure 3.8 which indicated the adiabatic curves that connects the energy levels of reactants lower than 15kcal/mol. It is obvious that the assumption of one barrier is sufficient, even if there is some pretty small well in higher levels, which won't give big effect. The transmittance probability is evaluated as bellow:

$$\delta = \frac{1}{\hbar} \int_{T_1}^{T_2} \sqrt{2\mu|E - V(s)|} ds \quad (3.20)$$

,where T_1 and T_2 are the turning points in each adiabatic curve. If the adiabatic curves are in parabolic shape, then the transmittance probability are in the form as equation (3.21) and (3.22):

$$P_{transmit\ tan\ ce} = \frac{e^{-2\delta}}{1 + e^{-2\delta}} \quad for\ E_{total} > E_{max} \quad (3.21)$$

$$P_{transmit\ tan\ ce} = \frac{e^{2\delta}}{1 + e^{2\delta}} \quad for\ E_{total} < E_{max} \quad (3.22)$$

, in which E_{total} is the total energy and E_{max} is the max energy in each adiabatic

curve. In type II, we obtain the result as figure 3.9. The deviation from Miller's result⁷ is not small. There are three possible reasons:

1. The linkage between reactants and products is not appropriate, since there two rotational related vibratioanl modes in product side, but three for reactant side. Possible solution would be the way of dealing with the mode, which shows vibrational behavior in one side but rotational behavior in other side. We should consider the evolution of this kind of mode from reactant to product, not just take one side as vibration and the evolution only in another side. Besides, the way of dealing with the evolution from vibration to rotation should be modified also, and this would be done in the future.
2. The non-adiabatic transition may cause some effect to the cumulative reaction probability.
3. The accuracy of the frequencies along the reaction coordinate would influence the density of states. For those big frequencies, the defects may be small ,but not the case for those small frequencies, especially those rotational related modes in the asymptotic regions.

Type III:

Since the adiabatic curves are not appropriate yet, in order to obtain the cumulative reaction probability, we've done following three assumptions:

1. The shape of upper levels is same as the ground state, and take all of curves as parabolic model
2. Take the energy level of transition state as the max energy, E_{max} , of each adiabatic curve.
3. From assumption 1 and 2, we could make a subroutine of δ vs ΔE for ground energy curve, where ΔE is the difference between E_{total} and E_{max} .

Then take this subroutine as the reference for upper energy levels. So for each adiabatic curves we only need to know two things, one is $E_{total} > E_{max}$ or $E_{total} < E_{max}$, another is difference between E_{max} and E_{total} . Then from the subroutine, we could get its correspond $\delta(\delta)$. For $E_{total} > E_{max}$, equation (3.21) is applied to get $P_{transmittance}$. For $E_{total} < E_{max}$, equation (3.22) is applied to get $P_{transmittance}$.

We call this model as adiabatic model. The energy diagram of this model is shown in figure 3.10. The δ (δ) vs δE for ground energy curve is displayed in figure 3.11 and the fitted δ (δ) vs δE is shown in equation (3.23):

$$\delta = -5.66455 \cdot 10^{-4} + 1.07919 \cdot \delta E + 7.40337 \cdot 10^{-4} \cdot \delta E^2 + 0.01189 \cdot \delta E^3 - 8.93079 \cdot 10^{-5} \cdot \delta E^4 \quad (3.23)$$

The cumulative reaction probability of $J = 0$ is in figure 3.12. We could found that it's much closer to Miller's result⁷ than type I, but still has not small difference. There would three possible reasons:

1. From figure 3.10, it is easy to see that the energy density of reactant side is larger than transition state, that is, the δ would be smaller than ground energy curve at the same δE for the upper curves, as the parabolic model still holds. So we've done some modification for upper curves as bellow:

$$\delta' = \delta \times \sqrt{1 + \frac{\Delta v}{v_0}} \quad \text{for } E_{total} > E_{max} \quad (3.24)$$

$$\delta' = \frac{\delta}{\sqrt{1 + \frac{\Delta v}{v_0}}} \quad \text{for } E_{total} < E_{max} \quad (3.25)$$

, where v_0 stands for the maximum of ground energy curve, E_{max} is the maximum

of adiabatic curve considered and Δv equals to $E_{\max} - v_0$. The result of this modification is shown in figure 3.13. No big difference between before and after modifications. But after directly multiple adiabatic models result by a factor 3.6 or the modification order change from 0.5 to 2.95 as bellow:

$$\delta' = \delta \times \left(1 + \frac{\Delta v}{v_0}\right)^{2.95} \quad \text{for } E_{total} > E_{\max} \quad (3.26)$$

$$\delta' = \frac{\delta}{\left(1 + \frac{\Delta v}{v_0}\right)^{2.95}} \quad \text{for } E_{total} < E_{\max} \quad (3.27)$$

we found that the result match Miller's result⁷ better. These are displayed in figure 3.14. The possible explanations would be the parabolic model is not appropriate or the density of state in transition state is not correct which would be explained in reason 3. We fit the ground energy curve in polynomial equation, and obtained the equation (3.28)

$$E(kcal/mol) = 5.48581 + 9.75594 \cdot s - 17.62052 \cdot s^2 - 6.5155 \cdot s^3 + 11.56263 \cdot s^4 + 3.61526 \cdot s^5 - 3.31808 \cdot s^6 - 1.04517 \cdot s^7 + 0.33778 \cdot s^8 + 0.11207 \cdot s^9 \quad (3.28)$$

From equation (3.28), we could find that s^2 is not the only dominated term, that is, parabolic model no longer good, but whether this is the main reason, it is still in request.

2. Non-adiabatic transition between each adiabatic curve may cause some effects, which would be shown in type IV.
3. The accuracy of the frequencies along the reaction coordinate would influence the density of states. For those big frequencies, the defects may be small, but not the

case for those small frequencies, especially those rotational related modes in the asymptotic regions.

Type IV:

In order to consider the influence of non-adiabatic transition, we use diabatic model to evaluate the energy curves for the transition state. In diabatic model, all modes in transition state preserve the properties of the motion in reactants. Since diabatic model keep all the properties from reactant to transition state, that is, the non-adiabatic coupling is considered entirely in each curves. So the five vibrational frequencies 546.6cm^{-1} , 609.94cm^{-1} , 1059.12cm^{-1} , 2479.16cm^{-1} and 3736.43cm^{-1} in transition state would be changed as bellow:

1. 546.6cm^{-1} : correlates to the rotation between OH and H_2 in asymptotic region, which is zero wave number in asymptotic region, but 4.89cm^{-1} in transition state, which the radius for moment inertia is calculated by the mass center of OH and H_2 .
2. 609.94cm^{-1} : correlates to the rotation of OH in asymptotic region, which is 18.601cm^{-1} in asymptotic region, but 18.6cm^{-1} in transition state. No big differences between asymptotic region and transition state, since OH can be seen as a spectator during the reaction.
3. 1059.12cm^{-1} : correlates to the rotation of H_2 in asymptotic region, which is 57.66cm^{-1} in asymptotic region, but 50cm^{-1} in transition state.
4. 2479.16cm^{-1} : correlates to the vibration of H_2 in asymptotic region, which is 4344.54cm^{-1} in asymptotic region, but 2479.16cm^{-1} in transition state.
5. 3736.43cm^{-1} : correlates to the rotation of OH in asymptotic region, which is 3714.33cm^{-1} in asymptotic region, but 3736.43cm^{-1} in transition state.

No big differences between asymptotic region and transition state, the reason is same as the concept mentioned in 609.94cm^{-1}

So, for the diabatic model, in order to preserve the properties, that is, the quantum numbers of those five motions in transition state should follow the quantum numbers of reactants. This is pretty different from adiabatic model. In adiabatic model, we count the number of possible tunneling amounts from reactants, and then the E_{max} of each adiabatic curve are taken from low level to high level, that is, the relation between each E_{max} and each state of reactants are decided by the sequence of the energy level of transition state and reactants. But for diabatic model, for every state of reactants, we should remember the quantum numbers of those 5 motions, and its corresponded E_{max} should have the same quantum numbers in order to preserve the properties. So the energy level of transition state would be like equation (3.29) :

$$E(J_{OH}, J_{H_2}, J_{OH/H_2}, \nu_{OH}, \nu_{H_2}) = \nu_0 + \nu_{H_2} \cdot 2479.16 + \nu_{OH} \cdot 3736.43 + J_{OH} (J_{OH} + 1) \cdot 18.6 + J_{OH/H_2} (J_{OH/H_2} + 1) \cdot 4.89 + J_{H_2} (J_{H_2} + 1) \cdot 50 \quad (3.29)$$

, where ν_0 is electronic energy plus zero point energy of transition state, J_{OH} , J_{H_2} , ν_{OH} , ν_{H_2} should be same as the J_{OH} , J_{H_2} , ν_{OH} , ν_{H_2} of reactants as bellow

$$E(J_{OH}, J_{H_2}, \nu_{OH}, \nu_{H_2}) = \nu_{H_2} \cdot 4344.54 + \nu_{OH} \cdot 3714.33 + J_{OH} (J_{OH} + 1) \cdot 18.601 + J_{H_2} (J_{H_2} + 1) \cdot 57.66 \quad (3.30)$$

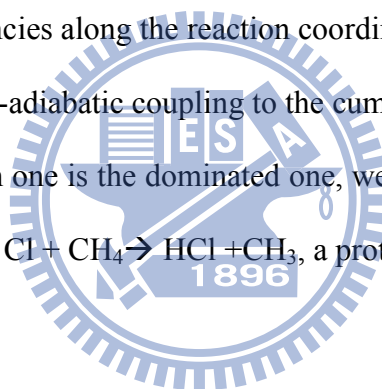
, and J_{OH/H_2} is $|J_{OH} + J_{H_2}|$, $|J_{OH} + J_{H_2} - 1|$, $|J_{OH} + J_{H_2} - 2|$, $|J_{OH} - J_{H_2}|$ in order to obtain total angular momentum equals to zero. Then we could get the energy diagram for diabatic model as figure 3.15. We could find out that the density of state in transition state is similar to the density in reactants, since it is diabatic model. Then the process to obtain cumulative reaction probability is entirely same as type III except the

linkage between E_{\max} and state of reactants. So we use the same equation (3.23) for δ vs ΔE , then we get the cumulative reaction probability of diabatic model as figure 3.16. In this figure, it also shows the adiabatic model. It's obvious to see that miller's result is between adiabatic model and diabatic model, that is to say, non-adiabatic coupling may give some contribution to the cumulative reaction probability, since diabatic model consider the non-adiabatic coupling entirely in each curve, but entirely no non-adiabatic coupling in adiabatic model.

From type III to type IV, it's easy to figure out that there are three possible reasons that influence the accuracy of the trends for cumulative reaction probability:

1. Whether the parabolic model for energy curve is appropriate or not.
2. Accuracy of the frequencies along the reaction coordinate
3. The contribution of non-adiabatic coupling to the cumulative reaction probability

In order to figure out which one is the dominated one, we would like to apply type III to type IV to a new system, $\text{Cl} + \text{CH}_4 \rightarrow \text{HCl} + \text{CH}_3$, a prototypical chemical reaction.



3-3.2 Cumulative reaction probability for $\text{Cl} + \text{CH}_4 \rightarrow \text{HCl} + \text{CH}_3$

Before applying those types of model to $\text{Cl} + \text{CH}_4 \rightarrow \text{HCl} + \text{CH}_3$, we would like to show some theoretical results that people have done before and my works.

3-3.2.1 Theoretical results for the MEP of $\text{Cl} + \text{CH}_4 \rightarrow \text{HCl} + \text{CH}_3$

Theoretically, there are several ab initio calculations investigating the barrier height and the heat of reaction with the calculated vibrational adiabatic ground-state barrier height; V_a^G , varying from 2.6 to 13.7 kcal/mol. Truong et al⁸ used the MP2-SAC2/MC-311G method, Dobbs and Dixon⁹ used QCISD(T) and CCSD(T) with a larger basis set (TZ+2P) and Hua-Gen and Gunnar Nyman obtained the

information of MEP by applying the hyper-spherical projection method to Rotating Line Approximation; RLA¹⁰, Rotating Line Umbrella; RLU¹¹ and Rotating Bond Umbrella; RBU¹² with the calculated London-Eyring-Polanyi-Sato (LEPS); which contains the zero-point energies of modes that are not explicitly treated in the quantum dynamics calculations. In this report, Gaussian 09 is used to calculate the reaction path of $\text{Cl} + \text{CH}_4 \rightarrow \text{HCl} + \text{CH}_3$ with CCSD/aug-cc-pvdz and CCSD(T)/aug-cc-pvdz//CCSD/aug-cc-pvdz. All the results are shown in table 3.6. From table 3.6, we could see that the energy correction by CCSD(T) is necessary, which match pretty well with Nyman's three results, Troung's result and the results of experiments within 1.5 kcal/mol, that is to say, the results of CCSD(T) energy correction is ok. And the comparison for MEP of my work between before and after energy correction by CCSD(T) shown in figure 3.17 indicates that the saddle point does not change to much compared to the one without energy correction. So we use the MEP calculated by CCSD(T)/ aug-cc-pvdz // CCSD aug-cc-pvdz

3-3.2.2 Geometries of transition state, products and reactants

Table 3.7 displays the geometries of transition state with CCSD/aug-cc-pvdz method, which predicted that the C-H length of Cl-H-CH₃'' is 1.0961 Å, which almost same as the CH'' of CH''₃ radical and the CH'' of H'CH''₃, but closer to CH''₃ radical more. This result match the concept that several studies bring out, which CH₃ can be seen as a spectator group during the reaction as Nyman does¹⁰⁻¹².

It was found that the transition state has a collinear structure along the Cl-H'-C reactive and is located near the product channel; HCl + CH₃.

3-3.2.3 Normal modes along reaction path

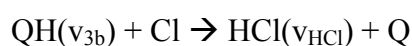
We've done the same process as $\text{OH} + \text{H}_2 \rightarrow \text{H}_2\text{O} + \text{H}$. Then we obtain the modified 11 frequencies along the reaction path as table 3.8 for $s < 0$, table 3.9 for $s > 0$ and figure 3.18 for both $s > 0$ and $s < 0$.

3-3.2.4 Cumulative reaction probability for $\text{Cl} + \text{CH}_4 \rightarrow \text{HCl} + \text{CH}_3$

As mentioned before, for hyper spherical radius coordinate and Jacobi coordinate, there's no exact solution for more than 5 atoms reaction, that is, only reduced dimension information is available. So we can only apply adiabatic model with the consideration of reduced dimension to do the comparisons, that is, only type III is going to be used. Below we would like to compare to Hua-Gen and Gunnar Nyman's^{10,11,12} three reduced dimension results; RLA, RLU and RBU.

RLA:

RLA stands for Rotating Line Approximation, which treats CH_4 as QH, where Q is a quasi-atom with the mass of CH_3 , that is, the reaction would be changed to $\text{QH} + \text{Cl} \rightarrow \text{Q} + \text{HCl}$. So in the RLA framework the studied reaction is written:

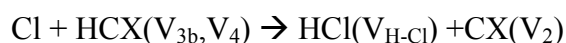


, where the quantum number v_{3b} represents the H-Q vibration and v_{HCl} represents the H-Cl vibration. The H-Q vibration is correlated to anti-symmetric stretching which is not adiabatically correlated to the vibration of HCl, that is, there are two dimensions in this model. It seems like that in order to do the comparison, we should consider all these two motions, but in fact, it's not the truth. For hyper-spherical radius (same for after projection), we can consider reactants and products separately, but for reaction coordinate, we need to consider them together, that is, the linkage between reactants and products is necessary for reaction coordinate but not the case for hyper-spherical radius (same for after projection). So for hyper-spherical radius

(same for after projection), the adiabatic energy curves for reactants only consider one dimension; the vibration of QH, and the adiabatic energy curves for products also only consider one dimension; the vibration of HCl. Both sides all only consider one dimension. But if we consider both the two dimensions in reaction coordinate, which makes both reactants and products two dimension, which is not the case in hyper-spherical radius (same for after projection). It's impossible for reaction coordinate to consider one side one motion and the other side another motion and there's no linkage between these two motions. In order to match the results of hyper-spherical radius (same for after projection), we only consider the motions of reactants, which is pretty reasonable. Since cumulative reaction probability is an effect of summation, as shown in equation (3.17) and (3.18). No matter how many final states you just sum all of them, it won't influence how much to go through, so the real one to decide how much to go through is the part of reactants. By using the W_{11} (anit-sym stretching of CH_4/CH_3) in table 3.8/table 3.9 and the calculated electronic by CCSD(T)/aug-cc-pvdz//CCSD/aug-cc-pvdz, we can obtain the reduced dimension energy diagram of adiabatic model as figure 3.19. And we repeat the same in type III, then we obtain the cumulative reaction probability as figure 3.20. We could find that the trend of my result goes well with Nyman's result, but the starting point is different. Besides that, we could find out there's strong resonance effect.

RLU:

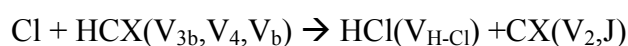
RLU stands for Rotating Line Umbrella. In the RLU model, the reaction $\text{Cl} + \text{CH}_4 \rightarrow \text{HCl} + \text{CH}_3$ is treated as a collinear four-atom reaction, $\text{Cl} + \text{HCX} \rightarrow \text{HCl} + \text{CX}$, where X has the mass of three hydrogen atoms and is located at their center of mass. So in the RLU framework, the studied reaction is written



, where v_{3b} is the quantum number correlated to anti-symmetric stretching of CH_4/CH_3 , V_4/V_2 are the quantum numbers of the umbrella type mode of CH_4/CH_3 fragments respectively and $V_{\text{H-Cl}}$ is the quantum number correlated to symmetric stretching of CH_4/HCl . So there are two dimensions in reactant side, two dimensions in product side and totally three dimensions. As the reasons mentioned in **RLA** section, we used W_7 , W_{11} in table 3.8/table 3.9 and the calculated electronic by $\text{CCSD(T)/aug-cc-pvdz//CCSD/aug-cc-pvdz}$, we can obtain the reduced dimension energy diagram of adiabatic model as figure 3.21 and the cumulative reaction probability as figure 3.22. The trend between my result and Nyman's seems almost the same, and the resonance effect becomes smaller.

RBU:

RBU stands for Rotating Bond Umbrella. In this model includes four internal physical motions: the H-C (V_{3b} ; anti-symmetric stretching of CH_4/CH_3) and H-Cl ($V_{\text{H-Cl}}$, symmetric stretching of CH_4/HCl) stretch, umbrella type mode of the CH_4/CH_3 fragments (V_4/V_2) and a rotation mode of CH_3 (J) which becomes a bending mode in CH_4 (V_b), that is, the studied reaction could be written:



So there are three dimensions in reactant side, three dimensions in product side and totally four dimensions Then we do the same thing as **RLA** and **RLB** section, we used the W_4 , W_7 , W_{11} in table 3.8/table 3.9 and the calculated electronic by $\text{CCSD(T)/aug-cc-pvdz//CCSD/aug-cc-pvdz}$, we get the reduced dimension energy diagram of adiabatic model as figure 3.23 and the cumulative reaction probability as figure 3.24. The trend of my result goes well with Nyman's and the resonance effect becomes smaller compared to **RLA** and **RLU**.

From **RLA** to **RBU** model, we found that adiabatic model goes well with

Nymans's results. But it is not the case in the full dimension case for $\text{OH} + \text{H}_2 \rightarrow \text{H}_2\text{O} + \text{H}_2$. It gives us a clue that we could find out the main reason from the three reasons we assumed after the section of $\text{OH} + \text{H}_2 \rightarrow \text{H}_2\text{O} + \text{H}_2$. Let's look at them one by one.

1. Parabolic model :

By fitting the ground energy curves of these three models, we found that none of these three curves has the dominated second order term, that is, this one is not the main reason for the deviation from exact one.

2. Non-adiabatic transition:

Since we are using adiabatic model with considering non-adiabatic transition, but we still get the right trend, that is, this may not give too big contribution.

3. The accuracies of the frequencies along the reaction path:

Since the frequencies used in full dimensions of $\text{OH} + \text{H}_2 \rightarrow \text{H}_2\text{O} + \text{H}_2$ have frequencies that are correlated to rotations in asymptotic regions, which are very small and easily contaminated by the gradient of reaction coordinate, rotations and translations. And in general, these modes control the density of states, since there are small. But for the cases in comparing with RLA, RLB and RBU, the frequencies used are those large frequencies which are in general correct. Even if there is still some difference between the frequencies I used and he used, but the difference compared to the frequency itself would be small, since these frequencies are not small. So in the total energy we are interested in, the difference won't be revealed.

So cumulative reaction probability is mainly decided by the accuracy of the density of states

Group	ΔE^*	ΔH^*	ΔE	ΔH	$E_a(300K)$
Zenner ¹	5.0	x	x	x	4.74
Schatz ²	7.4 ^a (6.2) ^b	(6.11) ^b	(15.18) ^b	x	5.59 ^b ₁ (4.75) ^b ₂
Truong ⁴	6.3 ^c (6.0) ^d	6.85 ^c (6.55) ^d	x	x	X
CCSD/dz	6.99	7.68	-14.02	-12.09	x
CCSD(T)/dz//CCSD/dz	5.63	6.38	-15.20	-13.27	x
CCSD(T)/tz//CCSD/dz	5.51	6.63	-15.13	-13.2	x
Experiments	x	x	x	-14.8 ^{s,e}	5.1 ^{s,e}

Table 3.1 All energy are in units of kcal/mol, ΔE^* is the classical barrier height, ΔH^* is the barrier height with ZPE, ΔE is the classical reaction energy, ΔH is the reaction energy with ZPE, dz stands for aug-cc-pv-dz and tz is aug-cc-pvtz (a) 3s3p1d/3s1p basis, (b) 4s3p2d/3s2p basis, (b₁) without tunneling (b₂) with tunneling (c) QCISD/ 6-311+G(d,p) method, (d) PMP4/ 6-311++G(2d f ,2pd)//QCISD/6-311+G(d,p) (e) All the results are at 0 K, except for the results notated e, which is at 300K

s(bohr)	W₁	W₂	W₃	W₄	W₅	W₆	W₇	W₈	W₉	W₁₀	W₁₁	W₁₂
-2.5	210.13	220.18	257.56	1715.67	3723.99	3842.01	-290.25	-56.13	-52.4	-0.02	0	0.03
-2.4	214.41	232.93	253.51	1715.4	3723.97	3842.45	-291.83	-64.6	-60.71	-0.02	0	0.03
-2.3	212.64	248.69	252.94	1715.07	3723.93	3842.65	-293.68	-73.7	-69.53	-0.01	-0.01	0.03
-2.2	210.02	242.83	274.96	1714.65	3723.85	3842.53	-171.09	-34.39	0	0	0	0
-0.1	-1769.0	610.76	640.39	1181.23	1995.49	3734.53	-0.15	-0.02	-0.01	116.26	165.7	165.97
0.0	-1338	501.63	593.51	1058.57	2460.84	3735.91	-9.84	0	0	0	0	6.01
0.1	-979.98	357.75	520.97	949.73	2916.27	3736.92	-155.85	-145.93	-101.88	0.04	0.07	1.05
1.7	-214.61	34.45	281.52	348.5	3738.4	4324.45	-117.19	-107.54	-1.67	-0.01	1.91	41.14
1.8	-199.38	-11.34	262.98	332.35	3738.36	4328.15	-110.91	-99.49	-2.73	0	1.39	24.35
1.9	-184.55	-38.34	245.85	316.21	3738.33	4330.78	-105.74	-91.7	-20.88	0	0.89	2.86
2.0	-165.87	-49.86	232.05	300.92	3738.29	4331.69	-102.33	-83.88	-28.29	0	0.44	2.04

Table 3.2 The frequencies are in cm^{-1} unit which are calculated by G09 with CCSD/aug-cc-pvdz method along reaction path

s(bohr)	W ₁	W ₂	W ₃	W ₄	W ₅	W ₆	W ₇	W ₈	W ₉	W ₁₀	W ₁₁	W ₁₂
-2.5	209.65	219.09	257.03	1715.49	3723.9	3842.02	0	0	0	0	0	0
-2.4	213.04	232.95	253.14	1715.25	3723.89	3842.5	0	0	0	0	0	0
-2.3	211.21	248.34	253.41	1714.93	3723.86	3842.75	0	0	0	0	0	0
-2.2	208.47	275.8	322.55	1714.52	3723.78	3842.7	-171.09	-34.39	0	0	0	0
-0.1	654.06	677.07	1183.33	1998.15	3734.95	-1850.8	0	0	0	0	23.41	31.96
0.0	546.6	609.94	1059.12	2479.16	3736.43	-1349.8	-9.84	0	0	0	0	6.01
0.1	414.35	537.49	949.11	2940.67	3737.36	-964.6	-23.31	-14.61	0	0	0	0
1.7	282.4	350.72	3738.99	4324.9	-195.1	-65.52	-45.35	0	0	0	0	28.28
1.8	264.39	332.23	3739.05	4328.4	-179.11	-68.57	-41.22	0	0	0	0	15.84
1.9	246.81	317.26	3738.84	4330.94	-166.35	-72.43	-51.21	-41.95	0	0	0	0
2.0	233.74	301.88	3738.92	4331.85	-145.2	-73.02	-57.03	-38.29	0	0	0	0

Table 3.3 The frequencies are in cm^{-1} unit which are calculated by Molpro by CCSD/aug-cc-pvdz method along reaction path with the geometries obtained by G09

s(bohr)	W ₁	W ₂	W ₃	W ₄	W ₅	s(bohr)	W ₁	W ₂	W ₃	W ₄	W ₅
-2.5	257.03	209.65	1715.49	3723.9	3842.02	0	546.6	609.94	1059.12	2479.16	3736.43
-2.4	253.14	213.04	1715.25	3723.89	3842.5	0.1	414.35	537.49	949.11	2940.67	3737.36
-2.3	248.34	211.21	1714.93	3723.86	3842.75	0.2	276.79	461.87	858.92	3294.27	3738.11
-2.2	-171.09	208.47	1714.52	3723.78	3842.7	0.3	91.63	389.89	783.85	3554.9	3738.69
-2.1	-170.9	205.23	1714.01	3723.67	3842.28	0.4	-203.94	330.09	720.49	3749.76	3734.49
-2	-171.34	201.18	1713.38	3723.52	3841.37	0.5	-259.11	280.27	664.13	3888	3738.07
-1.9	-174.32	194.84	1712.48	3723.41	3841.11	0.6	-292.84	227.58	615.83	3995.79	3738.99
-1.8	-177.29	188.63	1711.45	3723.13	3838.82	0.7	-308.32	188.82	571.37	4079.01	3739.12
-1.7	-182.22	180.74	1710.16	3722.76	3835.54	0.8	-313.62	158.88	531.17	4141.67	3739.2
-1.6	-189.9	169.92	1708.51	3722.23	3831.05	0.9	-314.34	136.78	494.61	4189.49	3738.97
-1.5	-199.97	157.08	1706.5	3721.34	3823.79	1	-283.18	119.03	460.87	4225.9	3739.26
-1.4	-216.85	136.13	1703.88	3720.24	3816.03	1.1	-287.63	105.57	421.97	4253.84	3739.24
-1.3	-237.48	108.13	1700.72	3718.15	3803.83	1.2	-264.05	86.33	398.04	4276.3	3739.21
-1.2	-266.71	53.09	1696.74	3714.74	3789.82	1.3	-267.32	80.46	372.07	4291.96	3739.18
-1.1	-302.3	-89.78	1691.81	3707.61	3772.87	1.4	-256.01	68.18	347.16	4304.57	3739.14
-1	-352.98	-148.3	1685.64	3692.1	3756.8	1.5	-232.57	53.63	323.92	4313.95	3739.07
-0.9	-399.03	-202.98	1677.81	3665.42	3746.76	1.6	-206.09	55.85	303.16	4318.83	3739.01
-0.8	-448.96	-248.57	1668.42	3612.78	3739.99	1.7	-195.1	28.28	282.4	4324.9	3738.99
-0.7	-300.81	-98.3	1660.29	3296.12	3732.7	1.8	-179.11	15.84	264.39	4328.4	3739.05
-0.6	426.97	315.67	1629.1	2620.87	3730.16	1.9	-166.35	-2.43	246.81	4330.94	3738.84
-0.5	585.94	522.75	1504.25	1900.22	3729.23	2	-145.2	-15.34	233.74	4331.85	3738.92
-0.4	636.88	535.27	1351.75	1642.58	3729.74						
-0.3	707.59	614.81	1344.17	1568.26	3731.06						
-0.2	681.3	651.5	1302.46	1675.79	3733.23						
-0.1	677.07	654.06	1183.33	1998.15	3734.95						

Table 3.4 The chosen frequencies along the reaction path are in cm^{-1} unit which are calculated in CCSD/aug-cc-pvdz method

s(bohr)	W ₁	W ₂	W ₃	W ₄	W ₅	s(bohr)	W ₁	W ₂	W ₃	W ₄	W ₅
H₂O	x	x	1648.89	3821.88	3937.11	0	644.9	632.52	1059.12	2479.16	3736.43
-2.5	14.91	11.93	1715.49	3723.9	3842.02	0.1	495.76	532.15	949.11	2940.67	3737.36
-2.4	14.94	11.95	1715.25	3723.89	3842.5	0.2	408.54	448.19	858.92	3294.27	3738.11
-2.3	15.02	12	1714.93	3723.86	3842.75	0.3	336.67	377.96	783.85	3554.9	3738.69
-2.2	15.18	12.1	1714.52	3723.78	3842.7	0.4	277.45	319.21	720.49	3749.76	3734.49
-2.1	15.5	12.34	1714.01	3723.67	3842.28	0.5	228.64	270.07	664.13	3888	3738.07
-2	16.1	12.83	1713.38	3723.52	3841.37	0.6	188.42	228.96	615.83	3995.79	3738.99
-1.9	17.18	13.81	1712.48	3723.41	3841.11	0.7	155.27	194.57	571.37	4079.01	3739.12
-1.8	19.09	15.69	1711.45	3723.13	3838.82	0.8	127.95	165.8	531.17	4141.67	3739.2
-1.7	22.3	19.13	1710.16	3722.76	3835.54	0.9	105.44	141.73	494.61	4189.49	3738.97
-1.6	27.53	25.11	1708.51	3722.23	3831.05	1	86.90	121.6	460.87	4225.9	3739.26
-1.5	35.73	35.05	1706.5	3721.34	3823.79	1.1	71.61	104.76	421.97	4253.84	3739.24
-1.4	48.09	50.74	1703.88	3720.24	3816.03	1.2	59.01	90.68	398.04	4276.3	3739.21
-1.3	66.01	74.33	1700.72	3718.15	3803.83	1.3	48.63	78.89	372.07	4291.96	3739.18
-1.2	90.95	108	1696.74	3714.74	3789.82	1.4	40.08	69.04	347.16	4304.57	3739.14
-1.1	124.3	153.6	1691.81	3707.61	3772.87	1.5	33.03	60.79	323.92	4313.95	3739.07
-1	166.9	212.1	1685.64	3692.1	3756.8	1.6	27.22	53.89	303.16	4318.83	3739.01
-0.9	219.2	282.7	1677.81	3665.42	3746.76	1.7	22.43	48.12	282.4	4324.9	3738.99
-0.8	280.2	362.8	1668.42	3612.78	3739.99	1.8	18.48	43.30	264.39	4328.4	3739.05
-0.7	347.8	447.3	1660.29	3296.12	3732.7	1.9	15.23	39.26	246.81	4330.94	3738.84
-0.6	418.8	529.4	1629.1	2620.87	3730.16	2	12.55	35.88	233.74	4331.85	3738.92
-0.5	488.5	601	1504.25	1900.22	3729.23	OH	x	x	x	x	3714.33
-0.4	551.6	654.1	1351.75	1642.58	3729.74	H₂	x	x	x	4344.54	x
-0.3	602.8	682.5	1344.17	1568.26	3731.06						
-0.2	637.3	682.6	1302.46	1675.79	3733.23						
-0.1	651.9	654.3	1183.33	1998.15	3734.95						

Table 3.5 The modified and fitted frequencies along the reaction path are in cm^{-1} unit which are calculated in CCSD /aug-cc-pvdz method

Group	ΔE^*	ΔH^*	ΔE	ΔH	$E_a(300K)$
CCSD/dz	9.8	5.6	7.2	2.2	x
CCSD(T)/dz//CCSD/dz	8.1	3.9	6.9	1.8	x
CCSD(T)/tz//CCSD/dz	7.8	3.6	6.5	1.4	x
Truong et al ^{8,a}	7.9	3.5	x	1.2	x
Dobbs and Dixon ^{9,b}	4.9	8.9	x	2.5	x
RLA ^{10,c}	7.3	3.5	x	1.0	x
RLU ^{11,d}	6.8	2.8	x	1.7	x
RBU ^{12,e}	x	3.5	x	1.2	x
Experiments	x	2.3 ^{f,15}	x	1.1 ± 0.1 ^{f,13}	2.6 ± 0.4 ^{g,14} 3.5 ± 0.5 ^{h,14}

Table 3.6 All energy are in units of kcal/mol, ΔE^* is the classical barrier height, ΔH^* is the barrier height with ZPE, ΔE is the classical reaction energy, ΔH is the reaction energy with ZPE, dz stands for aug-cc-pv-dz and tz is aug-cc-pvtz. (a) MP-SAC2/MC-311G(2d,d,p) (b) QCISD(T)/TZ+2P and for ΔH^* , the difference between QCISD(T)/TZ+2P and CCSD(T)/TZ+2P is within 0.1 kcal/mol (c) Rotating Line Approximation with LEPS (d) Rotating Line Umbrella with LEPS (e) Rotating Bond Umbrella with LEPS (f) Enthalpy of reaction at 0 K (g) Experimental activation energy in the range of 200–300 K (h) Experimental activation energy in the range of 300–500 K (i) Obtained by threshold method

Molecule	R(C-H') (Angstroms)	R(C-H'') (Angstroms)	R(Cl-H') (Angstroms)	L(H'-C-H'') (degree)	L(H''-C-H'') (degree)	L(Cl-H'-C) (degree)	D(H''CH''H'') (degree)
H'-CH''₃	1.1013	1.1013	x	109.4712	109.4712	x	120.0000
CH''₃	x	1.0920	x	x	119.9967	x	180.0000
Cl-H'	x	x	1.2906	1896	x	x	x
Cl-H'-CH''₃	1.4008	1.0961	1.4600	101.1251	116.3692	180.0000	143.0404

Table 3.7 The geometries of transition state, reactants and products in CCSD/ aug-cc-pvdz

s(bohr)	W ₁	W ₂	W ₃	W ₄	W ₅	W ₆	W ₇	W ₈	W ₉	W ₁₀	W ₁₁
HCl	x	x	x	x	x	x	x		x	x	x
CH₃	x	x	x	x	497.54	1413.2	1413.2	x	3116.1	3303.65	3303.65
-1.6	220.7	220.7	381.79	381.79	726.66	1411.51	1411.51	2746.32	3088.25	3286.07	3286.07
-1.7	227.63	227.63	394.28	394.28	740.96	1411.5	1411.5	2716.92	3085.81	3285.265	3285.265
-1.4	235.4	235.4	408.08	408.08	755.67	1411.58	1411.58	2682.86	3083.06	3283.91	3283.91
-1.3	242.19	242.19	422.21	422.21	770.2	1411.61	1411.61	2644.88	3080.59	3282.87	3282.87
-1.2	249.34	249.34	438.38	438.38	784.78	1411.68	1411.68	2599.82	3078.3	3281.7	3281.7
-1.1	257.41	257.41	456.65	456.65	799.37	1411.81	1411.81	2546.77	3076.01	3280.06	3280.06
-1	264.52	264.52	475.81	475.81	813.84	1411.96	1411.96	2486.82	3074.1	3278.36	3278.36
-0.9	272.64	272.64	498.23	498.23	828.34	1412.19	1412.19	2414.41	3072.43	3276.14	3276.14
-0.8	280.29	280.29	523.02	523.02	841.95	1412.38	1412.38	2329.57	3071.8	3274.1	3274.1
-0.7	289.02	289.02	551.23	551.23	854.81	1412.67	1412.67	2228.48	3071.49	3271.41	3271.41
-0.6	297.74	297.74	583.43	583.43	865.77	1412.97	1412.97	2106.79	3072.26	3268.76	3268.76
-0.5	306.8	306.8	620.015	620.015	873.3	1413.33	1413.33	1960.98	3073.78	3265.79	3265.79
-0.4	316.97	316.97	662.64	662.64	872.59	1413.77	1413.77	1783.57	3076.01	3262.69	3262.69
-0.3	327.88	327.88	712.25	712.25	851.02	1414.34	1414.34	1574.13	3078.65	3259.23	3259.23
-0.2	339.49	339.49	774.08	774.08	764.1	1415.02	1415.02	1357.31	3081.65	3256.36	3256.36
-0.1	351.39	351.39	841.83	841.83	610.14	1416	1416	1218.38	3084.16	3253.56	3253.56
0	360.62	360.62	923.09	923.09	495.28	1417.43	1417.43	1180.36	3085.59	3251.54	3251.54

Table 3.8 The modified and fitted frequencies for S > 0 are in cm⁻¹ unit which are calculated in CCSD /aug-cc-pvdz method

s(bohr)	W ₁	W ₂	W ₃	W ₄	W ₅	W ₆	W ₇	W ₈	W ₉	W ₁₀	W ₁₁
0	360.62	360.62	923.09	923.09	495.28	1417.43	1417.43	1180.36	3085.59	3251.54	3251.54
0.1	382.28	382.28	1010.21	1010.21	444.33	1419.66	1419.66	1191.2	3084.98	3249.89	3249.89
0.2	368.01	368.01	1095.13	1095.13	437.73	1423.19	1423.19	1227.39	3081.55	3248.48	3248.48
0.3	321.39	321.39	1168.55	1168.55	532.62	1428.8	1428.8	1300.08	3075.03	3247.96	3247.96
0.4	268.87	268.87	1223.22	1223.22	953.01	1437.67	1437.67	1540.26	3064.18	3249.12	3249.12
0.5	228.13	228.13	1255.33	1255.33	1139.1	1450.17	1450.17	2029.42	3047.46	3252.54	3252.54
0.6	202.67	202.67	1270.34	1270.34	1191.35	1463.09	1463.09	2416.09	3025.9	3259.08	3259.08
0.7	187.45	187.45	1279.23	1279.23	1215.45	1473.88	1473.88	2632.26	3006.02	3266.07	3266.07
0.8	176.09	176.09	1250.67	1250.67	1301.99	1482.8	1482.8	2756.25	2993.43	3271.3	3271.3
0.9	165.32	165.32	1258.79	1258.79	1309.35	1490.59	1490.59	2844.12	2988.42	3272.48	3272.48
1.0	155.42	155.42	1266.08	1266.08	1314.6	1497.41	1497.41	2908.07	2991.05	3270.27	3270.27
1.1	148.01	148.01	1272.79	1272.79	1318.3	1503.32	1503.32	2949.17	3004.05	3265.51	3265.51
1.2	143.46	143.46	1279.05	1279.05	1320.73	1508.54	1508.54	2970.01	3027.79	3258.88	3258.88
1.3	140.16	140.16	1285.07	1285.07	1322.45	1513.05	1513.05	2981.66	3052.22	3250.04	3250.04
1.4	136.39	136.39	1290.77	1290.77	1323.43	1516.98	1516.98	2991.19	3072.98	3240.15	3240.15
1.5	133.24	133.24	1296	1296	1323.85	1520.38	1520.38	3000.41	3089.83	3229.67	3229.67
CH₄	x	x	1329.82	1329.82	1329.82	1544.05	1544.05	3033.14	3158.52	3158.52	3158.52

Table 3.9 The modified and fitted frequencies for $S < 0$ are in cm^{-1} unit which are calculated in CCSD /aug-cc-pvdz method

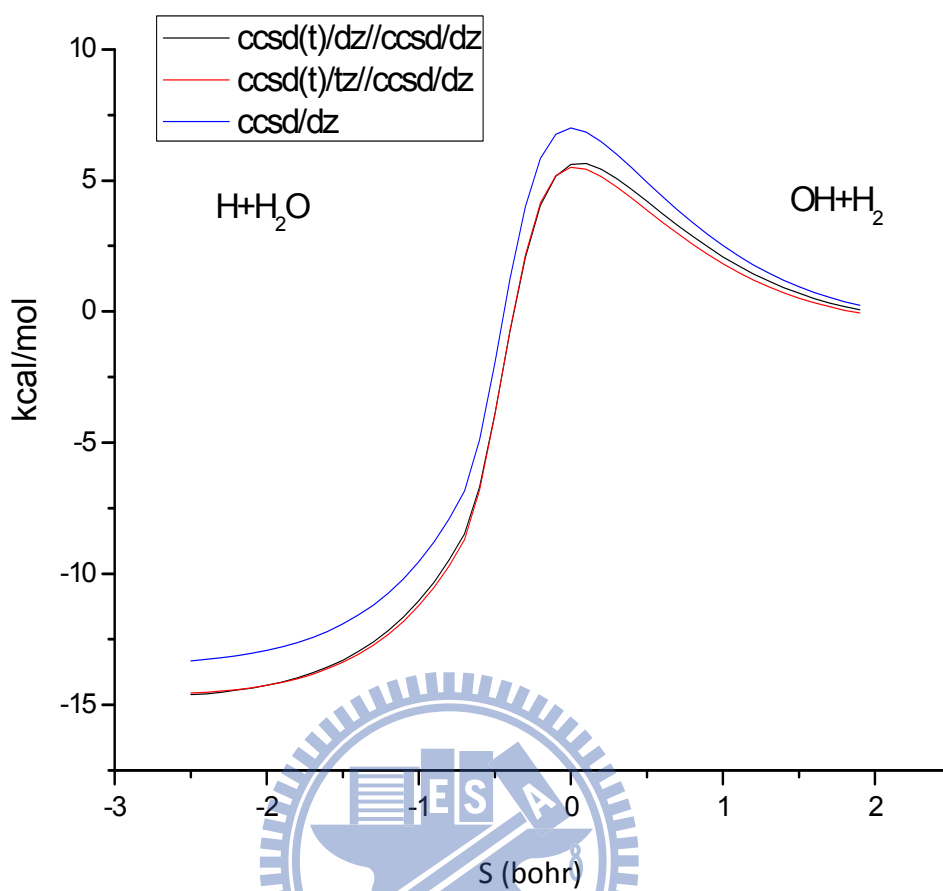


Figure 3.1 MEP of three different methods, where dz stands for aug-cc-pvdz and tz stands for aug-cc-pvtz.

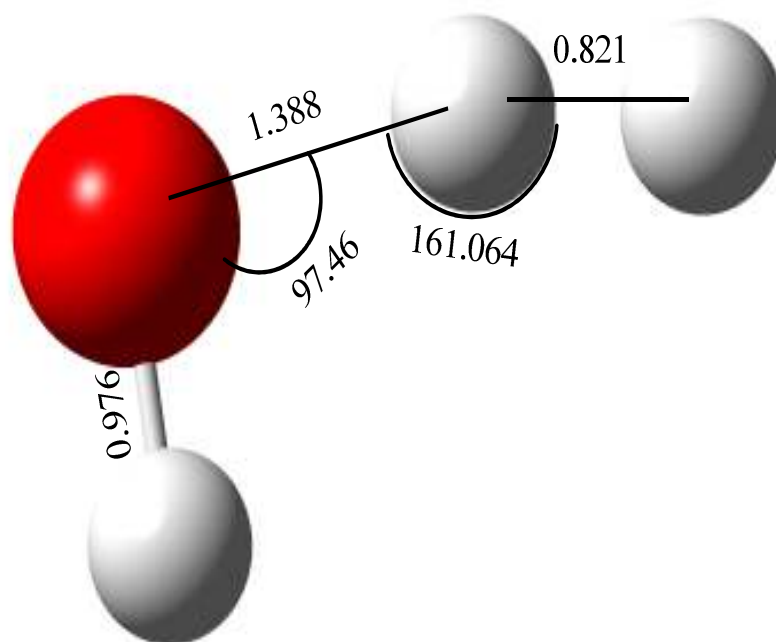


Figure 3.2 The geometry of transition state in CCSD/
aug-cc-pvdz



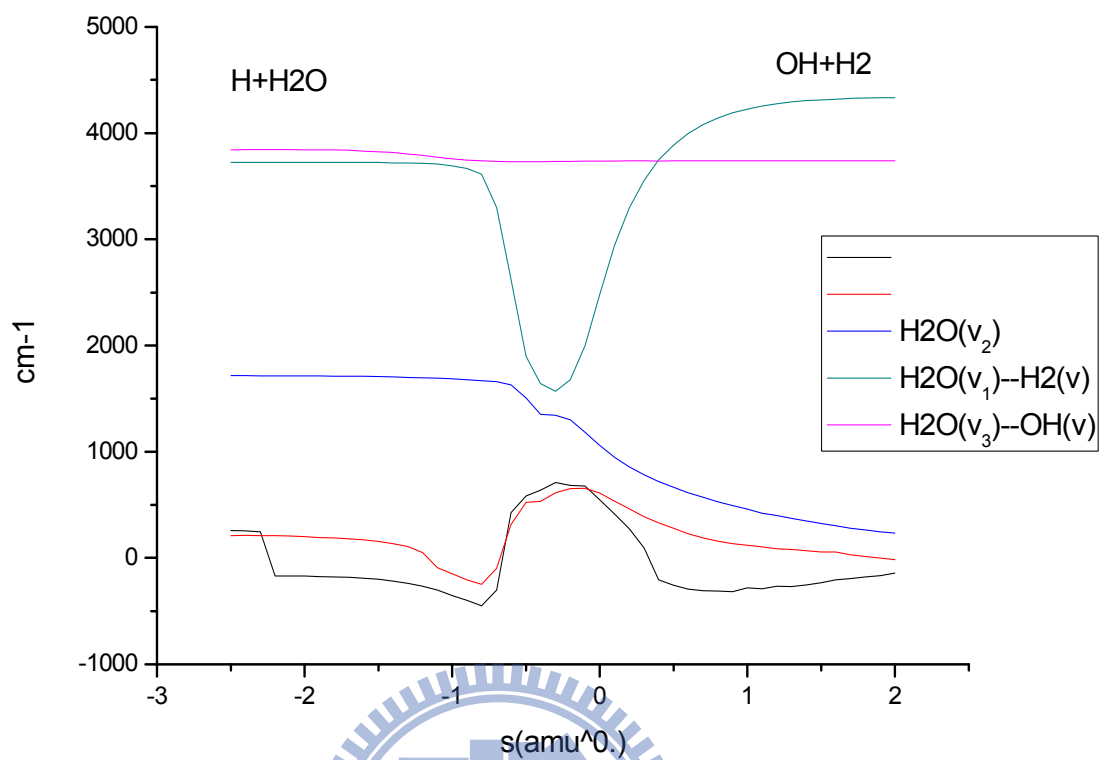


Figure 3.3 The evolution of frequencies along the reaction path. This result is calculated with ccSD/aug-cc-pvdz method.

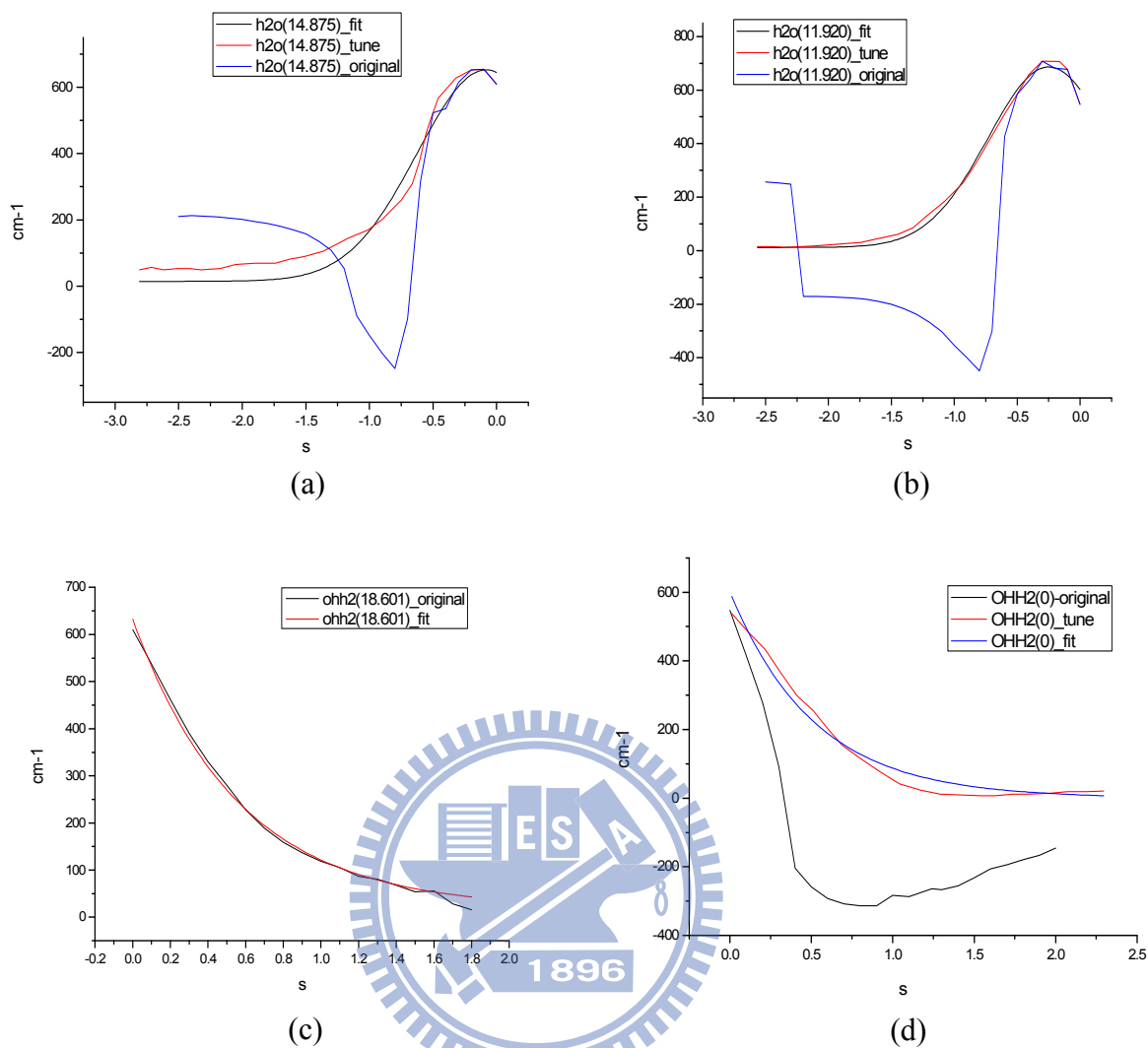


Figure 3.4 Schema of the modified and fitted frequencies of W_1 and W_2 . (a) W_2 of H_2O+H ; rotation of H_2O , (b) W_1 of H_2O+H ; k component of the rotation of H_2O (c) W_1 of $OH+H_2$; rotation of OH (d) W_1 of $OH+H_2$; the rotation of H_2 rotating around OH .

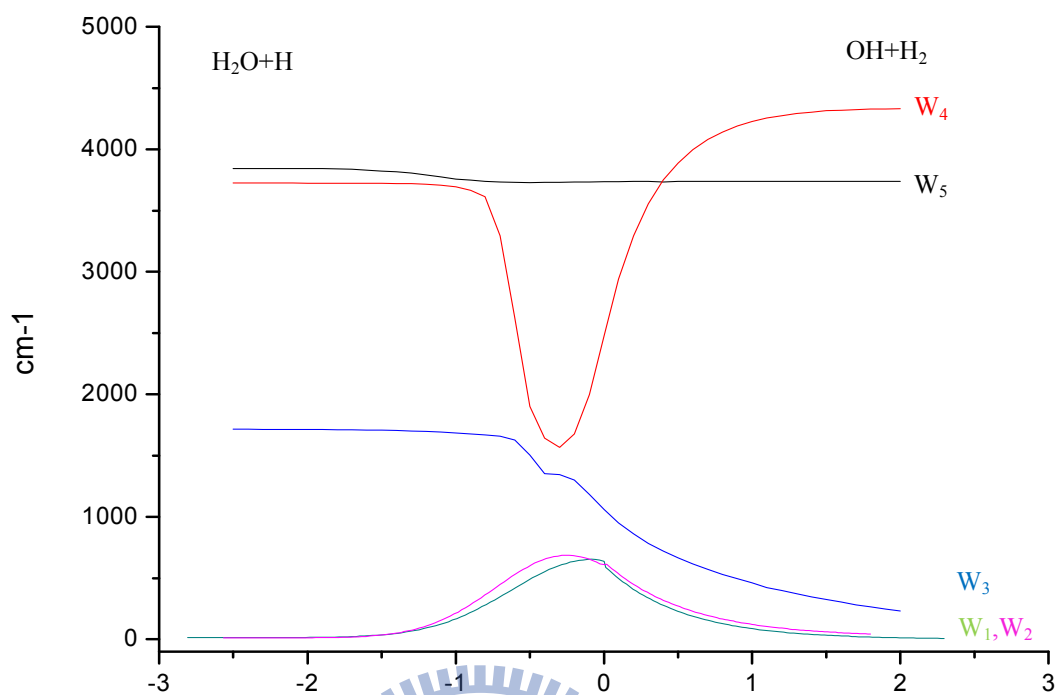


Figure 3.5 Fitted frequencies along MEP. This result is calculated with *ccsd/aug-cc-pvdz* method. W_i is the label used in table 3.5. From these labels, the correlation between asymptotic regions and the motion along reaction path could be understood clearly in table 3.5.

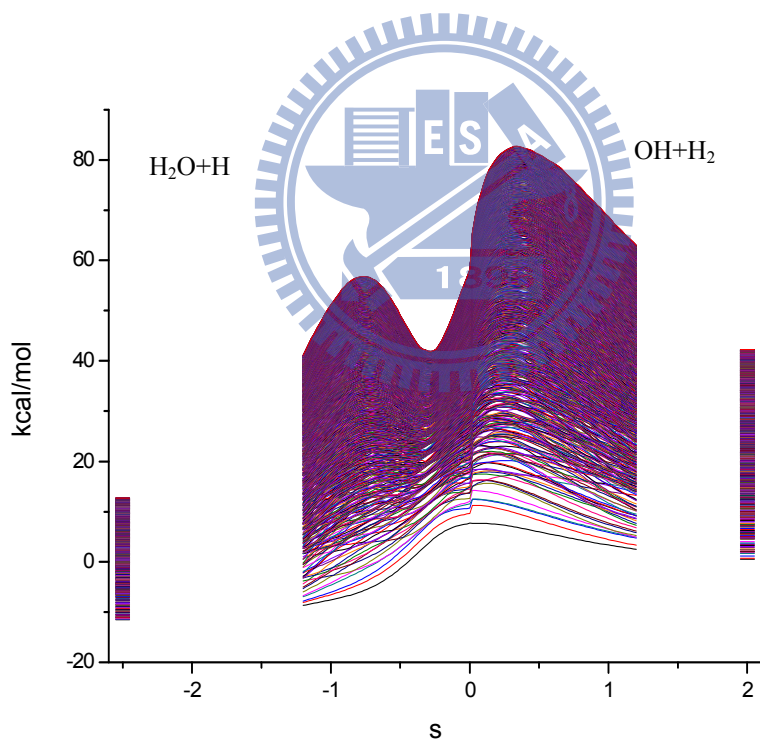
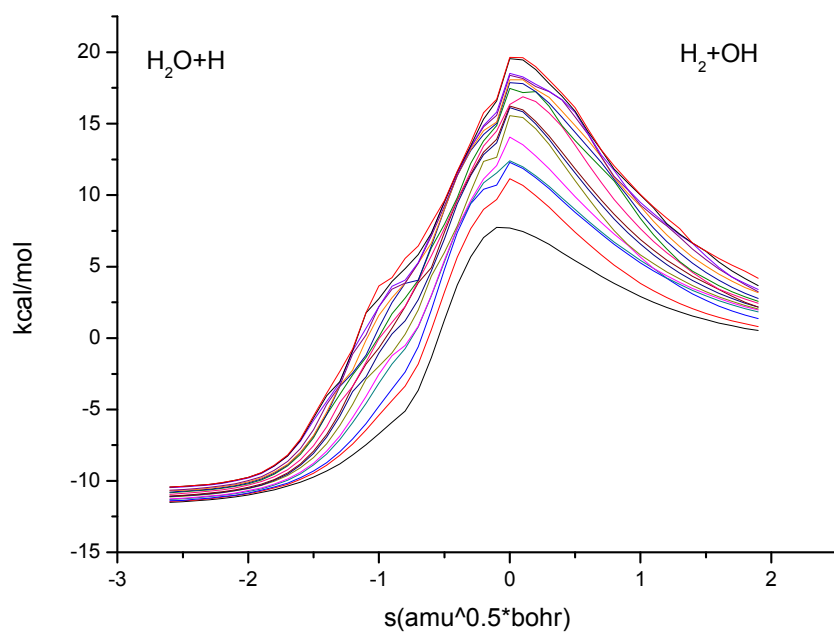


Figure 3.6 (a) 16 Adiabatic curves on reaction path (b)1500 Adiabatic curves on reaction path with rightmost and leftmost part are the energy level of reactants an products respectively.This result is calculated with ccSD(t)/aug-cc-pvdz //ccSD/aug-cc-pvdz for energy correction and ccSD/aug-cc-pvdz for frequencies along MEP

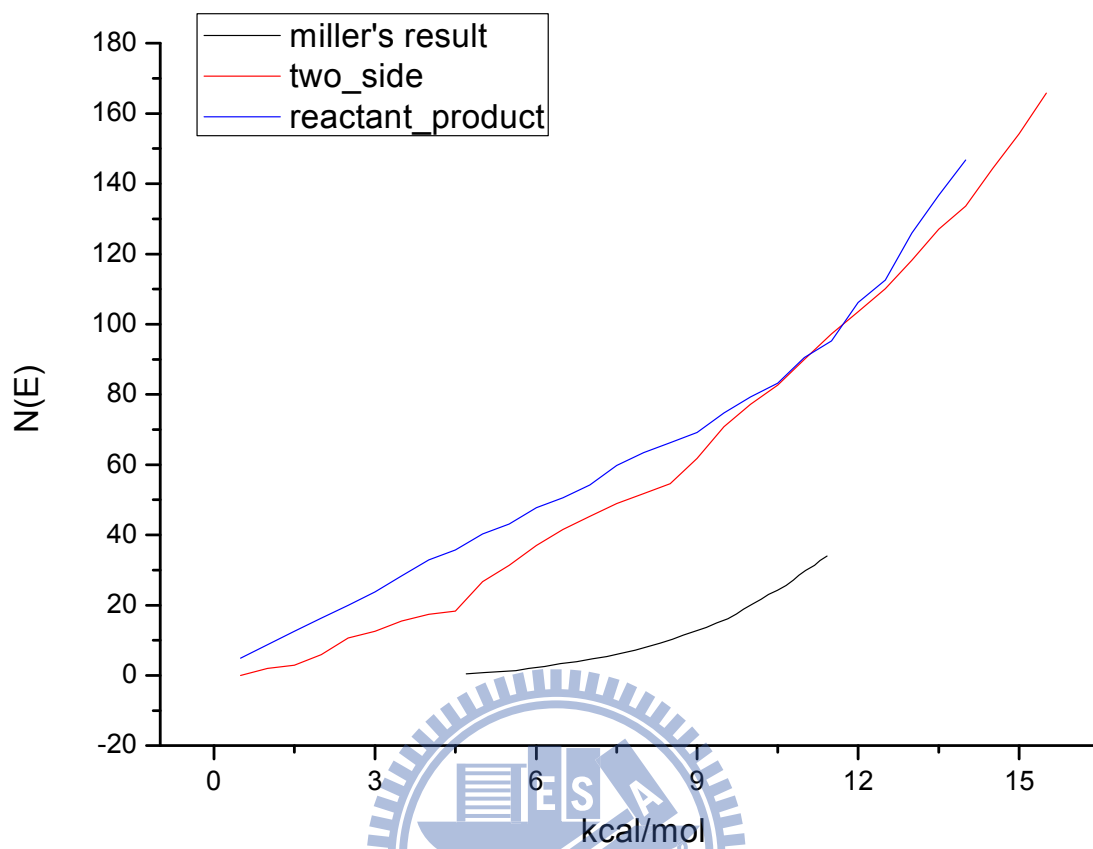


Figure 3.7 Reaction probability $N(E)$ of $J = 0$, black line is Miller's result, blue one is evaluated by reactants and product, red is $s = -2.5/2.0$ bohr. Red and blue are all evaluated with equation (3.17)

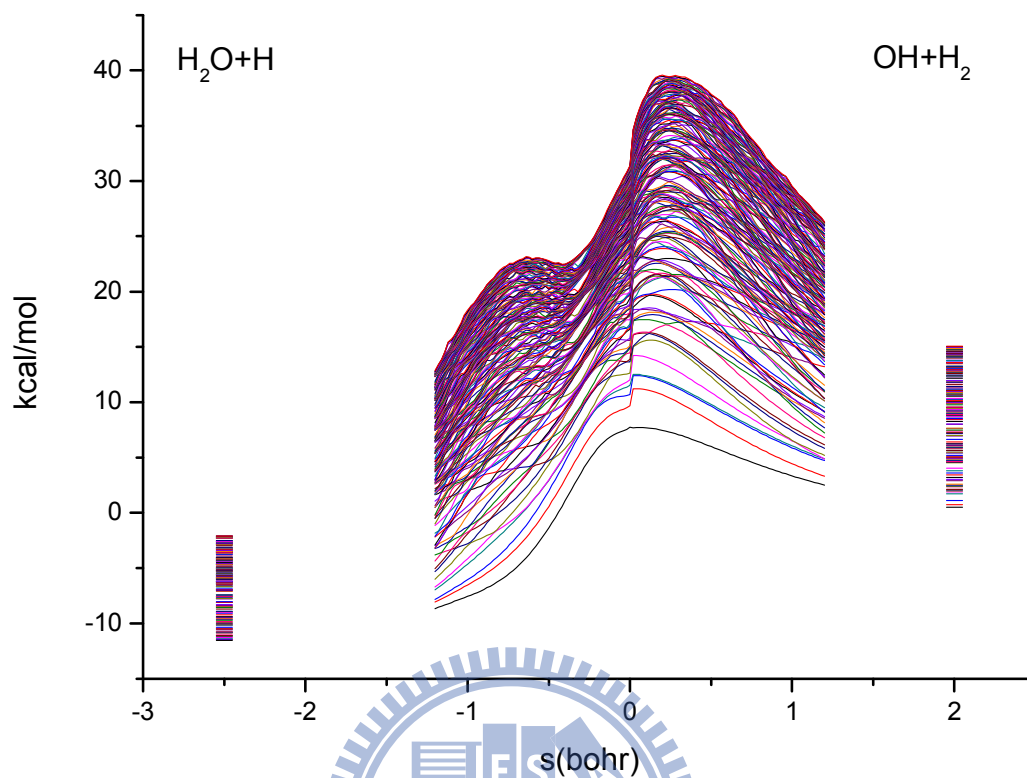


Figure 3.8 Adiabatic curves that connect reactant's energy curves lower than 15kcal/mol. This result is calculated with `ccsd(t)/aug-cc-pvdz//ccsd/aug-cc-pvdz` for energy correction and `ccsd/aug-cc-pvdz` for frequencies along MEP

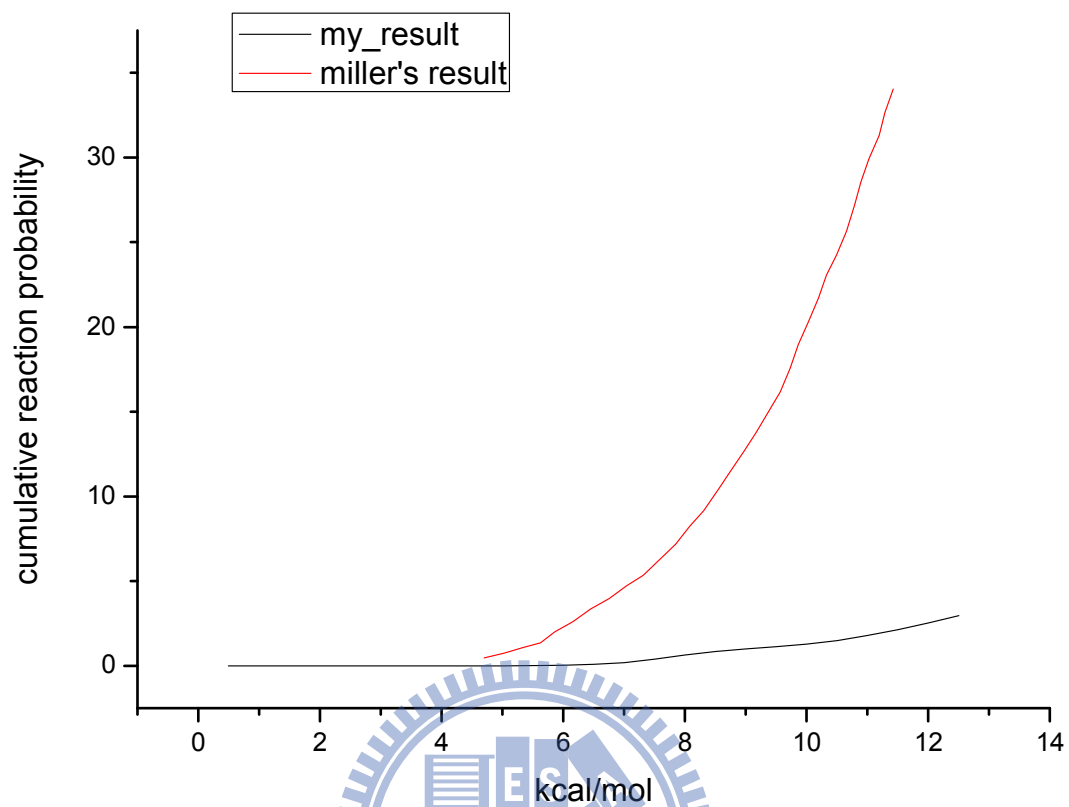


Figure 3.9 Cumulative reaction probability of $J = 0$, my result is evaluated with one barrier tunneling effect and parabolic model in `ccsd(t)/aug-cc-pvdz//ccsd/aug-cc-pvdz` for energy correction and `ccsd/aug-cc-pvdz` for frequencies along MEP

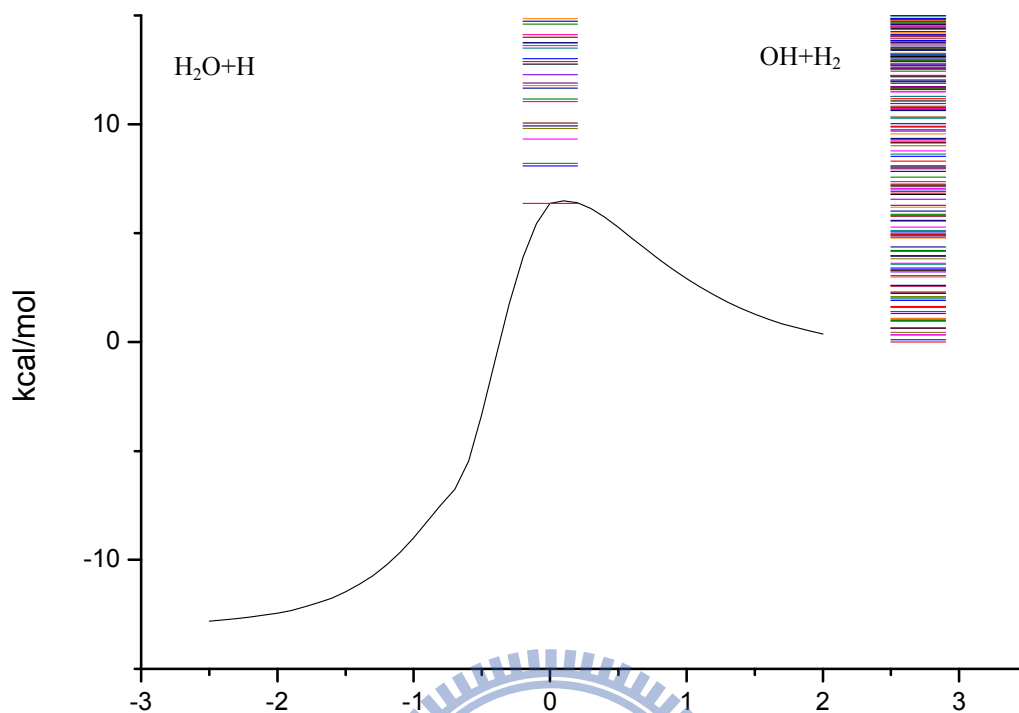


Figure 3.10 The energy diagram of adiabatic model, which show the energy levels of transition state in the middle and energy levels of reactant in the rightmost side. This result is calculated with `ccsd(t)/aug-cc-pvdz//ccsd/aug-cc-pvdz` for energy correction and `ccsd/aug-cc-pvdz` for frequencies along MEP

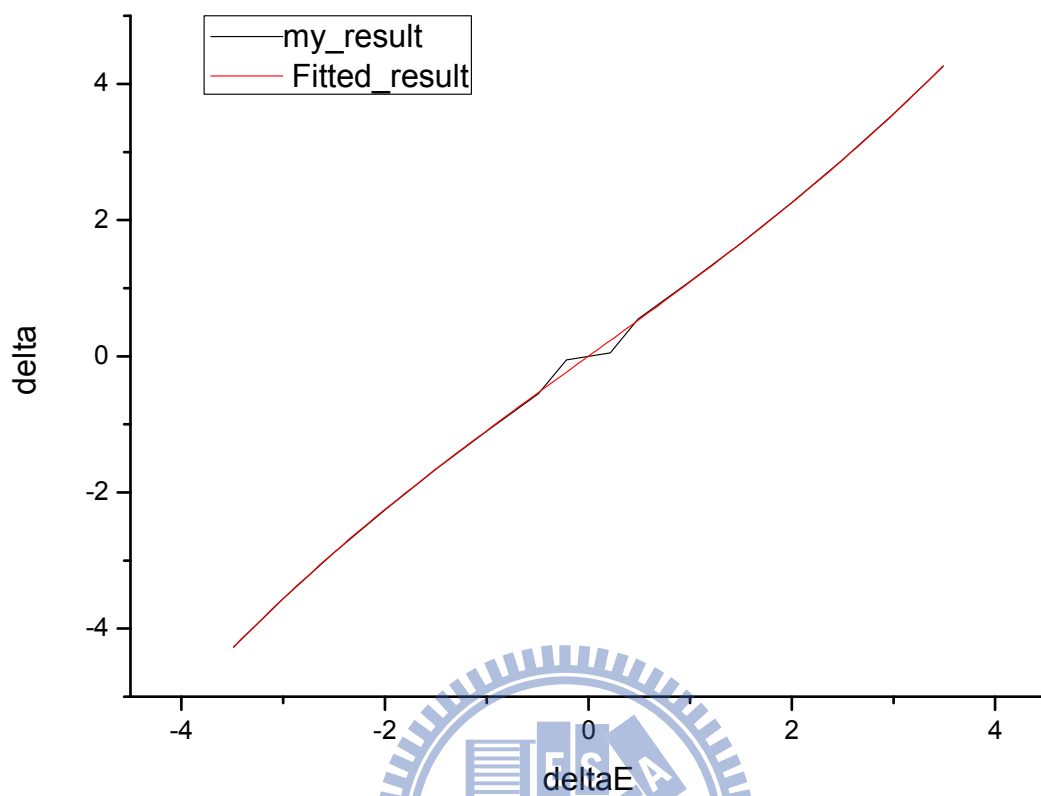


Figure 3.11 The diagram of delta (δ) vs deltaE for ground energy level in ccsd(t)/aug-cc-pvdz//ccsd/aug-cc-pvdz for energy correction and ccsd/aug-cc-pvdz for frequencies along MEP

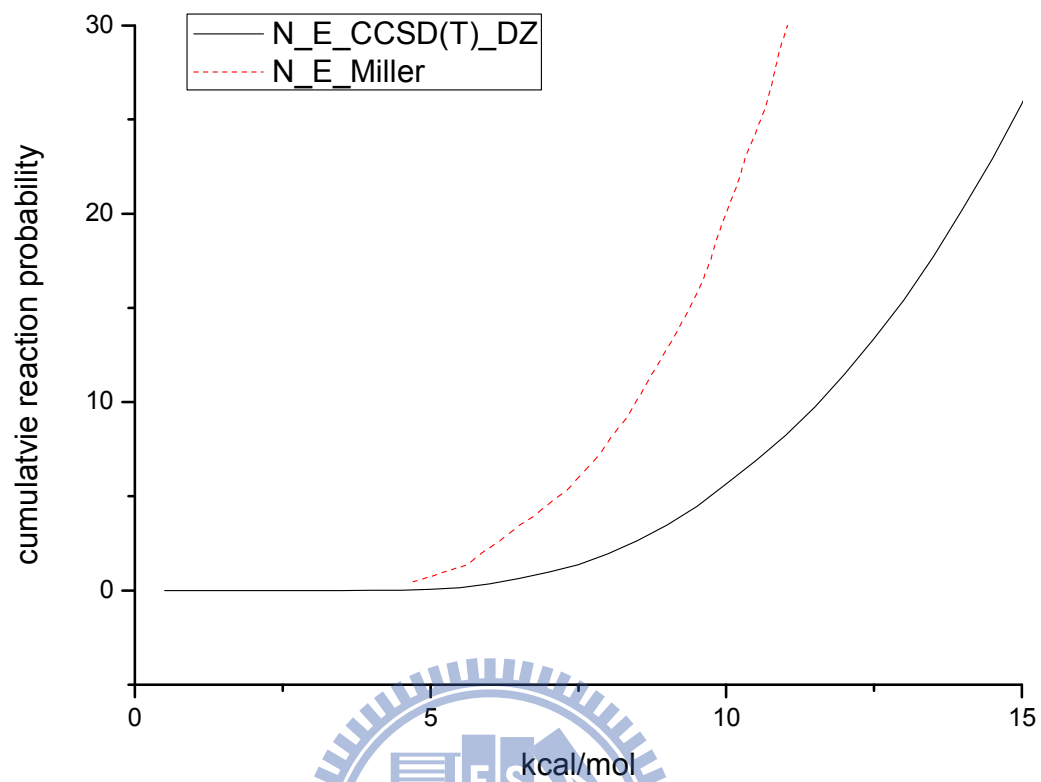


Figure 3.12 Cumulative reaction probability of $J = 0$ for adiabatic model and miller's result. This result is calculated with `ccsd(t)/aug-cc-pvdz//ccsd/aug-cc-pvdz` for energy correction and `ccsd/aug-cc-pvdz` for frequencies along MEP

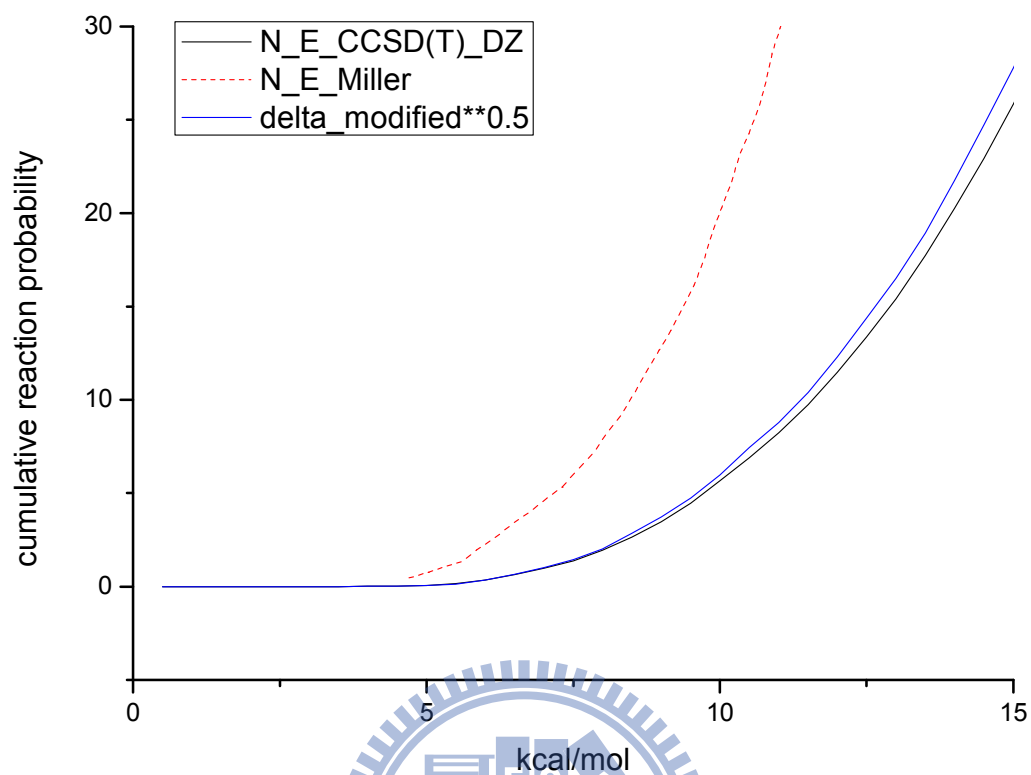


Figure 3.13 Cumulative reaction probability of $J = 0$ for adiabatic model with modified delta in order of 0.5 and miller's result. This result is calculated with ccSD(t)/aug-cc-pvdz//ccSD/aug-cc-pvdz for energy correction and ccSD/aug-cc-pvdz for frequencies along MEP

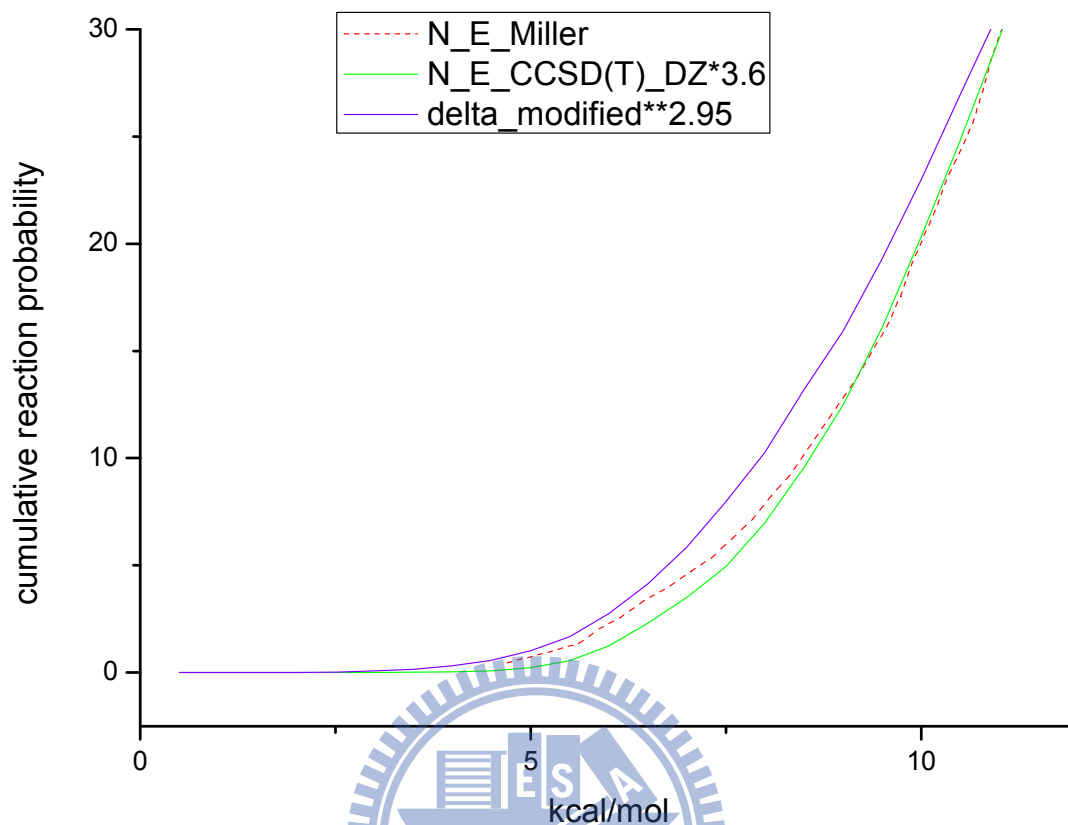


Figure 3.14 Cumulative reaction probability of $J = 0$ for adiabatic model with modified delta in order of 2.95 as equation (3.26) and (3.27), adiabatic model with a multiple factor 3.6 and miller's result. This result is calculated with ccSD(t)/aug-cc-pvdz//ccSD/aug-cc-pvdz for energy correction and ccSD/aug-cc-pvdz for frequencies along MEP

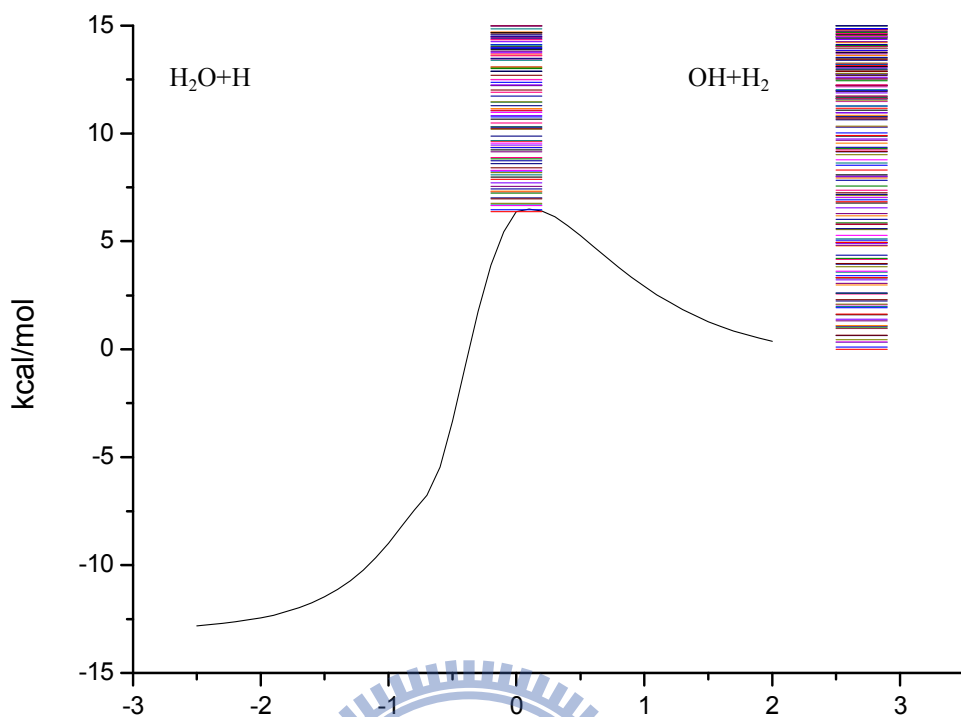


Figure 3.15 The energy diagram of diabatic model, which show the energy levels of transition state in the middle and energy levels of reactant in the rightmost side. This result is calculated with `ccsd(t)/aug-cc-pvdz//ccsd/aug-cc-pvdz` for energy correction and `ccsd/aug-cc-pvdz` for frequencies along MEP

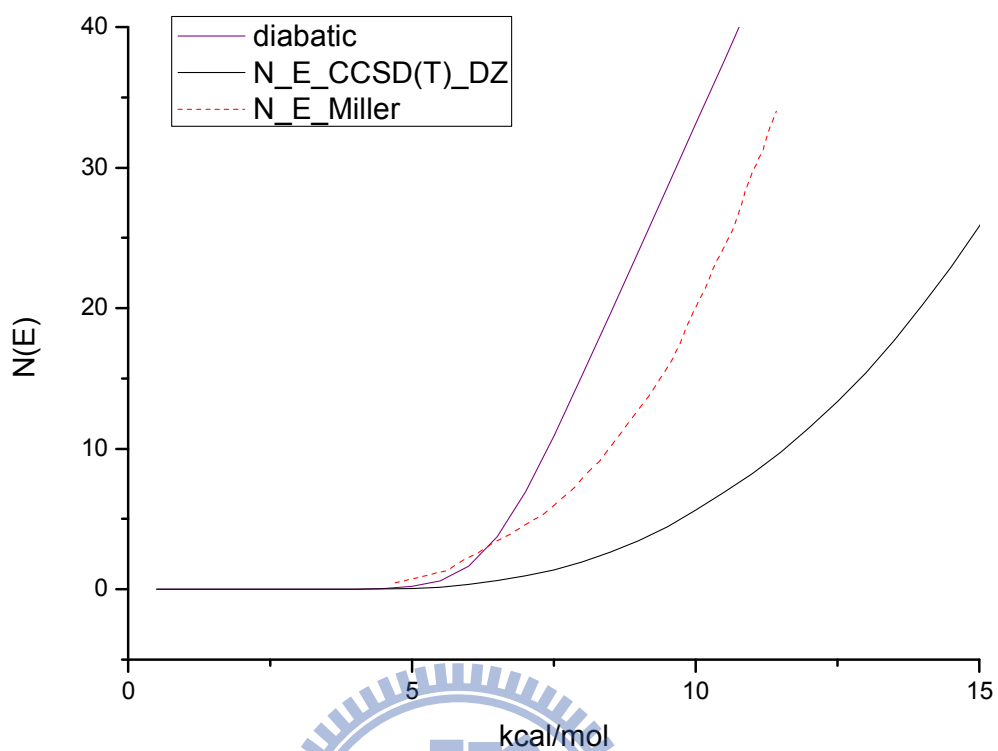


Figure 3.16 Cumulative reaction probability of $J = 0$ for diabatic model (purple line), adiabatic model (black line) and Miller's result (red dash line). This result is calculated with `ccsd(t)/aug-cc-pvd//ccsd/aug-cc-pvdz` for energy correction and `ccsd/aug-cc-pvdz` for frequencies along MEP

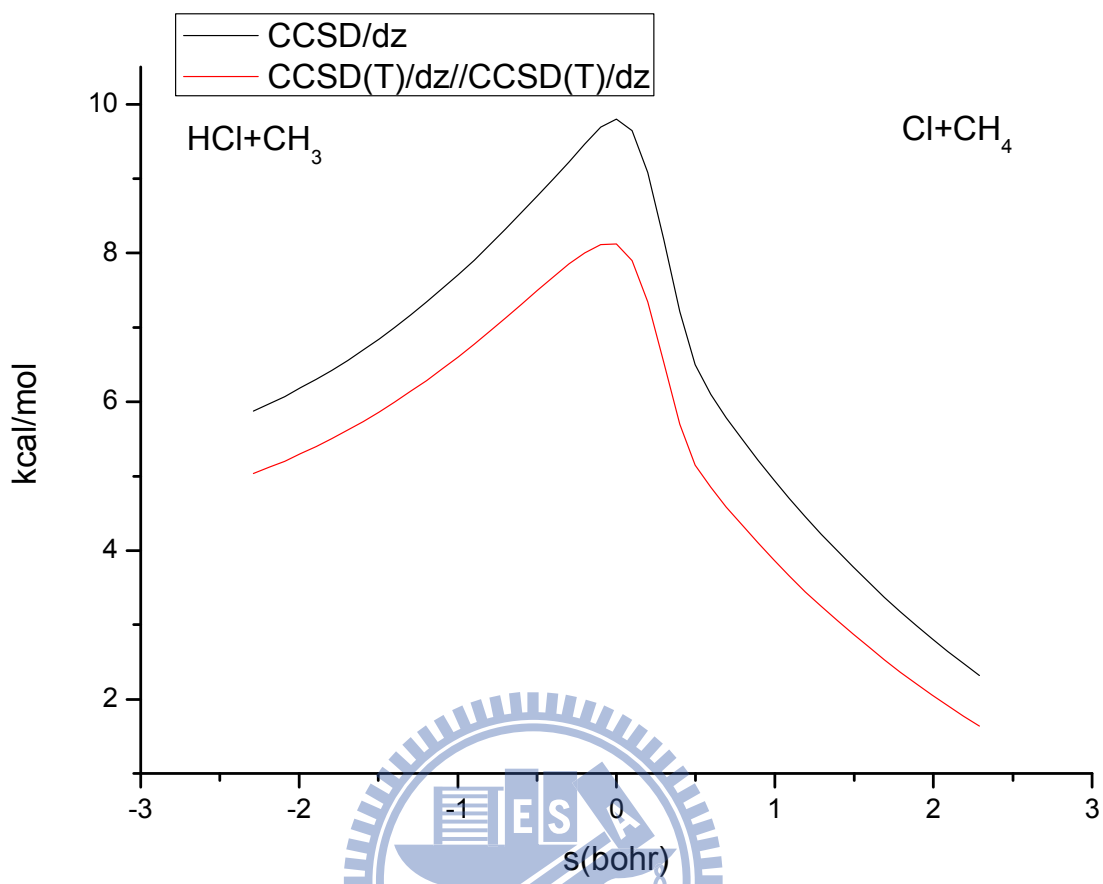


Figure 3.17 MEP of two different methods, where dz stands for aug-cc-pvdz and tz stands for aug-cc-pvtz.

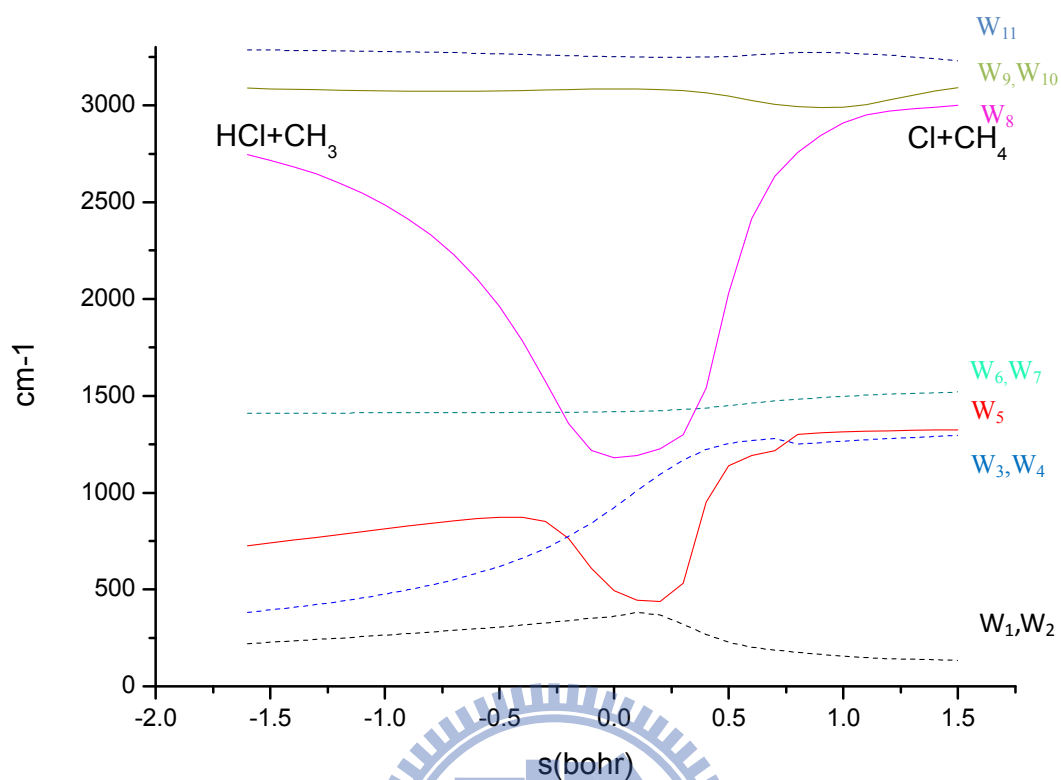


Figure 3.18 Fitted frequencies along MEP. This result is calculated with CCSD/aug-cc-pvdz method. W_i is the label used in table 3.8 and 3.9. From these labels, the correlation between asymptotic regions and the motion along reaction path could be understood clearly in table 3.8 and 3.9. Double degenerate modes are dashed curves, and non-degenerate modes are solid curves.

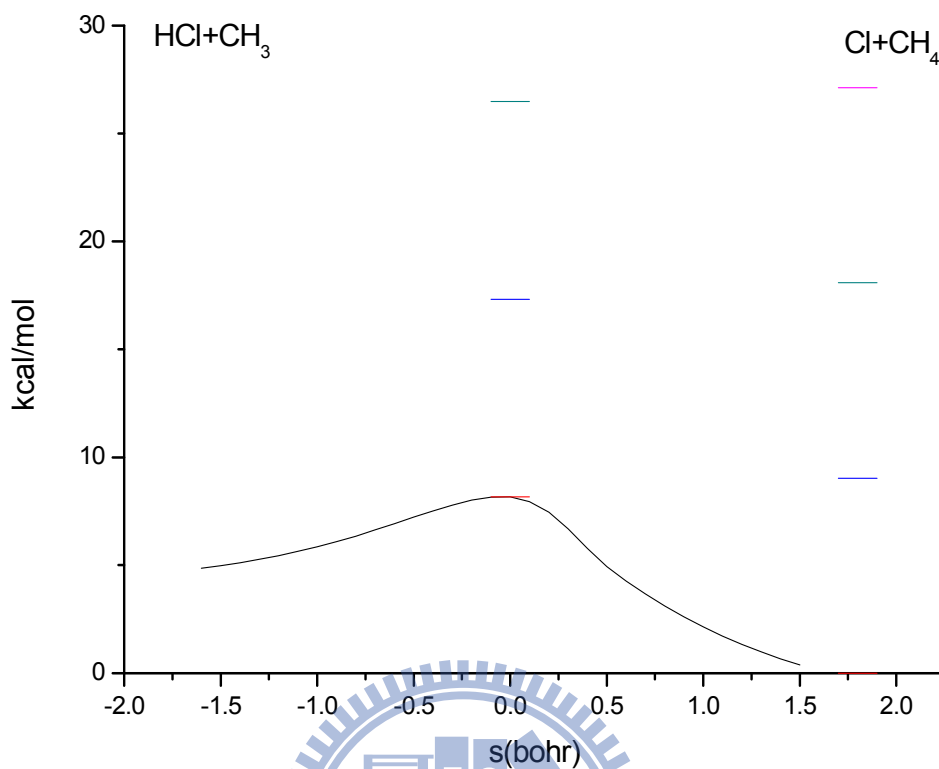


Figure 3.19 The energy diagram of diabatic model with only one dimension of the anti-sym stretching of CH₄/CH₃ considered, which show the energy levels of transition state in the middle and energy levels of reactant in the rightmost side. This result is calculated with `ccsd(t)/aug-cc-pvd//ccsd/aug-cc-pvdz` for energy correction and `ccsd/aug-cc-pvdz` for frequencies along MEP

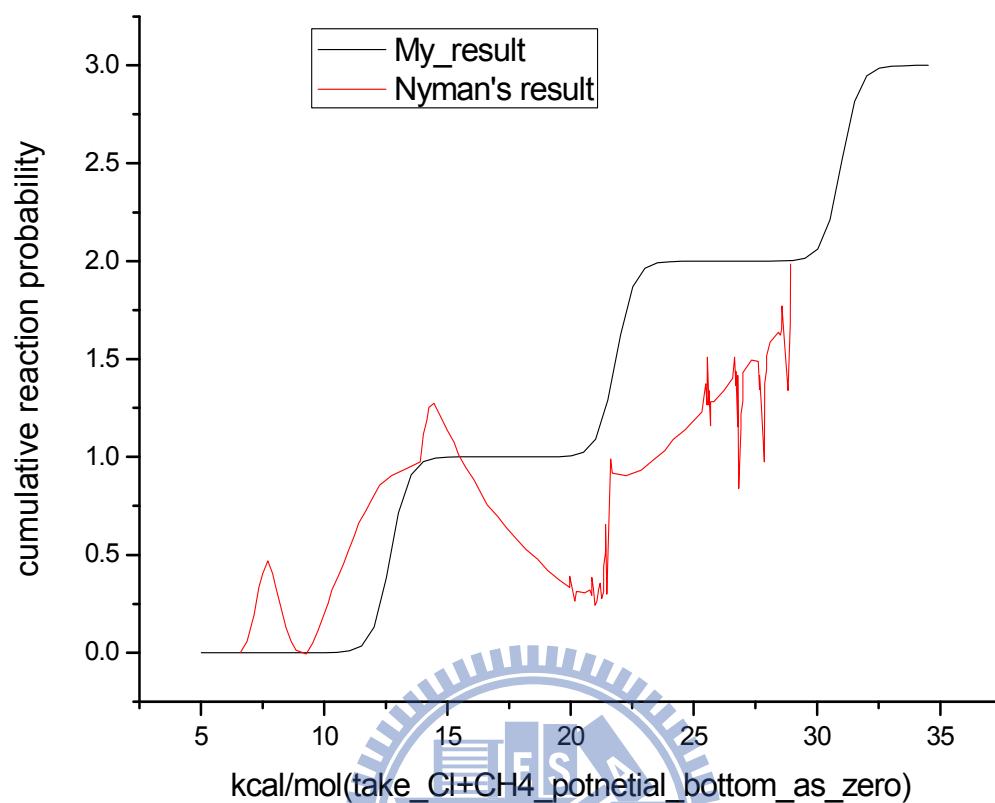


Figure 3.20 Cumulative reaction probability of $J = 0$ for adiabatic model with only one dimension of the anti-sym stretching of CH_4/CH_3 considered and Nyman's RLA result. This result is calculated with `ccsd(t)/aug-cc-pvd //ccsd/aug-cc-pvdz` for energy correction and `ccsd/aug-cc-pvdz` for frequencies along MEP

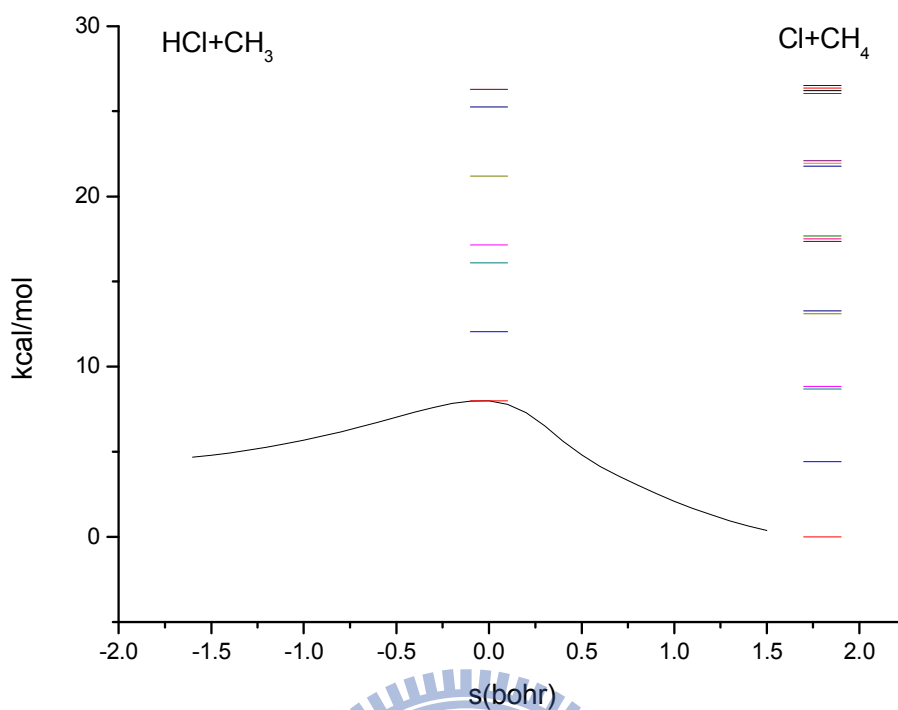


Figure 3.21 The energy diagram of diabatic model with only two dimensions of the anti-sym stretching of CH₄/CH₃ and the umbrella motion of CH₄/CH₃ considered, which show the energy levels of transition state in the middle and energy levels of reactant in the rightmost side. This result is calculated with ccSD(t)/aug-cc-pvd //ccSD/aug-cc-pvdz for energy correction and ccSD/aug-cc-pvdz for frequencies along MEP

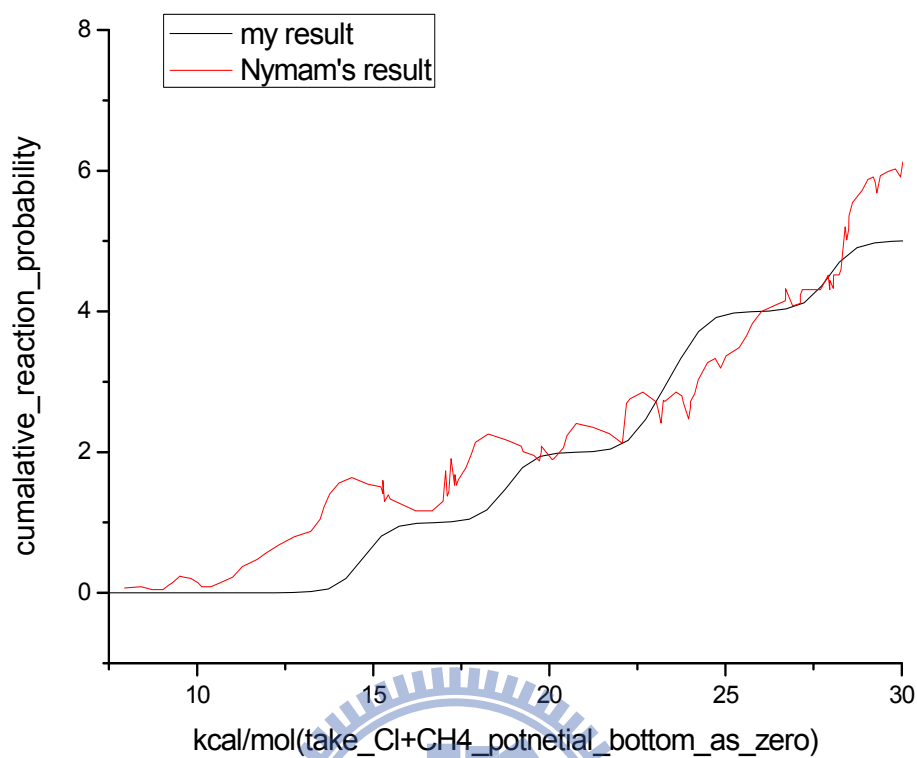


Figure 3.22 Cumulative reaction probability of $J = 0$ for adiabatic model with only two dimensions of the anti-sym stretching of CH_4/CH_3 and the umbrella motion of CH_4/CH_3 considered and Nyman's RLU result. This result is calculated with $\text{ccsd}(t)/\text{aug-cc-pvd}/\text{ccsd}/\text{aug-cc-pvdz}$ for energy correction and $\text{ccsd}/\text{aug-cc-pvdz}$ for frequencies along MEP

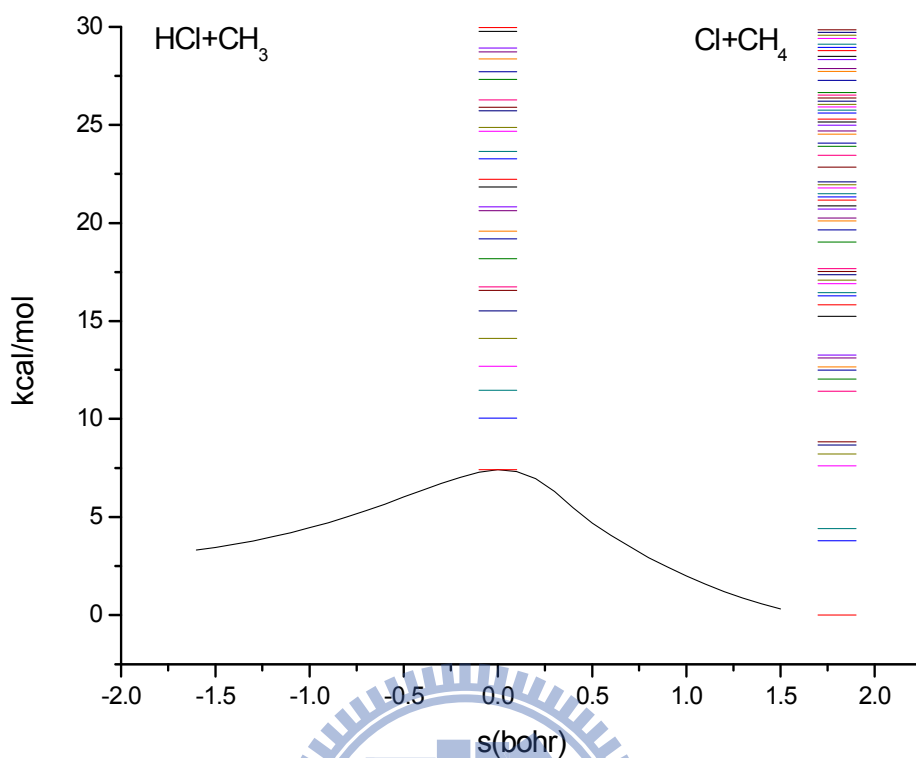


Figure 3.23 The energy diagram of diabatic model with only three dimensions of the anti-sym stretching of CH₄/CH₃, the umbrella motion of CH₄/CH₃ and the bending motion of CH₄ considered, which show the energy levels of transition state in the middle and energy levels of reactant in the rightmost side. This result is calculated with `ccsd(t)/aug-cc-pvd //ccsd/aug-cc-pvdz` for energy correction and `ccsd/aug-cc-pvdz` for frequencies along MEP

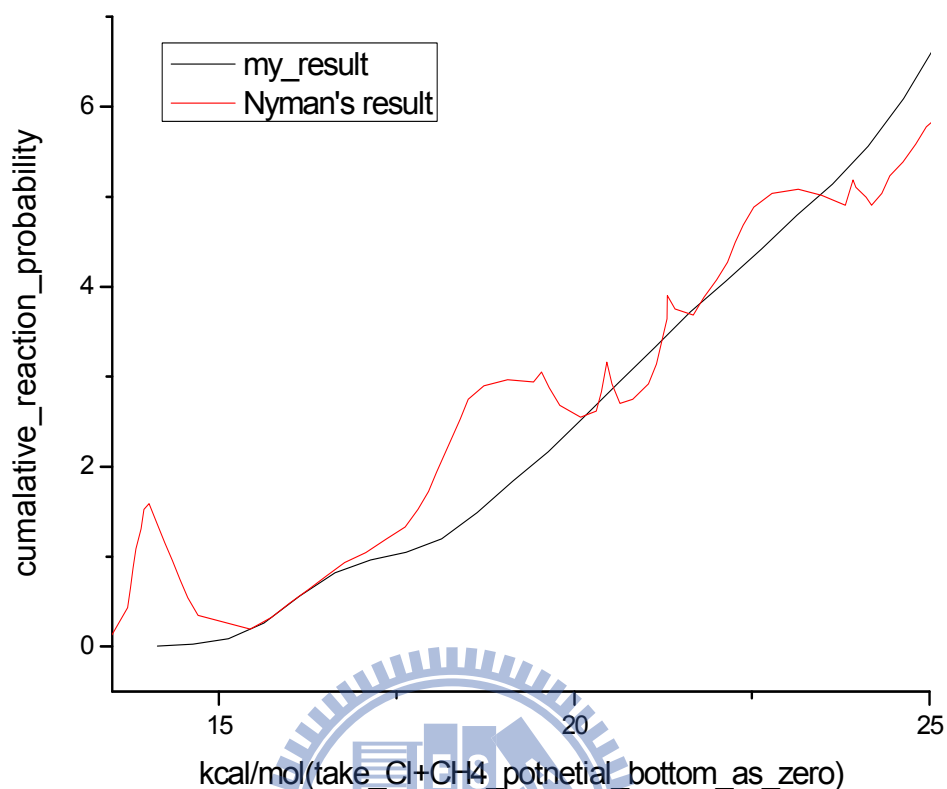


Figure 3.24 Cumulative reaction probability of $J = 0$ for adiabatic model with only three dimensions of the anti-sym stretching of CH_4/CH_3 , the umbrella motion of CH_4/CH_3 and the bending motion of CH_4 considered and Nyman's RLU result. This result is calculated with `ccsd(t)/ aug-cc-pvd//ccsd/aug-cc-pvdz` for energy correction and `ccsd/ aug-cc-pvdz` for frequencies along MEP

References:

1. W. M. Smith and R. Zellner, *J. Chem. Soc. Faraday Trans. II* **70**, 1045 (1974).
2. George C. Schatz and Stephen P. Walch *J. Chem. Phys.* **72**, 1 (1980)
3. P. J. Hay and T. H. Dunning, *J. Chem. Phys.* **64**, 5077 (1976); T. H. Dunning, *J. Chem. Phys.* **65**, 3854 (1976).
4. Thanh N. Truong, *J. Chem. Phys.* **102**, 13 (1995)
5. R.F. Heidner III, J.F. Bott, C.E. Gardner and J.E. Melzer, *J. Chem. Phys.* **72**, 4815. (1980)
6. Charles F. Jackels, Zhen Gu, and Donald G. Truhlar, *J. Chem. Phys.* **102**, 8 (1995)
7. Uwe Manthe, Tamar Seideman, and William H. Miller, *J. Chem. Phys.* **99**, 12 (1993)
8. T. N. Truong, D. G. Truhlar, K. K. Baldrige, M. S. Gordon and R. Steckler, *J. Chem. Phys.* **90**, 7137 (1989)
9. K. D. Dobbs and D. A. Dixon, *J. Phys. Chem.*, **98**, 12584 (1994)
10. Hua-Gen and Gunnar Nyman, *J. Chem. Phys.* **109**, 14 (1998)
11. Hua-Gen and Gunnar Nyman, *PCCP*, **1**, 1181, (1998)
12. Hua-Gen and Gunnar Nyman, *J. Chem. Phys.* **110**, 15 (1999)
13. NIST Computational Chemistry Comparison and Benchmark Database IVA Reaction Comparison Experimental Enthalpies at 0K, <http://srdata.nist.gov/ccbdb>
14. M. S. Zahniser, M. Berquist, and F. Kaufman, *Int. J. Chem. Kinet.* **10**, 15 (1978).
15. S. S. Yan, Y.-T. Wu, K. Liu, *Phys. Chem. Chem. Phys.* **9**, 250 (2007).

Chapter4 Conclusions

We constructed more general adiabatic energy curves of $J=0$ for $\text{OH} + \text{H}_2 \rightarrow \text{H}_2\text{O} + \text{H}$ by using, equation (3.15) and (3.16) but found the cumulative reaction probability of these adiabatic energy curves (without the effect of non-adiabatic coupling, only the effect of tunneling) is lower than the result of Miller. The possible reason would be the linkage between reactants and products. Since three rotational related vibration modes in reactant side, but two in product side. The evolution from rotation to vibration should be considered carefully. (In fact, the mode which evolves from rotation in H_2 to vibration in H_2O should be considered together, not in two parts; reactant and product.) So we applied the adiabatic model, modified adiabatic model and diabatic model to the cumulative reaction probability and then got three main possible reasons for the deviation from Miller's result¹. First is that the energy curves are not parabolic model, the second one is that the contribution of non-adiabatic coupling and the last one is the accuracies of the frequencies along the reaction path. In order to make sure which one is the main reason, we applied these three models to a larger but prototypical system. But for more than 5-atoms system, there's no exact solution no matter hyper-spherical (projected one is the same) or Jacobi coordinate. So only reduced dimensions information is available, that is, only the adiabatic model with reduced dimension could be applied to do comparisons. After comparing with

the three models; RLA, RLU, RBU, by Nyman², we found that the trends of our adiabatic models goes well Nyman's results and the effect of resonance becomes larger as the degree of freedom becomes smaller. From the result, we conclude that the last reason; the accuracies of the frequencies along the reaction coordinate dominate the accuracy of the result for the cumulative reaction probability.



Reference

1. As the reference 7 in chapter 3.
2. As the references 10~12 in chapter 3.

